NONSIMILAR SOLUTIONS FOR IMPACT-GENERATED SHOCK PROPAGATION IN SOLIDS

by

William J. Rae

prepared for

NATIONAL AERONAUTICS AND SPACE ADMINISTRATION

CONTRACT NO. NAS 3-2536

CORNELL AERONAUTICAL LABORATORY, INC.
of Cornell University
Buffalo, New York 14221

NOTICE

Requests for copies of this report should be referred to

National Aeronautics and Space Administration
Office of Scientific and Technical Information
Attention: AFSS-A
Washington, D.C. 20546

CASE FILE COPY

FINAL REPORT

NONSIMILAR SOLUTIONS FOR IMPACT-GENERATED SHOCK PROPAGATION IN SOLIDS

by

William J. Rae

prepared for

NATIONAL AERONAUTICS AND SPACE ADMINISTRATION

March 1965

CONTRACT NO. NAS 3-2536

CORNELL AERONAUTICAL LABORATORY, INC.
of Cornell University
Buffalo, New York   14221

N65 21625

FOREWORD

This document constitutes a final report on the application of the blast-wave theory of meteoroid impact to the problem of space radiator design. Other publications entitled "Comments on the Solution of the Spall-Fracture Problem in the Approximation of Linear Elasticity", CAL Report AI-1821-A-3, NASA CR-54250, and "On the Possibility of Simulating Meteoroid Impact by the Use of Lasers", CAL Report AI-1821-A-1, NASA CR-54029, have previously been generated under this NASA-sponsored program.

The present report is mainly concerned with the phenomena of shock propagation and fluid flow due to impact. The application of these results to the prediction of the deformation remaining after the fluid motion ceases is taken up in the report on spall fracture, mentioned above.

ABSTRACT

This report presents analytical solutions for the propagation of shock waves in dense targets struck by hypervelocity projectiles. The solutions considered deal mainly with the high-pressure phases of deformation, during which the material strength can be neglected. Several methods of solution are described. Their advantages and limitations are discussed, and their accuracy is estimated by comparing their predictions with experiment and with the results of numerical solutions. To illustrate the application of these approximate theories, an example is given of shock propagation in porous targets.

TABLE OF CONTENTS

LIST OF SYMBOLS

a^2 square of the sound speed, equal to $\left(\frac{\partial p}{\partial \rho}\right)_\sigma$

A^2 dimensionless sound speed squared, see Eq. (126)

b parameter related to Grüneisen constant at normal density, see Eq. (65)

c weak-wave limit of shock speed: $u_s = c + s u_1$

C_v specific heat at constant volume

D function defined in Eq. (47)

e internal energy per unit mass

$\hat{e}/c^2$ constant defined in Eq. (48)

E total energy in a blast wave, taken to be projectile kinetic energy

f $p / \rho_0 \dot{R}_s^2$

$f(v)$ function defined in Eq. (63)

$F(p, \rho)$ general form of state equation

g $(e - e_0) / \dot{R}_s^2$

$I(M)$ integral defined by Eq. (99) or (165)

K constant defined by Eq. (160)

M shock Mach number, u_s/c, or $\dot{R}_s/c$

M_0 value the shock Mach number had when it crossed a given particle

M_i value of u_s/c during plane-wave portion of projectile destruction

N exponent in $R_s \sim t^N$

p pressure

r, θ spherical polar coordinates

R_s shock radius

R_0 scaling length, defined by Eq. (102) or (167)

u, w velocity components in the r- and θ-directions

$\mathcal{A}$ entropy

s constant in the relation $u_s = c + s u_1$

t time

T temperature

τ specific volume, $1/\rho$

x, y variables defined in Eq. (104)

z variable defined in Eq. (75)

α defined by Eq. (119); also used to denote $(N-1)/N$

γ specific-heat ratio of a perfect gas

Γ Grüneisen parameter

$\Delta(\rho)$ see Eq. (24)

η $r/R_s(t)$

ν geometrical index, equal to 0, 1, or 2 for plane, cylindrical, or spherical flows

ρ mass density

σ_ν constant defined by Eq. (100) or (166)

τ angular velocity gradient, see Eq. (144)

ϕ $u/\dot{R}_s$

$\varphi(\rho)$ see Eq. (17)

Φ function defined by Eq. (73)

ψ p/p_0

Ψ function defined by Eq. (73)

ω $w/\dot{R}_s$

$( )_c$ denotes cohesive contribution

$( )_{FS}$ denotes free-surface conditions

$( )_H$ denotes Hugoniot conditions, e. g., p_H = Hugoniot (or shock) pressure

$( )_s$ denotes conditions at the shock, e. g., u_s = shock velocity

$( )_{0,1}$ denotes conditions ahead of, and behind, the shock

$(\,\dot{}\,)$ denotes time derivative

$( )'$ denotes $d/d\eta$

∞ denotes proportionality

INTRODUCTION

The deformation of a solid target by the impact of a high-speed projectile is an extremely complex phenomenon. Attempts to predict the behavior of real materials during such an intense disturbance are complicated by the presence of a variety of nonelastic, nonlinear effects. In recent years, however, interest in impact at the extreme velocities of meteoric particles (10 - 70 km/sec) has made it possible to neglect material strength during much of the deformation. This approximation is suggested by the fact that the pressures generated at impact are typically measured in megabars, and far exceed the strength of any common material. While the applicable equations of inviscid motion are considerably simpler than those in which material strength is accounted for, nevertheless their solution presents a formidable problem in time-dependent, multidimensional, compressible fluid flow. Numerical solutions of such problems for specific cases have been reported by Bjork[1,2] and by Walsh and his coworkers.[3,4] The latter results, in particular, have revealed the existence of certain scaling laws, but extensive correlations of the numerical results have not yet appeared. Parallel analytical treatments, while less specific, have also identified these scaling laws, and have been used[5] to correlate results from a variety of cases. The main purpose of this report is to review several of the more promising analytical approaches that have been used, to present some extensions of them, and to show their range of application.

The solutions described below deal exclusively with the inviscid-fluid model; the strength mechanisms by which the target material is eventually brought to rest are omitted. Consequently, the solutions offer

no direct information about target damage, but describe only the shock propagation and the flow behind the shock. Some implications of these results on the question of target damage are presented in the Concluding Remarks.

One of the main obstacles to finding analytic solutions for shock propagation in solids is that the powerful method of similarity cannot be used.[5] The reasons for this fact, which is associated with the equation of state of the material, are briefly reviewed in Section I. Various forms of the state equation are considered in Section II, and the particular form used in the present report is described in detail. The three types of non-similar solutions considered are taken up in Section III. The first of these, developed by Oshima[6] for a perfect gas, has perhaps the greatest analytical justification, and is here extended to the case of solids.

The second is the "Quasi-Steady" solution used previously[5] to achieve a fairly accurate correlation of impact-generated shock waves. This theory is also extended, so as to apply to the weaker, later stages of shock propagation, and is compared extensively with experiment and with numerical solutions. The third method reviewed was developed originally by Porzel[7] for the case of atmospheric blasts, and was later extended by Zaker[8] to the problem of a nuclear explosion inside a solid. The Porzel-Zaker theory is rederived here, in the light of new information now available about the equation of state of solids.

The application of these theories is illustrated in Section IV by considering shock propagation in porous targets, a situation which apparently has not yet been treated numerically. The report concludes with remarks intended to indicate what can and cannot be done at present by

analytical means, and to call attention to several lines of research that may be fruitful for achieving an improved analytical understanding of deformation due to hypervelocity impact.

I. SIMILARITY CONSIDERATIONS

When material strength is neglected, the equations expressing the conservation of mass, momentum, and energy reduce to the Euler equations of an inviscid, compressible fluid. Assuming that all motion is symmetric about an axis normal to the target surface, and using a spherical coordinate system with its center at the impact point, the equations of motion are

$$\frac{\partial \rho}{\partial t} + u \frac{\partial \rho}{\partial r} + \frac{w}{r} \frac{\partial \rho}{\partial \theta} + \rho \left(\frac{\partial u}{\partial r} + \frac{1}{r} \frac{\partial w}{\partial \theta} + \frac{\nu u}{r} + \frac{w}{r} \cot \theta \right) = 0 \qquad (1)$$

$$\frac{\partial u}{\partial t} + u \frac{\partial u}{\partial r} + \frac{w}{r} \frac{\partial u}{\partial \theta} - \frac{w^2}{r} + \frac{1}{\rho} \frac{\partial p}{\partial r} = 0 \qquad (2)$$

$$\frac{\partial w}{\partial t} + u \frac{\partial w}{\partial r} + \frac{w}{r} \frac{\partial w}{\partial \theta} + \frac{u w}{r} + \frac{1}{\rho r} \frac{\partial p}{\partial \theta} = 0 \qquad (3)$$

$$\frac{\partial e}{\partial t} + u \frac{\partial e}{\partial r} + \frac{w}{r} \frac{\partial e}{\partial \theta} - \frac{p}{\rho^2} \left(\frac{\partial \rho}{\partial t} + u \frac{\partial \rho}{\partial r} + \frac{w}{r} \frac{\partial \rho}{\partial \theta} \right) = 0 \qquad (4)$$

Here u and w denote velocity components in the r- and θ-directions, p denotes the pressure, ρ the density, and e the internal energy per unit mass. The index ν appearing in the continuity equation must, strictly speaking, be set equal to 2, since these equations apply only for a spherical problem. Its value is left arbitrary for the moment, since, when the θ-variation is discarded (as will be done shortly) the correct forms for the cylindrical and planar cases can be recovered by setting ν = 1 or 0.

These equations are completed by the equation of state, which is taken for the moment in the form

$$e = F(p, \rho) \qquad (5)$$

At the shock, the Rankine-Hugoniot conditions apply. Thus

$$\rho_0 u_s = \rho_1 (u_s - u_1) \qquad (6)$$
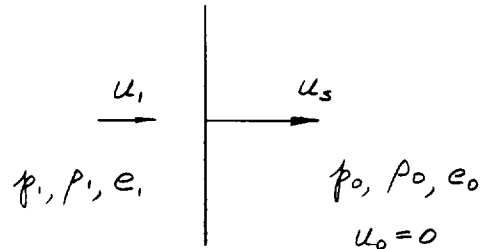
$$p_1 - p_0 = \rho_0 u_s u_1 \qquad (7)$$

$$e_1 - e_0 = \frac{1}{2}(p_0 + p_1)\left(\frac{1}{\rho_0} - \frac{1}{\rho_1}\right) \qquad (8)$$

where u_s is the velocity of any portion of the shock normal to itself, and subscripts 0 and 1 denote conditions ahead of and behind the shock.

The analysis presented in this report is based on the assumption that the shock is always a hemisphere, with center at the impact point on the surface. Such an assumption is supported by photographs of impact-generated shock waves in transparent targets, [9, 10, 11] by internal measurements of shock shape in wax targets, [12, 13] and by computer solutions

for impact into solids, at a sufficiently long time after impact. [1,2,3,4]
For impact into a gaseous target, the results of Walsh et al[4] indicate a
spherical shock whose center lies inside the original target surface, at
about one-third the distance traveled by the shock along the axis of sym-
metry.

The problem of predicting the flow field behind the shock wave as
it propagates into the target requires the solution of Eqs. (1) - (4), which
contain two spatial coordinates and time. One of the most fruitful
approaches to such a complicated problem has been the method of simi-
larity, which assumes that properly normalized distributions of the
various physical quantities (pressure, density, etc.) at each instant are
the same when viewed on a scale defined by the shock radius at that in-
stant. Thus each quantity, instead of varying independently with time and
with the spatial coordinate r (distance from the origin), is assumed to
be a function only of the similarity variable.

$$\eta = r/R_s(t) \tag{9}$$

where $R_s(t)$ is the instantaneous distance of the shock from the origin.
Mathematically speaking, the objective of the similarity assumption is to
suppress time as an explicit independent variable. To see how this is
done, and to set the stage for the introduction of Oshima's method below,
it is instructive to change independent coordinates from r, θ, t
to η, θ, $R_s(t)$, and to redefine the dependent variables in terms
of certain dimensionless functions:

$$u = \dot{R}_s \, \phi(\eta, \theta, R_s) \qquad p = p_o \dot{R}_s^{\;2} f(\eta, \theta, R_s)$$

$$w = \dot{R}_s \, \omega(\eta, \theta, R_s) \qquad \rho = \rho_o \, \psi(\eta, \theta, R_s) \qquad (10)$$

$$e - e_o = \dot{R}_s^{\;2} \, g(\eta, \theta, R_s)$$

In these terms, the basic differential equations become

$$(\phi - \eta) \frac{\partial \psi}{\partial \eta} + \frac{\omega}{\eta} \frac{\partial \psi}{\partial \theta} + \psi \left(\frac{\partial \phi}{\partial \eta} + \frac{1}{\eta} \frac{\partial \omega}{\partial \theta} + \nu \frac{\phi}{\eta} + \frac{\omega}{\eta} \cot \theta \right) = -R_s \frac{\partial \psi}{\partial R_s} \qquad (11)$$

$$\frac{R_s \ddot{R}_s}{\dot{R}_s^{\;2}} \phi + (\phi - \eta) \frac{\partial \phi}{\partial \eta} + \frac{\omega}{\eta} \frac{\partial \phi}{\partial \theta} - \frac{\omega^2}{\eta} + \frac{1}{\psi} \frac{\partial f}{\partial \eta} = -R_s \frac{\partial \phi}{\partial R_s} \qquad (12)$$

$$\frac{R_s \ddot{R}_s}{\dot{R}_s^{\;2}} \omega + (\phi - \eta) \frac{\partial \omega}{\partial \eta} + \frac{\omega}{\eta} \frac{\partial \omega}{\partial \theta} + \frac{\phi \omega}{\eta} + \frac{1}{\psi \eta} \frac{\partial f}{\partial \theta} = -R_s \frac{\partial \omega}{\partial R_s} \qquad (13)$$

$$2 \frac{R_s \ddot{R}_s}{\dot{R}_s^{\;2}} g + (\phi - \eta) \frac{\partial g}{\partial \eta} + \frac{\omega}{\eta} \frac{\partial g}{\partial \theta} - \frac{f}{\psi^2} \left\{ (\phi - \eta) \frac{\partial \psi}{\partial \eta} + \frac{\omega}{\eta} \frac{\partial \psi}{\partial \theta} \right\} =$$

$$(14)$$

$$= -R_s \frac{\partial g}{\partial R_s} + \frac{f}{\psi^2} R_s \frac{\partial \psi}{\partial R_s}$$

The assumption of similarity amounts to neglecting the right-hand sides of these equations -- i. e., it is assumed that the functions ϕ , ω ,

f , ψ , and q do not change with the scale R_s of the disturbance. In addition, similarity requires that the combination $R_s \ddot{R}_s / \dot{R}_s^2$ be a constant, which is satisfied if the shock radius is proportional to a power of the time

$$R_s \sim t^N \qquad (15)$$

The only remaining source of time dependence then comes from the boundary conditions. The Rankine-Hugoniot conditions, written in terms of the dimensionless functions introduced above, become

$$\psi_1 \left(1 - \phi_1 \right) = 1$$

$$f_1 = \phi_1 + \frac{p_o}{\rho_o \dot{R}_s^2} \qquad (16)$$

$$q_1 = \frac{1}{2} \left(f_1 + \frac{p_o}{\rho_o \dot{R}_s^2} \right) \left(1 - \frac{1}{\psi_1} \right)$$

$$\dot{R}_s^2 q_1 = F \left(\rho_o \dot{R}_s^2 f_1 , \rho_o \psi_1 \right)$$

where conditions ahead of and behind the shock are denoted by subscripts o and 1 , respectively. These equations show that an explicit time dependence can enter in either of two ways. The first occurs whenever the pressure ahead of the shock is comparable to $\rho_o \dot{R}_s^2$, which is of the order of the pressure behind the shock. The second possibility of time dependence comes from the state equation. As pointed out, for example by Kynch[14] and by Sedov,[15] similarity solutions are possible only if the equation of state has the form

$$e = p \varphi(\rho) \qquad (17)$$

where $\varphi(\rho)$ is any function of the density. When the state equation has this form, and when the term $p_0 / \rho_0 \dot{R}_s^2$ is negligible, it is possible to eliminate g_1 between the last two of Eqs. (16), and the result is an expression for the density ratio across the shock ψ_1, which remains constant

$$2 \rho_0 \, \varphi(\rho_0 \psi_1) - 1 + \frac{1}{\psi_1} = 0 \tag{18}$$

The equation of state of a perfect gas

$$e = \frac{p}{(\gamma - 1)\rho} \tag{19}$$

is of the form of Eq. (17). Thus, departures from similarity in the perfect-gas problem arise only from the term $p_0 / \rho_0 \dot{R}_s^2$. The situation is just the opposite for shock propagation in solids. There, the term $p_0 / \rho_0 \dot{R}_s^2$ is certainly negligible whenever the fluid-mechanical model itself is appropriate. On the other hand, the state equation appropriate to a high-pressure solid does not match the form required by Eq. (17), except in the limit of extremely high pressures, where, as will be seen below, the state equation approximates the required form, and the density ratio across the shock approaches a constant value. It is a matter of common experience, however, that the density ratios produced by impact-generated shock waves are far from constant. For impact speeds on the order of 10 km/sec, they may range as high as 2 or 3 at the impact point, but they drop rapidly as the wave expands, and quickly approach the elastic-wave limit of 1. Only the very early stages of impact at very high speed experience the constant density ratio required for similarity. Thus, as pointed out in Ref. 5, impact-generated shock propagation in solids is characteristically nonsimilar.

II. EQUATION OF STATE

The nonsimilar behavior of shock propagation in solids is caused by the form of the state equation. For the range of pressures encountered in hypervelocity impact, the Mie-Grüneisen equation of state is commonly used. In most numerical solutions, this equation is expressed in considerable detail, requiring the specification of a large number of constants. For present analytical purposes, a less cumbersome expression is desirable; this section describes an approximate form of the Mie-Grüneisen equation used in the analyses that follow. A complete description is given of the shock-wave relations and thermodynamic properties for such a state equation.

A. General Form

The Mie-Grüneisen equation is usually written in the form (see Ref. 16, Eq. (33))

$$e(p,\rho) - e_c(\rho) = \frac{p - p_c(\rho)}{\rho \Gamma(\rho)} \tag{20}$$

where the subscript c denotes the cohesive contribution, and where $\Gamma(\rho)$ is the Grüneisen factor, which depends weakly on ρ. It is convenient to express the cohesive quantities in terms of measured shock-wave data; along the Hugoniot, Eq. (20) takes the form:

$$e_H(\rho) - e_c(\rho) = \frac{p_H(\rho) - p_c(\rho)}{\rho \Gamma(\rho)} \tag{21}$$

Subtracting the left and right sides of this from the corresponding sides of (20) gives

$$e - e_H(\rho) = \frac{p - p_H(\rho)}{\rho \Gamma(\rho)} \tag{22}$$

This can be rearranged in the form

$$e = \frac{p}{\rho \Gamma(\rho)} - \Delta(\rho) \tag{23}$$

where

$$\Delta(\rho) = \frac{p_H(\rho)}{\rho \Gamma(\rho)} - e_H(\rho) = \frac{p_c(\rho)}{\rho \Gamma(\rho)} - e_c(\rho) \tag{24}$$

The presence of the second term in Eq. (23) renders a similarity solution inappropriate (compare with Eq. (17)) except in the limit of extremely high pressure, where $\Delta(\rho)$ is negligible compared to the first term.

B. Shock-Wave Relations for General Γ, Δ

The Rankine-Hugoniot condition expressing conservation of energy across a shock is

$$e_1 - e_0 = \frac{p_1 + p_0}{2\rho_0}\left(1 - \frac{\rho_0}{\rho_1}\right) \tag{25}$$

If all energies are measured with respect to e_0, the equation of state may be rewritten

$$e - e_0 = \frac{p}{\rho \Gamma(\rho)} - \Delta(\rho) \tag{26}$$

Equating these two expressions gives the Hugoniot curve in the form

$$\frac{p_1}{\rho_1 \Gamma(\rho_1)} - \Delta(\rho_1) = \frac{p_1}{2\rho_0}\left(1 - \frac{\rho_0}{\rho_1}\right) \tag{27}$$

where the approximation has been made that $p_0 \ll p_1$. An alternate form can be derived by using the other two Rankine-Hugoniot conditions

$$p_1 = \rho_0 u_s u_1 \qquad\qquad \rho_0 u_s = \rho_1 (u_s - u_1) \qquad (28)$$

This leads to

$$\left\{ 1 + \frac{2 \Delta(p_1)}{u_s^2} \right\} \left(\frac{\rho_1}{\rho_0} \right)^2 - 2 \left\{ \frac{1}{\Gamma(\rho_1)} + 1 \right\} \frac{\rho_1}{\rho_0} + \left\{ 1 + \frac{2}{\Gamma(\rho_1)} \right\} = 0 \qquad (29)$$

This relation is shown in Fig. 1. If information about the functions $\Gamma(\rho_1)$ and $\Delta(\rho_1)$ is available (perhaps from a theoretical estimate of the cohesive terms) this figure can be used, for a given value of ρ_1, to find the corresponding value of u_s.

C. Specialization for a c, s Medium

The steps indicated above can be reversed, and the measured Hugoniot data can be used to investigate the quantities $\Gamma(\rho)$ and $\Delta(\rho)$.[*] In particular, if $\Gamma(\rho)$ is known, Eq. (24) gives $\Delta(\rho)$ in terms of the Hugoniot data. These relationships take on an especially simple form for a substance whose Hugoniot displays a linear relation between the shock speed and the particle speed behind the shock

$$u_s = c + s u_1 \qquad (30)$$

Such a substance is here referred to as a c, s medium. A large number of materials are well approximated by such a relation. Reference 16, for example, presents a collection of values of c and s for various materials.

---

[*] As pointed out, for example, by Tillotson.[17]

In what follows, the explicit form of $\Delta(\rho)$ for such a material is derived. From Eq. (24)

$$\Delta(\rho) = \frac{P_H(\rho)}{2\rho} \left[\frac{2}{\Gamma} + 1 - \frac{\rho}{\rho_0} \right] \tag{31}$$

For the moment, Γ is assumed to be a known constant; its precise value will be specified later. For a C, S medium

$$P_H = \rho_0 u_s^2 \frac{u_1}{u_s} = \rho_0 c^2 \left(\frac{u_s}{c} \right)^2 \frac{u_1}{u_s} = \frac{\rho_0 c^2 \left(1 - \rho_0/\rho \right)}{\left[1 - s + s\rho_0/\rho \right]^2} \tag{32}$$

Thus

$$\frac{\Delta(\rho)}{c^2} = \frac{\left(\frac{\rho}{\rho_0} - 1 \right)\left(\frac{2}{\Gamma} + 1 - \frac{\rho}{\rho_0} \right)}{2 \left[s - (s-1)\rho/\rho_0 \right]^2} \tag{33}$$

In the limit of extremely strong shocks, where $u_s \to \infty$, the results of Fig. 1 indicate that the density ratio should approach $\frac{2}{\Gamma} + 1$. On the other hand, for a C, S medium,

$$\frac{\rho_1}{\rho_0} = \frac{s\, u_s/c}{(s-1)\, u_s/c + 1} \longrightarrow \frac{s}{s-1} \quad as \quad \frac{u_s}{c} \longrightarrow \infty$$

The constant value to be used for Γ is chosen so as to make these two limiting values for the density ratio equal, i.e.,

$$\frac{2}{\Gamma} + 1 = \frac{s}{s-1} \quad , \; or \quad \Gamma = 2(s-1) \quad , \; or \quad s = 1 + \frac{\Gamma}{2} \tag{34}$$

It would be more accurate to allow $\Gamma(\rho)$ to vary from this value at the limiting density ratio to the value $2S - 1$ at normal density,[16] perhaps in a linear fashion

$$\Gamma(\rho) = 2s-1 - (s-1)\left(\frac{\rho}{\rho_0} - 1\right) \tag{35}$$

but for purposes of convenience, the constant value $\Gamma = 2S - 2$ has been used throughout the analysis that follows.

With this specification, the final form of the state equation used below is

$$\frac{e - e_0}{c^2} = \frac{p/\rho_0 c^2}{2(s-1)\rho/\rho_0} - \frac{1}{2(s-1)} \frac{\frac{\rho}{\rho_0} - 1}{s - (s-1)\rho/\rho_0} \tag{36}$$

This representation has the advantage of generality. It shows that the equation-of-state data for a large number of materials can be correlated in terms of the dimensionless pressure $p/\rho_0 c^2$, density ρ/ρ_0 , and specific internal energy $\frac{e - e_0}{c^2}$, with only S remaining as a parameter.[*] Figure 2 is a plot of this equation for the cases $S = 2$ and $S = 1.5$. The qualitative resemblance to the specific state equation of iron used in Bjork's calculations (see Fig. 1 of Ref. 18) is obvious. Figure 2 shows the Hugoniot, which can be found from

$$\frac{e_H - e_0}{c^2} = \frac{1}{2} \frac{\left(\frac{\rho_H}{\rho_0} - 1\right)^2}{\left[s - (s-1)\rho_H/\rho_0\right]^2} \quad ; \quad \frac{p_H}{\rho_0 c^2} = \frac{\frac{\rho_H}{\rho_0}\left(\frac{\rho_H}{\rho_0} - 1\right)}{\left[s - (s-1)\rho_H/\rho_0\right]^2} \tag{37}$$

as well as a number of isentropes, about which more will be said below.

_____

[*] The fact that the internal energy scales with c^2 can be used to estimate how much the Hugoniot is changed by heating a target, such as a heated radiator tube, for example. Changes in e_0 due to heating are given by $C_v \Delta T$. Even for a temperature rise of 1000°K, $C_v \Delta T / c^2$ is on the order of a few percent. Thus the shock-wave properties of a given material are not appreciably altered by heating it, and it might be expected that changes in impact damage in heated targets are due mainly to the effects of temperature on strength.

The Hugoniot conditions can also be written conveniently in terms of the shock Mach number $M = u_s/c$. A few values of M are shown on Fig. 2. The corresponding values of pressure, density, internal energy, and particle velocity are

$$\frac{\rho_H}{\rho_0} = \frac{sM}{1 + (s-1)M} \tag{38}$$

$$\frac{e_H - e_0}{c^2} = \frac{(M-1)^2}{2s^2} \tag{39}$$

$$\frac{p_H}{\rho_0 c^2} = \frac{M(M-1)}{s} \tag{40}$$

$$\frac{u_1}{c} = \frac{M-1}{s} \tag{41}$$

The representation afforded by Eq. (36) ceases to be valid in the limit of extremely high pressures, where the linear u_s, u_1 relation no longer holds. As noted below, Eq. (36) is also incorrect at low pressures. It is, however, a simple and useful approximation in the intermediate range of pressures -- i. e. , in the range where the approximation of Eq. (30) is appropriate.

D. Isentropes; Low-Pressure Behavior

Along an isentrope, the relation

$$\frac{de}{d\rho} = \frac{p}{\rho^2} \tag{42}$$

AI-1821-A-2

together with the general form of the Mie-Grüneisen relation, gives the following linear differential equation

$$\frac{d}{d\rho} (e - e_0) - \frac{\Gamma(\rho)}{\rho} (e - e_0) = \frac{\Gamma(\rho) \Delta(\rho)}{\rho} \tag{43}$$

whose solution is

$$(e - e_0) \exp\left[-\int \frac{\Gamma}{\rho} d\rho\right] = const + \int \frac{\Gamma(\rho)\Delta(\rho)}{\rho} \exp\left[-\int \frac{\Gamma(\rho)d\rho}{\rho}\right] d\rho \tag{44}$$

For the special case of a C, S medium, taking $\Gamma = 2(S - 1)$ and using

$$\frac{\Delta(\rho)}{c^2} = \frac{1}{2(s-1)} \frac{\frac{\rho}{\rho_0} - 1}{s - (s-1)\rho/\rho_0} \tag{45}$$

the equation for the isentropes is found to be

$$\frac{e - e_0}{c^2} = \left(\frac{\rho}{\rho_0}\right)^{2(s-1)} \left\{\frac{\hat{e}}{c^2} + D\left(\frac{\rho}{\rho_0}; s\right)\right\} \tag{46}$$

where

$$D\left(\frac{\rho}{\rho_0}; s\right) = \int_1^{\rho/\rho_0} \frac{(\sigma - 1) d\sigma}{\sigma^{2s-1} \left[s - (s-1)\sigma\right]} \tag{47}$$

Equation (46) defines the isentrope passing through the point $\frac{e - e_0}{c^2} = \frac{\hat{e}}{c^2}$, $\frac{\rho}{\rho_0} = 1$. The constant $\hat{e}/c^2$ can be evaluated in terms of conditions along the Hugoniot; an isentrope starting from the point $\frac{e_H - e_0}{c^2}$, ρ_H/ρ_0 will have

$$\frac{\hat{e}}{c^2} = \left(\frac{\rho_H}{\rho_0}\right)^{-2(s-1)} \frac{e_H - e_0}{c^2} - D\left(\frac{\rho_H}{\rho_0}; s\right) \tag{48}$$

The function D can be evaluated explicitly whenever $2S-1$ is an integer. In particular

$$D\left(\frac{p}{p_0}; 1\right) = \frac{p}{p_0} - 1 - \ell n \frac{p}{p_0}$$

$$D\left(\frac{p}{p_0}; 1.5\right) = \frac{2}{3 p/p_0} - \frac{2}{3} - \frac{4}{9} \ell n \frac{3 - p/p_0}{2 p/p_0}$$
(49)

$$D\left(\frac{p}{p_0}; 2\right) = \frac{-1}{4 p/p_0} + \frac{1}{4(p/p_0)^2} - \frac{1}{8} \ell n \frac{2 - p/p_0}{p/p_0}$$

At low density, the function D is approximately:

$$D \simeq \frac{1}{S} \int_{p/p_0}^{1} \frac{d\sigma}{\sigma^{2S-1}} = \frac{1}{2S(S-1)} \frac{1}{(p/p_0)^{2(S-1)}}$$
(50)

Thus, all isentropes converge toward the value

$$\frac{e - e_0}{c^2} \longrightarrow \frac{1}{2S(S-1)} \quad as \quad \frac{p_1}{p_0} \longrightarrow 0$$
(51)

Since, in the same limit

$$\frac{\Delta}{c^2} \longrightarrow \frac{-1}{2S(S-1)}$$
(52)

it follows that $p/p_0 c^2$ also approaches zero along an isentrope. In fact, it is clear from Eq. (35) that $p/p_0 c^2$ approaches zero more rapidly than does p/p_0 .

The C , S form of the state equation derived in Eq. (36) is based on the linear approximation to the u_s , u_1 Hugoniot, and applies only when $p_1 \gg p_0$. Thus, it must be viewed with suspicion when p/p_0 becomes even as low as unity, to say nothing of the limit $\frac{p}{p_0} \longrightarrow 0$. One of the most serious deficiencies of Eq. (36) at low density is that negative

pressures are encountered along the isentropes. For example, when $S = 2$, the p and e coordinates of an isentrope are given by (defining $\psi \equiv P/\rho_0$)

$$\frac{p}{\rho_0 c^2} = -\frac{\psi^2}{4} + \frac{\psi^3 \ln \psi}{4} + 2\psi^3 \left(\frac{\hat{e}}{c^2} - \frac{\ln 2}{8} + \frac{1}{16} \right) + O(\psi^4) \qquad (53)$$

and

$$\frac{e - e_0}{c^2} = \frac{1}{4} - \frac{\psi}{4} + \frac{\psi^2 \ln \psi}{8} + \left(\frac{\hat{e}}{c^2} - \frac{\ln 2}{8} \right) \psi^2 + \frac{\psi^3}{16} + O(\psi^4) \qquad (54)$$

Figure 3 shows the low-density behavior, for $S = 2$, of isentropes start-
ing from density ratios at the shock of 1.2, 1.4, and 1.8. For the lower
entropy states (lower values of ψ_H) the negative pressures are encoun-
tered at higher density.

Usually, the negative pressures themselves can be tolerated, espec-
ially if they comprise only a small part of an otherwise high-pressure
solution. Their effect is often more serious, however, in that they may
lead to imaginary values of the sound speed. The square of the speed of
sound, equal to the slope of the curves in Fig. 3, is negative over a rather
wide range for the two lower-pressure isentropes shown.

In the analysis below, Eq. (36) is used for all values of ρ , in
spite of its improper behavior at low density. The justification for use of
such a model lies chiefly in the fact that the low-density states have no
appreciable effect on quantities such as the shock trajectory. Furthermore,
even if their effect were appreciable, it would be very difficult to select
a more accurate model. The states reached by a shocked material when

it is expanded to low pressure are understood far less fully than are the corresponding high-pressure states. If the material is completely vaporized, it may be possible to treat it as a perfect gas, but in other regimes, processes such as condensation render such an approximation invalid.

It is reasonable to expect that the shock-propagation solutions are insensitive to the low-density portions of the equation of state only for the semi-infinite-target problem, because most of the mass is concentrated in the high-pressure region near the shock, where the equation of state is valid. Since only a very small fraction of the total mass is described by the low-density portion of the state equation, the over-all error in quantities such as the shock trajectory is quite small.

The situation is not nearly as favorable in the case of the thin-plate perforation problem. There, the momentum distribution of the material ejected from the rear surface of the plate is an item of central interest. In predicting such a distribution, the mass and velocity acquired upon expansion to low pressure must be known accurately, and they may depend, in a sensitive manner, on the precise form used for the equation of state. It is noteworthy, in this connection, that most theoretical treatments of the thin-plate problem (see Ref. 19, for example) make use of the perfect-gas approximation.

Negative pressures are present in the state equations used for some of the computer solutions of hypervelocity impact. Riney,[20] for example, extends the state equation into the tensile regime by use of the formula

$$p = (\psi - 1)\left(\frac{\partial f}{\partial \psi}\right)_{\psi=1} + f\bigg)_{\psi=1} \quad , \quad \psi < 1 \tag{55}$$

where $p = f(\psi, e)$ is the state equation used for $\psi > 1$. The equation of state for iron used by Bjork[2] also predicts negative pressures. Whether the same remark applies to his calculations in aluminum[1] is uncertain, since the state equation used in those calculations has apparently not been published.

Walsh and his coworkers make use of a low-density equation presented by Tillotson[17] in which the pressure is expressed as the sum of a perfect-gas term plus a correction which vanishes exponentially as the density goes to zero. The boundary along which the state equation is changed from the condensed-state form to the expanded-state form has been slightly changed in recent work[4] from that used in previous publications.[3,17] In both formulations, it is possible to encounter negative pressures. Shanfield, Lee, and Bach,[21] for example, have recently found negative pressures in aluminum when applying Tillotson's formulation.

Figure 4 indicates the magnitude of the negative pressures that may be encountered. Shown here are the pressure-density states through which an iron particle passes after being compressed to twice normal density, according to the equations employed by Tillotson, Bjork, and Riney, and also according to the present formulation (Eq. (36)) using $S = 1.59$, $\rho_o c^2 = 1.259$ megabars. For convenience, the actual equations used are collected in Appendix A.

The fact that no difficulty caused by these negative pressures has ever been reported indicates that calculations in a semi-infinite target can safely be made. That such errors in the state equation can be tolerated in the thin-plate problem is much less likely.

E. Sound Speed and Temperature

As a final note on the thermodynamic properties of a c, s medium, it is of interest to calculate the sound speed and temperature field. The most convenient expression to use for the former is

$$a^2 = \left(\frac{\partial p}{\partial \rho}\right)_s = \frac{\frac{p}{\rho^2} - \left(\frac{\partial e}{\partial \rho}\right)_p}{\left(\frac{\partial e}{\partial p}\right)_\rho} \tag{56}$$

Use of Eq. (36) leads, after a little algebra, to the expression

$$\frac{a^2}{c^2} = (2s-1)\frac{p/\rho_0 c^2}{\rho/\rho_0} + \frac{\rho/\rho_0}{\left[s - (s-1)\rho/\rho_0\right]^2} \tag{57}$$

The temperatures reached by a compressed solid have been calculated in a number of different ways (see, for example, Refs. 22, 23, 24). Since a general form of the equation of state is being employed here, it is of interest to inquire whether the associated temperature field can be determined with a comparable degree of generality. For this purpose, the method advanced by Walsh and Christian in Ref. 24 is especially convenient. These authors determined the temperatures along the Hugoniot from the relation

$$\int_{s_0}^{s_1} \left[T\,ds\right]_{\substack{\text{along the}\\\text{Hugoniot}}} = e_1 - e_0 + \int_{v_0}^{v_1} \left[p\,dv\right]_{\substack{\text{along the}\\\text{Hugoniot}}}$$

$$= \frac{p_1 + p_0}{2}(v_0 - v_1) + \int_{v_0}^{v_1}\left[p\,dv\right]_{\text{Hug.}} \tag{58}$$

where $v = 1/\rho$ is the specific volume, and where the integration is carried out along the Hugoniot. On this path, the right-hand side of (58)

is known, and is, in fact, a function only of v_1 . Differentiating with respect to v_1 gives

$$\frac{d}{dv_1}\int_{s_o}^{s_1}\left[T ds\right]_{Hug.} = \frac{v_0 - v_1}{2}\frac{dp_1}{dv_1} + \frac{p_1 - p_0}{2} \tag{59}$$

An independent relation for the left-hand side of this equation can be found from

$$T ds = C_v \, dT + \left(\frac{\partial p}{\partial T}\right)_v T \, dv \tag{60}$$

Integrating along the Hugoniot, and differentiating with respect to v_1 gives

$$\frac{d}{dv_1}\int_{s_o}^{s_1}\left[T ds\right]_{Hug.} = C_v\frac{dT_1}{dv_1} + \left(\frac{\partial p}{\partial T}\right)_v T_1 \tag{61}$$

Equating (59) to (61) produces a linear differential equation for T_1

$$C_v\frac{dT_1}{dv_1} + \left(\frac{\partial p}{\partial T}\right)_v T_1 = f(v_1) \tag{62}$$

where

$$f(v) = \frac{1}{2}\frac{dp}{dv}(v_0 - v) + \frac{1}{2}(p_1 - p_0) \tag{63}$$

Assuming that C_v and $\left(\frac{\partial p}{\partial T}\right)_v$ are constants, the solution is

$$T_1(v_1) = T_0 \exp\left[b(v_0 - v_1)\right] + \exp\left[-b v_1\right]\int_{v_0}^{v_1}\left[\frac{f(v)\,e^{bv}}{C_v}\right]_{Hug.} dv \tag{64}$$

where the parameter b is related to the Grüneisen parameter at normal density, i.e.,

$$b = \frac{\left(\partial p/\partial T\right)_v}{C_V} = \rho_o \Gamma(\rho_o) \quad , \quad \text{since} \quad \Gamma = \frac{1}{\rho}\left(\frac{\partial p}{\partial e}\right)_\rho = \frac{1}{\rho C_V}\left(\frac{\partial p}{\partial T}\right)_\rho \tag{65}$$

Along the Hugoniot of a C, S medium

$$p_1 - p_o = \rho_o c^2 \frac{\frac{\rho}{\rho_o}\left(\frac{\rho}{\rho_o} - 1\right)}{\left[s - (s-1)\rho/\rho_o\right]} \tag{66}$$

A little algebra shows that

$$\frac{dp}{dv} = \rho_o^2 c^2 \psi^2 \frac{s - (s+1)\psi}{\left[s - (s-1)\psi\right]^3} \quad ; \quad f(v) = -s\rho_o c^2 \frac{\psi(\psi-1)^2}{\left[s - (s-1)\psi\right]^3} \tag{67}$$

where $\psi = \rho/\rho_o$. Substituting these into Eq. (64) leads to

$$\frac{T_H}{T_o} = \exp\left\{\frac{b}{\rho_o}\left(1 - \frac{1}{\psi_H}\right)\right\} + \frac{sc^2}{C_V T_o} G\left(\psi_H ; s, \frac{b}{\rho_o}\right) \tag{68}$$

where

$$G\left(\psi_H ; s, \frac{b}{\rho_o}\right) = \exp\left\{-\frac{b}{\rho_o \psi_H}\right\} \int_1^{\psi_H} \frac{\sigma(\sigma-1)^2 \exp\left(\frac{b}{\rho_o \sigma}\right)}{\left[s - (s-1)\sigma\right]^3} \frac{d\sigma}{\sigma^2} \tag{69}$$

It is clear from this analysis that the temperatures along the Hugoniot are controlled by the Grüneisen factor $\frac{b}{\rho_o}$, and by the characteristic temperature c^2/C_V . The values of these parameters given by Walsh and Christian[24] for Aluminum, Zinc, and Copper are listed in the table below.

Material	$\rho_0, \frac{gm}{cm^3}$	$C_v, \frac{ergs}{gm-K}$	$\left(\frac{\partial p}{\partial T}\right)_v, \frac{dynes}{cm^2-°K}$	$\frac{c^2}{c_v}, °K$	$\frac{b}{\rho_0}$
24ST Aluminum	2.785	$.92 \times 10^7$	50.6×10^6	37,000	1.97
Zinc	7.14	$.397 \times 10^7$	70×10^6	23,300	2.46
Copper	8.903	$.390 \times 10^7$	75.5×10^6	40,600	2.17

Having the temperatures along the Hugoniot, the temperature at any other state can now be determined by finding how the temperature falls along an isentrope. This relationship has been given by a number of authors (see Ref. 16, for example), and is rederived in an alternate way in Appendix B. It has the form

$$\frac{T}{T_H} = exp\left[- \int_\rho^{\rho_H} \frac{\Gamma(\rho)\, d\rho}{\rho} \right] \qquad (70)$$

For the particular case of a C, S medium, this takes the simple form

$$\frac{T}{T_H} = \left(\frac{\rho}{\rho_H}\right)^{2(s-1)} \qquad (71)$$

It is interesting that this expression has the same form as that of a perfect gas of constant specific-heat ratio γ

$$\frac{T}{T_H} = \left(\frac{\rho}{\rho_H}\right)^{\gamma-1} \qquad (72)$$

in spite of the presence of the term $\Delta(\rho)$.

F. <u>Comparison with Enig's Formulation</u>

Enig[25] has recently derived an analytical formulation of the equation of state of a C, S medium by pursuing the logical consequences of

the "mirror image" approximation. This approximation assumes that the pressures and particle speeds experienced by a particle in a planar isentropic expansion wave are mirror images of the Hugoniot curve:
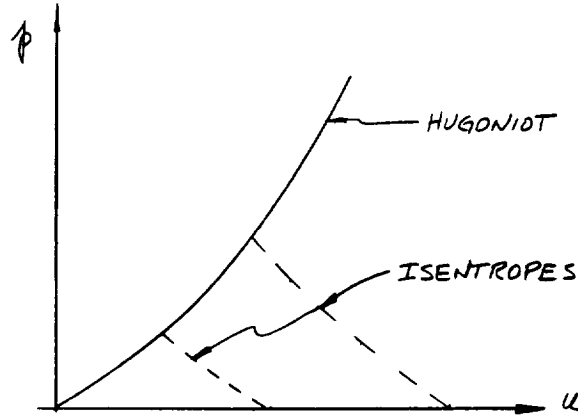
This approximation is consistent with another well-established approximation that the free-surface velocity acquired by isentropic expansion from a point on the Hugoniot is twice the particle speed on the Hugoniot.[24] Enig noted that the "mirror-image" assumption implies an equation of state, and found a closed-form expression for this equation for the case of a C, S medium. In the present notation, Enig's result is

$$4s^2 \frac{e-e_0}{c^2} = \frac{s\phi}{\rho_0 c^2} + s\left(\frac{\rho_0}{\rho} - 1\right) + \oint\left(\Psi\right)$$ (73)

where

$$\Psi = \left(1 + 4\frac{s\phi}{\rho_0 c^2}\right) exp\left[4s\left(\frac{\rho_0}{\rho} - 1\right)\right]$$ (74)

and where the functional dependence of $\oint$ on Ψ is given parametrically by

$$\Psi = (2z + 1)^2 exp\left[-\frac{4z}{1+z}\right] \quad ; \quad \oint = \frac{z^3}{1+z}$$ (75)

This equation of state is shown in Fig. 5. It is noteworthy that only the parameters $S\dfrac{p}{\rho_0 c^2}$, $S\left(\dfrac{\rho_0}{\rho}-1\right)$, and $S^2\dfrac{e-e_0}{c^2}$ appear. There is no other dependence on the parameter S .

Enig goes on to calculate the temperature, using the assumption that the thermal coefficient of volume expansion at low pressure is constant. The resulting specific heat at constant pressure exhibits a rather singular behavior at low pressure, indicating that a satisfactory state equation cannot be derived under the simultaneous assumption of the mirror-image approximation, the linear U_s , U_1 relation, and the constancy of the thermal coefficient of volume expansion at low pressure. The formulation involving only e , p , and ρ is perfectly satisfactory, however, and can be used in its present form if one is willing to dispense with its temperature predictions at low pressure.

The present form of the Mie-Grüneisen equation does not recover the mirror-image approximation. To illustrate this, calculations were made, for $S = 2$, of the free-surface velocity acquired by a shocked particle. Along an isentrope, $dp = -\rho a\,du$, or

$$\frac{U_{FS}}{c} = \int_0^{p_H/\rho_0 c^2} \frac{d\left(p/\rho_0 c^2\right)}{\dfrac{\rho}{\rho_0}\dfrac{a}{c}} + \frac{U_1}{c} \tag{76}$$

where subscript FS stands for free surface, and where the sound speed is given by Eq. (57). Because of the improper behavior of the present formulation at low pressure, the sound speed is imaginary over an appreciable range of pressure, as shown in the sketch below.

$$\frac{p}{\rho_0 c^2}$$

$a^2 < 0$ in this range

$\rho = const$

A

$-\rho/\rho_0$
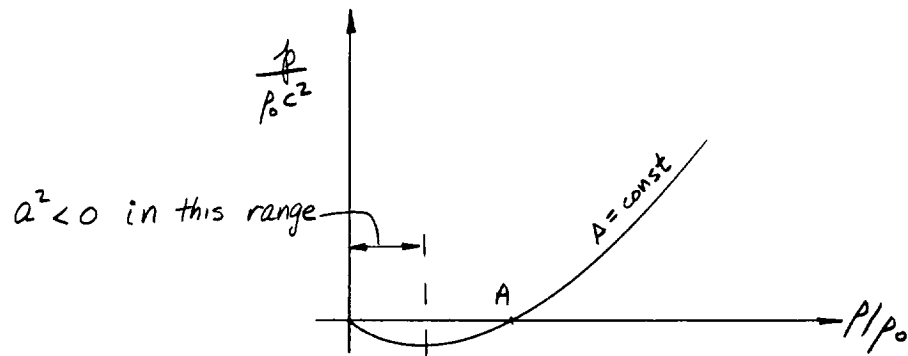
If the integration is started at the point A, the results are as follows

ρ_H/ρ_0	u_s/c	u_1/c	u_{FS}/u_1
1. 8	9	4	3. 04
1. 4	7	2/3	2. 10

The principal contributions to the integral in Eq. (76) come from the low-density range. It is clear from these results that the present formulation would be quite inadequate for any study (such as the thin-plate problem) where low-density behavior is important. It also serves to indicate that caution must be used in interpreting results from computer solutions whose low-density state equations allow negative pressures.

III. METHODS OF NONSIMILAR SOLUTION

This section describes three approximate analytical methods that have been used for predicting some of the features of the flow patterns set in motion by hypervelocity impact. The objective of these solution methods is to produce simple formulae for the location and strength of the main shock wave, and for some of the details of the flow pattern behind the shock. None of the three methods uses a similarity assumption, and thus their success is measured by their ability to achieve maximum accuracy with minimum complexity, by making the proper approximation.

It should be emphasized that the only class of problem considered is that for which the projectile may be represented by a point disturbance. Thus, the analysis will not be valid for greatly elongated projectiles. Moreover, even for cubic or spherical projectiles, the analysis only applies when the scale of the disturbance is large compared with the scale of the projectile.

A. Oshima's Method

The literature of blast waves in gases contains a number of analytic methods for dealing with the nonsimilar effect. Notable among these are perturbation methods, explored by Sakurai,[26] among others. Such perturbation methods, which describe the first-order departure from similarity, have been applied, for example by Kochina,[27] to shock propagation in condensed media. Another method, due to Oshima,[6,28] offers the possibility of a wider range of validity than that of the perturbation techniques, for a comparable expenditure of effort. Furthermore, the method, developed originally to handle nonsimilarity arising from counterpressure

p_0 in the perfect-gas case, can easily be adapted to handle that result-
ing from the equation of state in the present case.

The first of the subsections that follow contains a review of
Oshima's technique for the perfect-gas case, together with a few addi-
tional features not explicitly mentioned in his original paper. The second
section below then presents the application of Oshima's technique to the
case of shock propagation in a C, S medium.

1. Review of the Perfect-Gas Case

a) General Analysis

Consider the case of a symmetric flow, where the index ν is 0
for the planar case, 1 for the cylindrical case, and 2 for the spherical
case. Oshima begins by making the change of independent variables from
r and t to η and $R_s(t)$. Thus the Euler equations become

$$(\phi - \eta)\frac{\partial \psi}{\partial \eta} + \psi \left(\frac{\partial \phi}{\partial \eta} + \nu \frac{\phi}{\eta}\right) = -R_s \frac{\partial \psi}{\partial R_s} \tag{77}$$

$$\frac{R_s \ddot{R}_s}{\dot{R}_s^2} \phi + (\phi - \eta)\frac{\partial \phi}{\partial \eta} + \frac{1}{\psi}\frac{\partial f}{\partial \eta} = -R_s \frac{\partial \phi}{\partial R_s} \tag{78}$$

$$2\frac{R_s \ddot{R}_s}{\dot{R}_s^2} g + (\phi - \eta)\frac{\partial g}{\partial \eta} - \frac{f}{\psi^2}(\phi - \eta)\frac{\partial \psi}{\partial \eta} = \tag{79}$$

$$= -R_s \frac{\partial g}{\partial R_s} + \frac{f}{\psi^2} R_s \frac{\partial \psi}{\partial R_s}$$

These equations contain no approximations beyond those implied by use of an inviscid fluid. The terms on the right-hand sides come from the time derivatives in the original equations, and represent the change in the dependent variables with respect to the scale R_s of the disturbance. For the case of a perfect gas, where

$$q = \frac{f}{(\gamma-1)\psi} \tag{80}$$

the energy equation becomes

$$2\frac{R_s \ddot{R_s}}{\dot{R_s}^2} f + (\phi - \eta)\left\{\frac{\partial f}{\partial \eta} - \frac{\gamma f}{\psi}\frac{\partial \psi}{\partial \eta}\right\} = -R_s\left\{\frac{\partial f}{\partial R_s} - \frac{\gamma f}{\psi}\frac{\partial \psi}{\partial R_s}\right\} \tag{81}$$

The boundary conditions at the shock can be written conveniently in terms of the shock Mach number M

$$M = \dot{R_s}/c_o \tag{82}$$

where the sound speed ahead of the shock, c_o, is

$$c_o^2 = \frac{\gamma p_o}{\rho_o} \tag{83}$$

In terms of M, the Rankine-Hugoniot conditions for a perfect gas are

$$\phi(1, R_s) = \frac{2}{\gamma+1}\left(1 - \frac{1}{M^2}\right)$$

$$f(1, R_s) = \frac{2}{\gamma+1} - \frac{\gamma-1}{\gamma(\gamma+1)M^2} \tag{84}$$

$$\psi(1, R_s) = \frac{(\gamma+1)M^2}{(\gamma-1)M^2 + 2}$$

At this point, a similarity solution would require three steps. First, derivatives with respect to R_s must be assumed to vanish. Second, the combination $R_s \ddot{R}_s / \dot{R}_s^2$ must be assumed constant, which implies that $R_s \sim t^N$. Finally, the shock Mach number must be taken to be large, so that M^{-2} is small compared to unity.

Oshima uses the notation

$$\frac{R_s \ddot{R}_s}{\dot{R}_s^2} = \frac{d \ln \dot{R}_s}{d \ln R_s} = -\frac{1-N}{N} \tag{85}$$

The value of N is not assumed to be constant, however, as it would in a similarity solution, but is permitted to vary with $R_s(t)$. The next step is to approximate the derivatives with respect to R_s. This is done by first replacing these derivatives by derivatives with respect to the shock Mach number, and by then approximating the result. If $\mathcal{Y}$ stands for either ϕ, f, or ψ, the final form is

$$R_s \frac{\partial \mathcal{Y}}{\partial R_s} = R_s \frac{\partial \mathcal{Y}}{\partial \dot{R}_s} \frac{d \dot{R}_s}{d R_s} = -\frac{1-N}{N} \dot{R}_s \frac{\partial \mathcal{Y}}{\partial \dot{R}_s} = -\frac{1-N}{N} M \frac{\partial \mathcal{Y}}{\partial M} \tag{86}$$

using the definition given in Eq. (85). The problem is thus converted into one of approximating $\partial \mathcal{Y} / \partial M$. (It is possible, of course, to proceed to this point directly from the basic partial differential equations, by using η and M as independent variables.)

The essential feature of Oshima's method is his approximation for $\partial \mathcal{Y} / \partial M$, namely

$$\left. \frac{\partial \mathcal{Y} / \partial M}{\mathcal{Y}} \right)_{\text{any value of } \eta} = \left. \frac{\partial \mathcal{Y} / \partial M}{\mathcal{Y}} \right)_{\eta = 1} \tag{87}$$

The Rankine-Hugoniot conditions can be used to evaluate the right-hand side. Using (87), Oshima has, in general

$$R_s \frac{\partial \mathcal{J}}{\partial R_s} = - \frac{1-N}{N} M \frac{\left(\frac{\partial \mathcal{J}}{\partial M}\right)_{\eta=1}}{\mathcal{J}(1)} \mathcal{J}(\eta, M) \qquad (88)$$

Note that the right-hand side depends only on η , with M as a parameter. Thus the equations of motion have been reduced to a set of ordinary differential equations, which are found, after a little algebra, to be

$$(\phi - \eta) \psi' + \psi \left(\phi + \eta \frac{\phi}{\eta}\right) = \frac{1-N}{N} \frac{4}{2+(\gamma-1)M^2} \psi \qquad (89)$$

$$- \frac{1-N}{N} \phi + (\phi - \eta) \phi' + \frac{f'}{\psi} = 2 \frac{1-N}{N} \frac{\phi}{M^2-1} \qquad (90)$$

$$-2\frac{1-N}{N} f + (\phi - \eta)\left\{f' - \frac{\gamma f}{\psi} \psi'\right\} = \frac{1-N}{N} \left\{\frac{2(\gamma-1)}{2\gamma M^2 - (\gamma-1)} - \frac{4\gamma}{2+(\gamma-1)M^2}\right\} f \qquad (91)$$

These equations differ from those of the similarity analysis by the presence of the parameter M . For $M \rightarrow \infty$, they reduce to the self-similar relations which were first derived and solved numerically by G. I. Taylor.[29]

Equations (89) to (91) can be solved for the derivatives in the form

$$\psi' = \frac{(\phi - \eta) R_1 + R_3 - \psi R_2}{(\phi - \eta)^2 - \gamma f/\psi} \qquad (92)$$

$$\phi' = \frac{(\phi - \eta)R_2 - \frac{\gamma f}{\psi^2}R_1 - \frac{(\phi - \eta)}{\psi}R_3}{(\phi - \eta)^2 - \gamma f/\psi} \qquad (93)$$

$$f' = \frac{(\phi - \eta)^2 R_3 - \gamma f R_2 + \frac{\gamma f}{\psi}(\phi - \eta)R_1}{(\phi - \eta)^2 - \gamma f/\psi} \qquad (94)$$

where

$$R_1 = \frac{1-N}{N} \frac{4}{2+(\gamma-1)M^2} \psi - \gamma \frac{\psi\phi}{\eta} \qquad (95)$$

$$R_2 = \frac{1-N}{N} \frac{M^2+1}{M^2-1} \phi \qquad (96)$$

$$R_3 = \frac{1-N}{N} \left\{ 2 + \frac{2(\gamma-1)}{2\gamma M^2 - (\gamma-1)} - \frac{4\gamma}{2+(\gamma-1)M^2} \right\} \frac{f}{\phi - \eta} \qquad (97)$$

For a given value of γ , these equations must be solved anew for each value of M . In doing so, the value of N for each given value of M must be chosen. Oshima points out in his original article that, for each M , there is only one value of N which produces a solution free of singularities. When N differs from this value, the solution encounters one of two singularities, because either $(\phi - \eta)^2 - \gamma f/\psi$ or $\phi - \eta$ vanishes. The existence of a single value of N leading to a

regular solution has been demonstrated both by Oshima's own calcula-tions for $\eta = 1$, [6] and also by some more accurate calculations of Lewis[30] for $\eta = 0, 1, 2$. Both these authors terminate the integration at a small, nonzero value of η , which they refer to as the core radius. The value of $N(M)$ which they find varies from the classical strong-blast limit of $2/\eta+3$ at $M = \infty$, to the value $N = 1$ at $M = 1$, consistent with the fact that the shock expands like a strong blast wave at first, and ultimately decays to a sound wave, for which $R_s \sim t$.

The distributions of pressure and density found by Oshima's method for $\eta = 2$ bear a strong resemblance to the results of machine solu-tions of the full partial differential equations. Lewis' results,[30] for ex-ample, can be compared with the correlated numerical solutions shown by Sedov (Ref. 15, pp. 246-248). The velocity distribution is not nearly as well recovered, however; the Oshima result has u always positive, whereas the numerical result shows both positive and negative regions. The more gross properties of the solution, such as the predicted shock trajectory, agree well with machine solutions, and also with experiment.

In order to determine the shock trajectory, the conservation of total energy is used

$$E = \sigma_{\eta} \int_0^{R_s} \left(e - e_o + \tfrac{1}{2} u^2 \right) r^{\eta} \rho \, dr$$

(98)

$$= \sigma_{\eta} R_s^{\eta+1} \gamma p_o \left(\frac{\dot{R}_s}{c_o} \right)^2 I \left(\frac{\dot{R}_s}{c_o} ; \gamma \right) - \frac{\sigma_{\eta}}{\eta+1} \frac{p_o}{(\gamma-1)} R_s^{\eta+1}$$

where

$$ I = \int_0^1 \left(\frac{f}{(\gamma-1)\psi} + \tfrac{1}{2}\phi^2 \right) \psi \eta^\nu d\eta \qquad (99) $$

and

$$ \sigma_\nu = 2,\ 2\pi,\ 4\pi \qquad for \quad \nu = 0, 1, 2 \qquad (100) $$

The constant E has the dimensions of energy, energy per unit length, or energy per unit area, according as ν = 2, 1, or 0. Equation (98) can be written in a form valid for any E and p_0

$$ \frac{R_s}{R_0} = \left\{ \gamma M^2 I(M;\gamma) - \frac{1}{(\nu+1)(\gamma-1)} \right\}^{-1/(\nu+1)} \qquad (101) $$

where, as in all explosion problems,[31] the scaling length depends on the energy release divided by the characteristic pressure in the medium

$$ R_0 = \left(\frac{E}{\sigma_\nu p_0} \right)^{1/(\nu+1)} \qquad (102) $$

Once the shock radius-shock speed relation is known, the shock trajectory is found from the identity

$$ \frac{c_0 t}{R_0} = \int_0^{R_s/R_0} \frac{1}{M} d\left(\frac{R_s}{R_0} \right) \qquad (103) $$

b) Qualitative Nature of the Flow

The role played by the singularities of Eqs. (92) to (94) and the general nature of the flow they define can be seen by rewriting the equations in the (x, y) coordinate system used by Sedov:[15]

$$x = \frac{N\phi}{\eta} \qquad y = \frac{N^2}{\eta^2}\frac{\gamma f}{\psi} \qquad (104)$$

In terms of these variables, the equations of motion can be written in the form

$$\frac{d \ln \psi}{d \ln \eta} = \frac{(x-N)F_1 + F_3/\gamma - F_2}{(x-N)^2 - y} \qquad (105)$$

$$\frac{dx}{d \ln \eta} = \frac{(x-N)F_2 - yF_1 - (x-N)F_3/\gamma}{(x-N)^2 - y} \qquad (106)$$

$$\frac{dy}{d \ln \eta} = \frac{\left[(x-N)^2 - y/\gamma\right]F_3 - (\gamma-1)yF_2 + (\gamma-1)y(x-N)F_1}{(x-N)^2 - y} \qquad (107)$$

where the functions F_1 , F_2 , and F_3 depend only on x and y

$$F_1 = -(\gamma+1)x + \frac{4(1-N)}{2+(\gamma-1)M^2} \qquad (108)$$

$$F_2 = -x(x-N) + (1-N)\frac{M^2+1}{M^2-1}x - \frac{2y}{\gamma} \qquad (109)$$

$$F_3 = \frac{y}{x-N}\left\{(1-N)\left[2 + \frac{2(\gamma-1)}{2\gamma M^2-(\gamma-1)} - \frac{4\gamma}{2+(\gamma-1)M^2}\right] - 2(x-N)\right\} \qquad (110)$$

The use of the Sedov variables achieves the same result here as it does in the similarity limit, namely, the variable γ does not appear explicitly. Thus, by dividing Eq. (107) by (106), a single differential equation for dy/dx as a function of x and y can be derived, and is useful in any detailed study of the singularities of this set of equations. The boundary values at the shock are

$$X_s = \frac{2N}{\gamma+1}\left(1 - \frac{1}{M^2}\right) \ , \quad y_s = \frac{\gamma-1}{\gamma+1}\gamma N^2\left(\frac{2}{\gamma+1} - \frac{\gamma-1}{(\gamma+1)\gamma M^2}\right)\left(1 + \frac{2}{(\gamma-1)M^2}\right) \quad (111)$$

The singularities of this system of equations occur at the points $x - N = 0$ and $(x-N)^2 - y = 0$. A plot of the solutions found by Lewis[30] for a typical Mach number and for various values of N has the appearance:
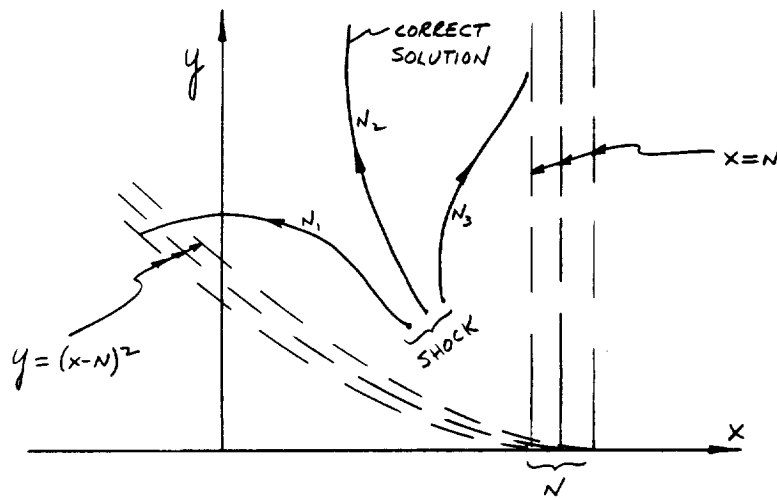
For values of N different from that which gives $\phi(o) = 0$, the solution encounters one of the singular lines, as shown in the sketch.

The nature of the flow is the same as that of the similarity solution[18] $(M = \infty)$. The quantity $(x-N)^2 - y$ always remains negative, approaching $-\infty$ as $\gamma \to 0$.

c) A First Integral

The similarity equations ($M=\infty$) have a first integral, that has been derived, among others, by Lees and Kubota.[32] The quasi-similar equations have an analogous integral. It can be derived by writing the basic equations in the form

$$(\phi - \eta)\psi' + \psi\left(\phi' + \vartheta\frac{\phi}{\eta}\right) = H_1\psi \tag{112}$$

$$(\phi - \eta)\phi' + \frac{f'}{\psi} = H_2\phi \tag{113}$$

$$(\phi - \eta)\left(f' - \frac{\gamma f}{\psi}\psi'\right) = H_3 f \tag{114}$$

where

$$H_1 = \frac{1-N}{N}\frac{4}{2+(\gamma-1)M^2} \tag{115}$$

$$H_2 = \frac{1-N}{N}\frac{M^2+1}{M^2-1} \tag{116}$$

$$H_3 = \frac{1-N}{N}\left\{2 + \frac{2(\gamma-1)}{2\gamma M^2 - (\gamma-1)} - \frac{4\gamma}{2+(\gamma-1)M^2}\right\} \tag{117}$$

If (112), divided by $\psi(\phi-\eta)$, is added to (114) divided by $H_3 f(\phi-\eta) \big/ (1+\vartheta - H_1)$, the resulting equation can be integrated, to give

$$\psi^{1-\alpha\gamma} f^{\alpha} |\phi-\eta| |\eta|^{\nu} = const \tag{118}$$

where

$$\alpha = \left(1+\nu- H_1\right) \big/ H_3 \tag{119}$$

The same first integral has also been treated by Oshima,[33] but his result appears to contain a misprint.[*]

For the similarity case ($M=\infty$) Von Neumann[34] and, independently, Sedov[15] have derived an exact solution of the entire problem by expressing, in terms of the similarity variables, the statement that the time rate of change of the energy enclosed between two surfaces must equal the rate at which work is being done on the surfaces, less the flux out. The same exact solution has been later rediscovered by J. L. Taylor,[35] Latter,[36] Sakurai.[37]

For the quasi-similar case $\left(M \neq \infty\right)$ the same approach does not produce an exact solution.

d) Mass Conservation

Oshima's approximation does not conserve mass. The integrated value of the mass distribution from the origin to the shock should yield the same value as the product of the undisturbed density and the volume swept out by the shock, i. e.

$$\sigma_{\nu} \int_{0}^{R_s} \rho r^{\nu} dr = \sigma_{\nu} \rho_0 \frac{R_s^{\nu+1}}{\nu+1}$$

---

[*] The exponent on the quantity $\left[h\left(x-f\right) x^{\delta}\right]$ should be multiplied by α in Eq. (24) of Ref. 33.

or

$$\int_0^1 \psi \eta^\nu \, d\eta = \frac{1}{\nu+1} \tag{120}$$

The alteration that is made to the continuity equation in the quasi-similar approximation violates this fact. The continuity relation, Eq. (112), can be written in the form

$$\frac{d}{d\eta} (\phi\psi) = \eta\psi' - \nu\frac{\psi\phi}{\eta} + H_1\psi \tag{121}$$

Multiplying by η^ν and integrating by parts gives

$$(\nu+1-H_1)\int_a^b \psi\eta^\nu d\eta = -\left[\eta^\nu\psi(\phi-\eta)\right]_a^b \tag{122}$$

If the limits are taken from zero to one, and the first of Eqs. (16) is used, the result is

$$\int_0^1 \psi\eta^\nu \, d\eta = \frac{1}{\nu+1-H_1} \tag{123}$$

The right-hand side of this equation, evaluated from Lewis' calculations,[30] is shown in Fig. 6 for $\nu = 2$. The maximum error, about 40%, occurs near $M = 2$. Such an overestimate of the total mass present is quite significant, and is partly responsible for the distorted particle trajectories described below.

e) Approximate Solution for $\eta \rightarrow 0$

The perfect-gas solutions reported by Oshima and by Lewis show a constant, nonzero pressure near the origin ($\eta = 0$), while the density vanishes as a power of η

$$\phi \approx A\eta \quad , \quad f \approx f_o \quad , \quad \psi \approx B\eta^b \qquad (124)$$

Substituting these into the continuity and energy equations ((112) and (114)) gives, respectively, the relations

$$(A-1)\,b + A\,(\nu+1) = H_1 \qquad , \qquad -\gamma(A-1)\,b = H_3 \qquad (125)$$

whose solution is

$$A = \frac{H_1 + H_3/\gamma}{\nu+1} \qquad\qquad b = \frac{(\nu+1)\,H_3/\gamma}{\nu+1 - H_1 - H_3/\gamma} \qquad (126)$$

In order to completely specify the solution, it is also necessary to know f_o and B . There appears to be no way of determining these analytically. They are related to each other, however, so an estimate of f_o (perhaps from numerical solutions for $\mathcal{N}$ close to the proper value, and η close to the origin) can be used to find an estimate of B . The relation, which comes from the first integral described above (118), is

$$B^{1-\gamma\alpha}\, f_o^{\alpha}\, |A-1| = \left[\psi(1)\right]^{1-\gamma\alpha} \left[f(1)\right]^{\alpha} \left|\,\phi(1)-1\,\right| \qquad (127)$$

2. <u>Asymmetric Disturbances in a Solid</u>

a) General Analysis

The foregoing discussion deals exclusively with symmetric disturbances, such as a spherical blast. Because the impact problem is asymmetric with respect to the target surface, the θ-variations in the equations of motion must be reinstated before any meaningful results can be ex-

tracted. When such variations are permitted, however, it is necessary to solve a set of partial differential equations, even if the similarity assumption is made. At present, there are no analytic solutions accounting for asymmetry, either with or without the similarity assumption.

Limited analytical progress has been made in the similarity limit, however, by restricting attention to the axis of symmetry.[18] Approximate solutions along that axis have been made by approximating the off-axis pressure distribution. It was found that for a wide range of off-axis distributions, the solution was virtually the same, and was quite close, in many respects, to the solution of the symmetric problem. That evidence, which was restricted to the perfect-gas (or extremely high pressure) limit, suggested that the impact process could be considered as one half of a spherically symmetric disturbance, whose scale is controlled by the energy of the projectile, its momentum playing a secondary role. Walsh and his coworkers have recently presented an exact numerical solution of the perfect-gas problem.[4] Several important features of their results are matched closely by the approximate solution.

An approximate treatment of the asymmetric, perfect-gas problem has also been given by Rayzer.[38] His solution is quite close to the symmetric, constant-energy solution in many important respects.[*]

Finally, mention should be made of two other papers in which the asymmetric problem is discussed. In one of these,[40] a brief reference is made (p. 63) to the use of a dipole representation. The other paper[41]

---

[*] The case of impact into a half-space of gas represents the spherical generalization of the planar "sharp-blow" problem, which is discussed in detail by Mirels.[39]

is chiefly a presentation of experimental data on the cylindrical problem of shock propagation due to a sudden energy release along a line (an exploding wire) at the free surface of a half-space of water. The paper refers to an analytical treatment of the problem in a Russian dissertation.[42]

The main conclusion drawn from the perfect-gas studies was that approximate solutions for quantities like the shock trajectory could be obtained by assuming the disturbance to be equivalent to one half of a spherically symmetric disturbance. It was emphasized, at the time that conclusion was presented,[5] that the evidence for it was limited to the perfect-gas, or similarity limit. In taking up the nonsimilar nature of the problem, then, one of the first questions to be answered is whether the same conclusion can be reached at finite values of the shock speed. The evidence presented below indicates an affirmative answer to this question. After the evidence has been reviewed, the discussion then centers on the symmetric solutions.

The basic differential equations in the η , θ , R_s coordinate system are given above in Eqs. (11) - (14). To these must be added the equation of state, which in these variables is

$$ g = \frac{1}{2(s-1)} \left\{ \frac{f}{\psi} - \frac{\psi - 1}{M^2 \left[s - (s-1)\psi \right]} \right\} \qquad (128) $$

The boundary conditions at the shock for a C , S medium, written in terms of the shock Mach number $M = \dot{R}_s / c$, take the form:

$$ f(1, \theta, R_s) = \phi(1, \theta, R_s) = \frac{1}{s} \left(1 - \frac{1}{M} \right) \qquad (129) $$

$$\psi\left(1, \theta, R_s\right) = \frac{SM}{1 + (S-1)M} \tag{130}$$

$$g\left(1, \theta, R_s\right) = \frac{1}{2}\left[\phi\left(1, \theta, R_s\right)\right]^2 = \frac{1}{2S^2}\left(1 - \frac{1}{M}\right)^2 \tag{131}$$

For a spherical shock, there is no tangential component of velocity immediately behind the shock. Thus

$$\omega\left(1, \theta, R_s\right) = 0 \tag{132}$$

Using the same notation as for the perfect-gas case, a new symbol is introduced for the decay coefficient

$$\frac{R_s \ddot{R}_s}{\dot{R}_s^2} = -\frac{1-N}{N} \tag{133}$$

and the Oshima approximation is again made, by use of the relation

$$R_s \frac{\partial \mathcal{F}}{\partial R_s} = -\frac{1-N}{N} M \frac{\left(\frac{\partial \mathcal{F}}{\partial M}\right)_{\eta=1}}{\mathcal{F}(1)} \mathcal{F} \tag{134}$$

The derivatives of ϕ , ψ , and f are readily found from this formula. It cannot be used for the derivative of ω , however, since that function is identically zero along a hemispherical shock. This derivative is retained, for the moment, in its original form.

There are two possible ways of calculating the derivative of g . The first is to apply Eq. (134) to the boundary value of g , giving

$$R_s \frac{\partial q}{\partial R_s} = -2 \frac{1-N}{N} \frac{q}{M-1} \tag{135}$$

The equation of state, (128), can now be used to replace q in terms of f and ψ . The seond way of calculating the derivative of q is to reverse these two steps, substituting (128) first, and then applying formula (134). The result is completely different

$$R_s \frac{\partial q}{\partial R_s} = -\frac{1-N}{N} \frac{1}{2(s-1)} \left\{ \frac{1}{M-1} \frac{f}{\psi} + \frac{2(\psi-1)}{M^2 [s-(s-1)\psi]} - \left[\frac{f}{\psi^2} + \frac{1}{M^2 [s-(s-1)\psi]^2} \right] \frac{1}{1+(s-1)M} \right\} \tag{136}$$

These two approximations are referred to in what follows as the first and second forms of Oshima's method. The former has the advantage of greater simplicity, while the latter appears to be a more consistent formulation. Only the first form has been used in the calculations reported here.

The same ambiguity is present in the perfect-gas case.[6] In the derivation outlined in Eqs. (79), (80), (81), and (91), the equivalent second form was derived. The first-form result is quite different, and in fact is considerably more complex.

When the first form for a C , S medium is used, the basic equations become

45   AI-1821-A-2

$$(\phi-\eta)\frac{\partial\psi}{\partial\eta} + \frac{\omega}{\eta}\frac{\partial\psi}{\partial\theta} + \psi\left(\frac{\partial\phi}{\partial\eta} + \frac{1}{\eta}\frac{\partial\omega}{\partial\theta} + \nu\frac{\phi}{\eta} + \frac{\omega}{\eta}\cot\theta\right) =$$

$$\text{(137)}$$

$$= \frac{1-N}{N}\frac{1}{1+(s-1)M}$$

$$-\frac{1-N}{N}\phi + (\phi-\eta)\frac{\partial\phi}{\partial\eta} + \frac{\omega}{\eta}\frac{\partial\phi}{\partial\theta} - \frac{\omega^2}{\eta} + \frac{1}{\psi}\frac{\partial f}{\partial\eta} = \frac{1-N}{N}\frac{\phi}{M-1} \qquad \text{(138)}$$

$$-\frac{1-N}{N}\omega + (\phi-\eta)\frac{\partial\omega}{\partial\eta} + \frac{\omega}{\eta}\frac{\partial\omega}{\partial\theta} + \frac{\phi\omega}{\eta} + \frac{1}{\psi\eta}\frac{\partial f}{\partial\theta} = -R_s\frac{\partial\omega}{\partial R_s} \qquad \text{(139)}$$

$$-2\frac{1-N}{N}q + (\phi-\eta)\frac{\partial q}{\partial\eta} + \frac{\omega}{\eta}\frac{\partial q}{\partial\theta} - \frac{f}{\psi^2}\left\{(\phi-\eta)\frac{\partial\psi}{\partial\eta} + \frac{\omega}{\eta}\frac{\partial\psi}{\partial\theta}\right\} =$$

$$\text{(140)}$$

$$= 2\frac{1-N}{N}\frac{q}{M-1} - \frac{1-N}{N}\frac{f/\psi}{1+(s-1)M}$$

For the case of a symmetric solution, where all θ-derivatives are zero, or for a "centerline" solution (i. e., along the axis $\theta=0$ in the asymmetric case) these take the form

$$(\phi-\eta)\psi' + \psi\left(\phi' + \nu\frac{\phi}{\eta} + \frac{\tau}{\eta}\right) = \frac{1-N}{N}\frac{\psi}{1+(s-1)M} \qquad \text{(141)}$$

$$-\frac{1-N}{N}\phi + (\phi-\eta)\phi' + \frac{f'}{\psi} = \frac{1-N}{N}\frac{\phi}{M-1} \qquad (142)$$

$$-2\frac{1-N}{N}g + (\phi-\eta)g' - \frac{f}{\psi^2}(\phi-\eta)\psi' = 2\frac{1-N}{N}\frac{g}{M-1} - \frac{1-N}{N}\frac{f/\psi}{1+(s-1)M} \qquad (143)$$

where τ is defined for $\nu = 2$ as

$$\tau = 2\frac{\partial\omega}{\partial\theta}(\eta,0) \qquad (144)$$

A different definition would be appropriate for a centerline solution in the cylindrical case ($\nu = 1$), while for a planar case, τ must be identically zero.

If the function g is now expressed in terms of f and ψ, the energy equation is

$$f' - A^2\psi' = \frac{2\frac{1-N}{N}\frac{M}{M-1}g - \frac{1-N}{N}\frac{f/\psi}{1+(s-1)M}}{(\phi-\eta)\left(\frac{\partial g}{\partial f}\right)_\psi} \qquad (145)$$

where the function A^2, defined as

$$A^2 = \frac{\frac{f}{\psi^2} - \left(\frac{\partial g}{\partial\psi}\right)_f}{\left(\frac{\partial g}{\partial f}\right)_\psi} = (2s-1)\frac{f}{\psi} + \frac{\psi}{M^2\left[s-(s-1)\psi\right]^2} \qquad (146)$$

is a dimensionless sound speed (squared), i.e., (see Eq. (57))

$$a^2 = \left(\frac{\partial p}{\partial \rho}\right)_{A} = \frac{\frac{p}{\rho^2} - \left(\frac{\partial e}{\partial \rho}\right)_{p}}{\left(\frac{\partial e}{\partial p}\right)_{\rho}} = \dot{R}_s^2 A^2 \tag{147}$$

With these definitions, the final form of the quasi-similar equations is

$$(\phi - \eta)\, \psi' + \psi \phi' = R_1 \tag{148}$$

$$(\phi - \eta)\, \phi' + \frac{f'}{\psi} = R_2 \tag{149}$$

$$f' - A^2 \psi' = R_3 \tag{150}$$

where

$$R_1 = \frac{1-N}{N}\; \frac{1}{1+(s-1)M}\; - \nu\, \frac{\psi \phi}{\eta} - \frac{\psi \tau}{\eta} \tag{151}$$

$$R_2 = \frac{1-N}{N}\; \frac{M}{M-1}\; \phi \tag{152}$$

$$R_3 = \frac{2(s-1)\psi}{\phi - \eta}\; \frac{1-N}{N}\; \left\{ \frac{1}{s-1}\; \frac{M}{M-1}\; \left[\frac{f}{\psi} - \frac{\psi-1}{M^2\left[s-(s-1)\psi\right]} \right] \right.$$
$$\left. - \frac{f/\psi}{1+(s-1)M} \right\} \tag{153}$$

Solved for the derivatives, these equations become

$$\psi' = \frac{(\phi-\eta)R_1 + R_3 - \psi R_2}{(\phi-\eta)^2 - A^2} \tag{154}$$

$$\phi' = \frac{(\phi-\eta)R_2 - \frac{A^2}{\psi}R_1 + \frac{(\phi-\eta)}{\psi}R_3}{(\phi-\eta)^2 - A^2} \tag{155}$$

$$f' = \frac{(\phi-\eta)^2 R_3 - A^2 \psi R_2 + A^2(\phi-\eta)R_1}{(\phi-\eta)^2 - A^2} \tag{156}$$

These equations are identical in form to those which apply for the perfect-gas case, [18] to which they reduce as $M \to \infty$. They have the same singularities as those for $M = \infty$; one is at the point where $\phi = \eta$ $(R_3 \to \infty)$, and the other is at the "sonic line", [18] where $|\phi - \eta|$ is equal to the local sound speed.

The Oshima approximation for a C, S medium fails to conserve the total mass, just as in the perfect-gas case. Following the same series of steps as is used in deriving Eq. (123), the result (which applies only for a symmetric case) is

$$\int_0^1 \psi \eta^\nu d\eta = \frac{1}{\nu+1 - G_1} \tag{157}$$

where

$$G_1 = \frac{1-N}{N} \frac{1}{1 + (S-1)M} \tag{158}$$

b) Results of Calculations

Equations (154) to (156) were solved numerically on an IBM 704 computer* for the spherical case (ν = 2), with S = 2 , and using the first-form definition of R_3 . Spherically symmetric solutions (τ = 0) were done for M = 8, 4, 2.5, 2, 1.5, and 1.25, and "centerline" solutions ($\tau \neq 0$) for M = 8, 4, 2, and 1.5. The results are shown in Fig. 7. The solution for $M = \infty$ would be the same as the perfect-gas similarity solution[18] for γ = 3.

The solutions with $\tau \neq 0$ require an additional equation specifying τ . In the absence of an exact solution, some approximation must be used. The approximation used here is to relate τ to the off-axis pressure distribution in the same manner as used in the similarity solution[18] -- i.e., the term $R_s \partial \omega / \partial R_s$ in Eq. (139) is assumed to be zero, the resulting differential equation is differentiated with respect to θ , and then θ is set equal to zero. The result is

$$ -\frac{1}{2} \frac{1-N}{N} \tau + \frac{1}{2} (\phi - \eta) \tau' + \frac{\tau^2}{4\eta} + \frac{\phi \tau}{2\eta} + \frac{1}{\eta \psi} \frac{\partial^2 f}{\partial \theta^2} (\eta, 0) = 0 \qquad (159) $$

The pressure variation is then approximated in the form

$$ \frac{\partial^2 f}{\partial \theta^2} = -K (1-\eta) f \qquad (160) $$

The value K = 10 , which was found satisfactory in the perfect-gas case, has been used in all the calculations reported here. With this specification, the variation of τ can be found as part of the solution.

Near the shock, the only important terms in Eq. (159) are

$$\frac{1}{2}(\phi - \eta)\tau' \approx -\frac{1}{\eta\psi}\frac{\partial^2 f}{\partial\theta^2} = \frac{K}{\eta\psi}(1-\eta)f \tag{161}$$

whose approximate solution

$$\tau \approx \frac{K f(1)(1-\eta)^2}{[1-\phi(1)]\psi(1)} = K f(1)(1-\eta)^2 \tag{162}$$

explains the parabolic variation of τ that is evident in Fig. 7.

For each value of M, various values of N must be tried until a solution is found which is free of singularities. In general, only one value of N leads to such a solution. When N is less than this number, the quantity $(\phi-\eta)^2 - A^2$ vanishes at some nonzero value of η, and when N is greater than this value, the solution encounters the singularity at $\phi = \eta$.

The results shown in Fig. 7 suggest that, just as in the similarity ($M = \infty$) limit, the three-dimensional effects are not large, at least as far as quantities like the shock trajectory are concerned. The evidence for this conclusion comes from two sources. First, as will be seen below, the shock trajectory is mostly affected by the mass-averaged values of velocity, pressure, and density. Because such averaging introduces a factor $\psi \eta^2$ into the integrands, only the values very close to the shock are influential. Thus, the relatively large differences in the distributions of ϕ, ψ, and f between symmetric ($\tau = 0$) and asymmetric ($\tau \neq 0$) solutions are not likely to be reflected in comparably large differences in shock trajectory.

AI-1821-A-2

The second line of evidence concerning the insensitivity of shock trajectory to asymmetry lies in the values of N . Regarding N as a function of M , the shock trajectory can be found by integrating Eq. (85) in the form

$$d \ln \frac{R_s}{R_0} = F(M) \, d \ln M \qquad\qquad (163)$$

where $F = -(1-N)/N$, and where the normalizing constant R_0 is defined below. The fact is that N has approximately the same value, at given M , for both the symmetric and asymmetric solutions. Thus the shock trajectory is not markedly affected by symmetry considerations.

It is interesting to observe that the value of N for the asymmetric solutions is always less than its corresponding value for the symmetric solutions. At the perfect-gas limit, Walsh[4] has pointed out that the value N_{asym} = .375 agrees with the result $\alpha = \frac{N}{1-N}$ = .59 found from his calculations. It appears that the present results for α exhibit the same ratio as that for $M = \infty$.

M	N_{sym}	N_{asym}	α_{sym}	α_{asym}	$\frac{2}{3} \cdot \frac{\alpha_{asym}}{\alpha_{sym}}$
∞	.400	.375	.667	.600	.600
8	.444	.4175	.798	.718	.599
4	.489	.4575	.955	.843	.589
2	.591	.5495	1.447	1.22	.562
1.5	.681	.6365	2.13	1.751	.549

The fact that this ratio is approximately constant is presumably related to the constancy of α revealed by Walsh's solutions. There is at present no analytical proof of this assertion, however.[*]

c) Further Discussion of Symmetric Solutions

Given that the symmetric solutions can be used for a crude approximation to the shock trajectory, it is of interest to examine in detail their distributions of pressure, density, and particle velocity. These results are shown in Fig. 7. As M gets closer to one, a narrow region appears, in which large gradients of velocity, pressure, and density occur. These large gradients are not associated with singularities of the differential equations (the solutions are free of such singularities), and the question arises whether they represent the appearance of an entropy line[39] or perhaps of a second shock. In connection with the latter possibility, it must be recognized that, in a gross sense, the terms which are introduced by Oshima's method are not unlike the artificial viscosity terms[43] which are often used for the express purpose of generating shock waves.

In order to identify the source of these steep-gradient regions, a calculation was made of the trajectories followed by various particles. There are two ways of calculating such trajectories. One is to integrate the relation $dr/dt = u$, while the second is to follow lines of constant entropy (since the entropy of a particle does not change, once the particle

---

[*] It should also be observed that N_{asym} was found to increase with increasing γ , and hence with increasing S , in the perfect-gas ($M = \infty$) results of Ref. 18. The same tendency presumably persists at finite values of M , indicating that materials with larger values of S will be associated with larger values of N and α .

has crossed the shock). For an exact solution of the partial differential equations, of course, both methods would lead to the same trajectories. Within the framework of Oshima's approximation, however, they do not necessarily lead to the same result, and the closeness between the two may be used to judge the validity of the approximation.

The first trajectory calculated is that of the shock. Conservation of energy gives

$$E = \sigma_\nu \int_0^{R_s} \left(e - e_0 + \tfrac{1}{2} u^2 \right) r^\nu \rho \, dr$$

$$= \sigma_\nu R_s^{\nu+1} M^2 \rho_0 c^2 \, I(M; s) \qquad (164)$$

where

$$I(M; s) = \int_0^1 \left(g + \tfrac{1}{2} \phi^2 \right) \psi \eta^\nu \, d\eta \qquad (165)$$

and

$$\sigma_\nu = 1, \ \pi, \ 2\pi \quad ; \ for \ \nu = 0, 1, 2 \qquad (166)$$

σ_ν is defined here as one-half the value used in Eq. (100), to facilitate application to impact problems, where it will be assumed (as in Ref. 5) that all the available energy goes into one half of a symmetric disturbance. It is interesting to note how the quantity $\rho_0 c^2$ presents itself as the proper quantity to use as an ambient pressure. This pressure, and the total energy E, can be scaled out of the problem by the definition

$$R_0 = \left(\frac{E}{\sigma_\nu \rho_0 c^2} \right)^{1/(1+\nu)} \qquad (167)$$

In these terms, the shock radius-shock speed relation is

$$\frac{R_s}{R_o} = \left\{ M^2 \, I(M; s) \right\}^{-1/(1+\nu)} \tag{168}$$

Figure 8 shows the result for $s = 2$, compared with the earlier[5] Quasi-Steady solution. The shock trajectory itself, found by integrating the identity

$$\frac{ct}{R_o} = \int_0^{R_s/R_o} \frac{1}{M} \, d\left(\frac{R_s}{R_o}\right) \tag{169}$$

is shown in Fig. 9.

This figure also shows particle paths, found as lines of constant entropy. This is done by first finding from Eq. (46) the variation, with η, of the quantity $\hat{e}/c^2$, for a given value of M, i.e., at a given instant. From Eq. (48), it is also possible to find the values of $\hat{e}/c^2$ that exist along the shock. A graphical solution of these two relations then makes it possible to identify, for each η at a given M, the value M_o which the shock Mach number had at the instant when that particle was traversed by the shock. The results are shown in Fig. 10. Note that horizontal lines (constant M_o) trace the history of a given particle. Thus, the particle intercepted by the shock ($\eta = 1$) at the instant when $M = 2.5$ has dropped back to the point $\eta = .75$ at the later instant when $M = 2$. Using these results, one can find the coordinates $r/R_o = \eta \, R_s/R_o$, ct/R_o, along a particle path. The results, shown in Fig. 9, suggest that the steep-gradient regions are associated with an entropy line, and not a second shock.

While the trajectories of the high-entropy particles (those processed by the strong portions of the shock) are reasonable, those crossing the shock at later time make no sense. All particles should initially follow the shock -- i.e., they should be deflected to the right. At late time ($M \rightarrow 1$), however, the particles appear to start in the opposite direction. In addition to this obvious fault, these trajectories do not agree with what would be had by integrating the velocity field. In all the solutions of Fig. 7, the quantity ϕ is always positive. However, the constant-entropy lines of Fig. 9 show regions of negative velocity.

In spite of its internally inconsistent description of particle trajectories, the Oshima solution makes an accurate prediction of the shock trajectory. The path traversed by the shock in Fig. 9 is, if anything, closer to experiment than the Quasi-Steady solution presented previously.[5]

In general, Oshima's method appears to work best at early time, when most of the mass is concentrated near the shock. During the weaker stages of shock propagation, the errors introduced by its approximations become more important, and its predictions of distributions of physical quantities less reliable. Throughout the entire range of shock strength, however, the integrated quantities required for shock-trajectory determinations are adequately handled.

B. Quasi-Steady Method

In the foregoing discussion of Oshima's method, the point has been made repeatedly that accurate shock-trajectory predictions require the distributions of pressure, density, and velocity only very near to the shock. Oshima's method is specifically designed to yield the exact values at the shock for these variables, and excellent approximations to their

first derivatives with respect to η [*]. Thus, any other approximation which is accurate at the shock is likely to be adequate for shock-trajectory calculations, even though its analytical basis might not be as rigorous as that of the Oshima method. One such approximation, called the "Quasi-Steady" method, was advanced in Ref. 5. In the sections that follow, this method is reviewed, extended to later, weaker stages of shock propagation, and compared extensively with experiment and with computer solutions.

The Quasi-Steady method is based on the observation that, for shock-trajectory calculations, the only quantity needed is the integral I in Eq. (165), which depends on the shock speed M with material properties (such as S) appearing as parameters. The Quasi-Steady approximation equates this integral to the value I_1 that it would have for a perfect-gas similarity solution with γ so chosen as to give the correct values of pressure, density, and particle velocity at the shock. In the perfect-gas similarity solution, the boundary values at the shock are given in terms of γ by [**]

$$\phi_1 = \frac{u_1}{u_s} = f_1 = \frac{p_1}{\rho_0 u_s^2} = \frac{2}{\gamma+1} \quad ,$$

$$\frac{\rho_1}{\rho_0} = \frac{\gamma+1}{\gamma-1} \quad , \qquad \frac{e-e_0}{u_s^2} = \frac{2}{(\gamma+1)^2}$$

(170)

---

[*] The derivatives at $\eta = 1$ are not quite exact, since they depend on N , which in turn depends on the entire approximation scheme over the whole range of η from zero to one.

[**] It should be noted that the Quasi-Steady method cannot be used to describe the nonsimilarity arising from counterpressure in the perfect-gas problem. The reason is that the Quasi-Steady method always has $\phi = f$ at the shock, whereas they are in general different for a perfect gas (see Eq. (84)).

In applying the Quasi-Steady solution, the Hugoniot values u_1, p_1, ρ_1, e_1, are regarded as known, and the corresponding value of γ is then found from any one of the relations

$$\gamma = 2 \frac{u_s}{u_1} - 1 = 2 \frac{\rho_0 u_s^2}{p_1} - 1 = \frac{\frac{p_1}{p_0} + 1}{\frac{p_1}{p_0} - 1} = \sqrt{\frac{2 u_s^2}{e_1 - e_0}} - 1 \qquad (171)$$

For example, when the shock speed is such as to create a density ratio $\rho_1/\rho_0 = 1.5$, the integral I is assumed to be the same as it would be in a similarity solution with $\gamma = \frac{1.5 + 1}{1.5 - 1} = 5$. At a later instant when $\rho_1/\rho_0 = 1.4$, γ is taken to be 6, etc. For a point-source solution, the shock speed is initially infinite, and the density ratio ρ_1/ρ_0 is equal to its limiting value. Thus γ starts out with the value $\left[\left(\rho_1/\rho_0 \right)_{lim} + 1 \right] \Big/ \left[\left(\frac{\rho_1}{\rho_0} \right)_{lim} - 1 \right]$. As the shock speed decreases, ρ_1/ρ_0 decreases, and thus γ increases, approaching infinity as ρ_1/ρ_0 approaches one. The large values of γ that are thus encountered in an attempt to account for nonsimilarity constitute, in a sense, the counterpart of the strong-blast theory in which γ is allowed to approach 1.[44]

It should be emphasized that the Quasi-Steady method can be quickly applied to any material whose Hugoniot is known. A graph, for example, of p_1 vs. u_s will give γ vs. u_s, from Eq. (171). The corresponding values of I_1, found from Fig. 11, are then used in Eq. (164) to give the shock radius-shock speed relation

$$R_s = \left\{ \frac{E}{2\pi \rho_0 \dot{R}_s^2 \, I_1 \left[\gamma(\dot{R}_s) \right]} \right\}^{1/3} \qquad (172)$$

The shock trajectory is then found from the identity

$$t = \int_0^{R_s} \frac{dR_s}{\dot{R}_s}$$

(173)

These relationships hold for any Hugoniot curve.

For the special case of a C, S medium, the shock-trajectory relations can be worked out once and for all in general form. The basic equations are the same as Eqs. (167) - (169):

$$\frac{R_s}{R_0} = \left\{ M^2 I(M, s) \right\}^{-\frac{1}{3}} \quad , \quad \frac{ct}{R_0} = \int_0^{R_s/R_0} \frac{1}{M} d\left(\frac{R_s}{R_0}\right)$$

(174)

where

$$I(M, s) = I_1 \left[\gamma(M, s) \right]$$

(175)

and where γ is defined by

$$\gamma = \frac{(2s-1) M + 1}{M - 1}$$

(176)

Curves of $1/M$ and ct/R_0 vs. R_s/R_0, for $S = 1.2$, 1.5, and 2.0, were presented in Ref. 5. Those results were based on values of γ extending up to 20, and provided results out to around $R_s/R_0 = 7$, where $1/M$ was between .8 and .9, and ct/R_0 was approximately 4. The calculations have now been extended to weaker shock strengths, by adding the cases $\gamma = 40$, 70, and 100, for which the distributions behind the shock are shown in Fig. 12. The new shock-trajectory results, shown as the solid lines in Figs. 13 and 14, extend to $R_s/R_0 \approx 19$, where $1/M$ lies between .96 and .98, and where ct/R_0 is about 15. In addition, curves have been prepared which show the pressure and density

at the shock as a function of the depth to which the shock has penetrated. These results, which can be found from Eqs. (174), (38), and (40), are shown in Figs. 15 and 16. For convenience in re-plotting, coordinates of all these curves are given in Tables I and II.

It is also possible to find the distributions of various quantities behind the shock, using the distributions for the various values of γ, given in Figs. 7a-j of Ref. 18, and in Fig. 12 of the present report. For example, the pressure distribution can be given as a function of r/R_o and M by using the relations

$$\frac{p}{\rho_o c^2} = M^2 f(\eta) \quad , \quad \frac{r}{R_o} = \eta \frac{R_s}{R_o} \tag{177}$$

These calculations have been done for $\gamma \leq 20$, and for $S = 1.2, 1.5,$ and 2.0. The results are shown in Figs. 17a-c. Unfortunately, there are very few numerical solutions available at present with which to compare these results.

Solution at Early Time

At early time, a point-source solution must contain a finite amount of energy in an infinitesimal volume. Thus the initial shock speed is predicted to be infinite. In actuality, the disturbance in the near vicinity of the impact point is not well represented by a point source, but at first exhibits a structure that is governed by the details of the geometrical configuration in which the projectile and target come together. Shortly after contact is made, the shock entering the target tends to become planar and parallel to the target surface. Its plane portion is soon affected by rarefaction waves originating at the intersection of the projectile with the free surface, but the interaction near the impact point is

roughly one-dimensional until the time when the shock has propagated into the target a distance on the order of the projectile length. During this initial period an exact solution for the (constant) shock speed can be found, from the Hugoniot curves of the projectile and target (see, for example, Ref. 18, page 17). The Quasi-Steady theory is improved by using the constant-speed solution up to the point where it intersects the point-source curve, using that curve thereafter. Curves showing constant multiples of the stress-wave speed, designated M_i , have been added to Fig. 13, which presents shock trajectories for the special case of a C , S medium.

Solution at Intermediate Time

Once the early-time phase has been completed, the shock speed ceases to be constant, and makes a transition to the point-source curve. If the impact speed is sufficiently high, so that the early-time shock speed is many times the stress-wave speed, then the transition to the point-source solution occurs in the strong-shock portion of the point-source solution, where the shock radius expands in proportion to the 2/5 power of time. As the shock continues to expand, it slows down further, and the power of time according to which it expands (essentially the slope of the log-log R_s, t curve) becomes larger, approaching the constant stress-wave speed ($R_s \sim t$) at late time. For a less severe impact, the transition to the point-source solution occurs at sufficiently late time that the 2/5-power-law variation is not detected. The speeds presently attainable in laboratory experiments are not sufficiently high to produce a $t^{2/5}$ variation (even if the very early time data could be properly resolved).

Such variations do appear, however, in computer solutions. Bjork's data for iron striking tuff[2] at 30 km/sec, for example, show this behavior, as do the results of Walsh et al[3] for an iron-iron impact at 40 km/sec.

Thus, in general, the shock expands according to the first power of time, both early and late. During the intermediate period, a variable power of the time is observed. The power may initially be as low as 2/5 for a very high-speed impact; it is higher for more moderate impacts, and in all cases tends toward 1 at late time.

It should be pointed out that a different interpretation has been advanced by Heyda and Riney.[45] These authors believe that the solution for the late stages of the hydrodynamic flow is of the form $R_s \backsim t^{2/3}$, with the transition to the form $\dot{R}_s = c$ occurring only when material-strength effects become important. The present results indicate that, even without any strength influence, the wave speed in the inviscid solution asymptotically approaches the acoustic velocity of the fluid being considered. In support of the variation $R_s \backsim t^{2/3}$, Heyda and Riney present a large number of computed results for Aluminum-Aluminum and Lead-Lead impacts. However, the data (which are listed in Appendix C) only extend to shock radii on the order of $R_s/R_o \approx 5$. Reference to Fig. 13 will show that the slope of the $\log R_s$, $\log t$ curve is indeed around 2/3 in this region. It appears that the calculations must be extended to later times ($R_s > 10 R_o$) before truly asymptotic conditions are achieved.

Solution at Late Time

For the case of a point-source disturbance in a perfect gas, where nonsimilarity is caused by counterpressure, the solution at late time

finds the wave speed approaching the sound speed ($M \rightarrow 1$), while the excess pressure (shock pressure less the ambient pressure) decays inversely as the first power of the shock radius. The present problem involves nonsimilarity due to the form of the state equation only; the counterpressure term is always neglected. Thus it is not surprising to find in the present results that, while $M \rightarrow 1$ at late time, the law of pressure decay differs from the acoustic ($p \sim 1/R_s$) relation. Instead, the pressure decays as approximately the -7/4 power of R_s .

This result can be demonstrated by noting that the function $I_1(\gamma)$ for $\gamma > 10$ is closely approximated by the relation

$$ I_1(\gamma) \approx \frac{K}{\gamma^n} \tag{178} $$

where $K = 0.366$, $n = 1.7$. As M is allowed to approach one, γ becomes very large

$$ M \rightarrow 1, \quad \gamma \approx \frac{2s}{M-1} \tag{179} $$

Thus

$$ I_1\left[\gamma(M)\right] \approx \frac{K}{(2s)^n}(M-1)^n \tag{180} $$

The shock-radius, shock-speed relation then becomes

$$ R_s/R_0 \approx \left\{ \frac{(2s)^n}{K(M-1)^n} \right\}^{1/3} \tag{181} $$

or

$$ M-1 \approx \frac{2s}{K^{1/n}}\left(\frac{R_s}{R_0}\right)^{-3/n} \tag{182} $$

This expression then gives the asymptotic law of pressure decay as

$$\frac{p_{SH}}{\rho_o c^2} = \frac{M(M-1)}{s} = \frac{2}{K^{1/n}} \left(\frac{R_s}{R_o}\right)^{-3/n}$$ (183)

For $n = 1.7$, $K = 0.366$, this becomes

$$\frac{p_{SH}}{\rho_o c^2} \approx 3.61 \left(\frac{R_s}{R_o}\right)^{-1.765}$$ (184)

It should be noted that if $I(M)$ were proportional to $(M-1)^2$ as $M \to 1$, then the pressure would decay as the -3/2 power of R_s. It is quite possible that a theory more accurate than the Quasi-Steady approximation would indeed reveal such a variation. For example, it is reasonable to assume that, at late time, the quantity $g + \frac{1}{2}\phi^2$ is always equal to its value at the shock. Thus $I(M)$ would be given by

$$I(M) \approx \left(g + \frac{1}{2}\phi^2\right)_{SH} \int_0^1 \psi \eta^2 d\eta = \frac{1}{3}\left(\frac{M-1}{sM}\right)^2 \approx \frac{(M-1)^2}{3s^2}$$

and the -3/2 power-law decay of shock pressure results. The same result would be found if $I_1(\gamma)$ were assumed inversely proportional to γ^2.

The present results are not capable of resolving exactly what the pressure-decay law is. However, it appears not to be the inverse first-power familiar in gaseous acoustics, and is probably closer to the 3/2 power mentioned above.

Comparison with Experiment and with Calculated Solutions

Figure 13 shows a correlation of the experimental data available at present on the propagation of impact-generated shock waves. Included are some measurements taken from a set of high-speed photographs of a

Lucite target, made by Mr. Robert Piacesi of the Naval Ordnance Laboratory.[*] Also included are the numerical results of Bjork for iron striking tuff at 30 km/sec[2] and iron on iron at 5 km/sec,[1] the results of Walsh et al[3] for iron-iron at 40 km/sec, and Riney's data[45] in Aluminum and Lead, referred to above. Particularly for the high-speed numerical results, the different regimes are clearly shown. Most of the experimental data lie in a range so close to the stress-wave speed that the shock trajectory is essentially a constant-speed line throughout.

Data on shock pressure as a function of shock radius are shown in Fig. 15. One set consists of the results computed by Walsh and Tillotson[3] for iron striking iron at 40 km/sec. Another set is a group of experimental measurements made by Charest.[46] In addition, Riney's results in Aluminum and Lead[45] are shown. The agreement is quite good in all cases, and indicates a decay law where $p_1 \sim R_s^{-2}$ for $\frac{R_s}{R_o} \approx 1$, tending toward $p_1 \sim R_s^{-1.5}$ for R_s/R_o on the order of ten.

Charest[46] notes that his data, as well as some calculations done for his case by Walsh and by Riney, are correlated by a -1.6 power law, and is careful to stress that this law must not be extrapolated beyond the range where it has been observed. The correlation shown in Fig. 15 indicates some guidelines for making such an extrapolation. If one moves in the direction of smaller R_s/R_o, a more rapid decay is to be expected. Very near the surface, of course, the pressure will level off at the value appropriate to the impact point. In the direction of larger R_s/R_o,

---

it is probable that the $R_s^{-1.6}$ law is still valid, at least to the point where strength effects become important. Unfortunately, there is at present no reliable estimate of the point at which this occurs.

The coordinate of all the points shown in Figs. 13 and 15 are collected for easy reference in Appendix C.

Comparison with Shock-Speed Data in Wax Targets

Karpov[47] has recently presented a refined set of wave-speed measurements in a wax target, and compares the data with the constant C, S form of the Quasi-Steady theory. Actually, the Hugoniot for the particular target material is not characterized by a single pair of parameters C and S, but is better approximated by

$$U_s = 2.91 + 1.48 \, U_1 \ \ \text{(km/sec) for} \ \ p_1 > 20 \ \text{kbar}$$

$$U_s = 1.85 + 7.32 \, U_1 \ \ \text{(km/sec) for} \ \ p_1 < 20 \ \text{kbar}$$

An improved Quasi-Steady prediction can be made by using the complete Hugoniot. The results are shown in Fig. 18. The agreement is improved, compared to that found using the constant values $C = 2.91$ km/sec, and $S = 1.48$. The theory still overestimates the shock speed, however, by as much as 20%.

It is possible that part of the discrepancy can be traced to strength effects,* which have been shown to influence plane-wave propagation.[50] In the later portions of Karpov's data ($R_s > 6 cm$) the density change across the shock is only a few percent. Thus a serious question exists as to whether or not an inviscid model has any relevance.

---

* Part is also due to the failure of energy scaling, and part may be due to a two-wave structure[48, 49] of the main shock.

Summary

On the whole, the Quasi-Steady theory makes a satisfactory pre-
diction of shock-wave trajectories, and provides a quantitative estimate,
in terms of R_0 , of the extent of the strong-shock, transitional, and
stress-wave regimes. It can be quickly and easily applied to any mater-
ial whose Hugoniot is known. Its chief drawbacks are that it is based
on pure energy scaling, and that it gives no information about the three-
dimensional character of the solution, although the distributions it
predicts behind the shock appear reasonable near the shock and near the
axis of symmetry.

The deficiencies of the Quasi-Steady solution are essentially the
same as those of Oshima's method. Thus, in spite of its lack of rigor,
the Quasi-Steady solution is probably preferable, because of its ease of
application.

C. Porzel-Zaker Method

An approximate analytic solution for strong blast waves in gases
was developed some years ago by Porzel.[7] His purpose was to account
for departures from ideal-gas behavior. In 1959, Zaker[8] adapted the
analysis so as to make it applicable to the nonsimilar problem, and pre-
sented a solution for a point-source explosion in a solid. In view of the
relative unimportance of asymmetry on quantities like the shock trajec-
tory, Zaker's results also have application to the present problem. In
the subsections that follow, the Porzel-Zaker method is reviewed, and
modified slightly so as to incorporate the C , S state equation described
above.

1. Approximate Solution

The basic idea behind the Porzel-Zaker method is the observation that the continuity and momentum equations involve only p, ρ, and u. Thus, an approximation to any one of these can be used to find corresponding approximations to the other two. The basic quantity for which an approximation is chosen is the density, which is assumed to vary as a power of the distance from the shock:[*]

$$\frac{\rho}{\rho_1} = \left(\frac{r}{R_s}\right)^{q} = \eta^{q} \tag{185}$$

where, as before, subscript 1 denotes conditions immediately behind the shock, and where the exponent q, a function only of time, is found from the mass conservation law

$$\frac{4}{3}\pi\rho_0 R_s^3 = \int_0^{R_s} 4\pi\rho\, r^2 dr \tag{186}$$

which gives

$$q = 3\left(\frac{\rho_1}{\rho_0} - 1\right) \tag{187}$$

This approximation reproduces other solutions to a remarkable degree. For example, the perfect-gas similarity solutions are extremely well recovered. In particular, the case $\gamma = 7$, for which $\frac{\rho_1}{\rho_0} = 4/3$, leads to $q = 1$, which is the exact solution for that case.

To find the velocity field, the conservation law is written for the mass lying between the origin and a given particle path, as shown in the following sketch.

---

[*] Solutions of this sort have also been considered briefly by Nowak.[51]
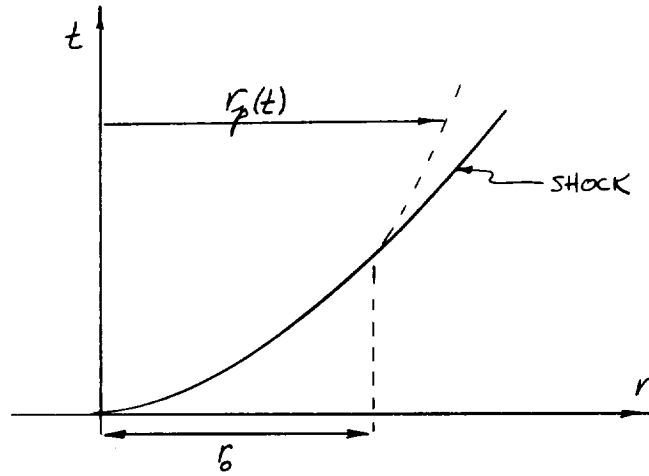
Here $r_p(t)$ is the Lagrangian coordinate of the particle which was originally situated a distance r_0 from the origin. Taking the time derivative of this equation along a particle path gives an expression for $D\rho/Dt$, which can then be equated to the value of $D\rho/Dt$ given by the continuity equation. The result is

$$\rho \frac{d}{dt} \ln (q+3) - \frac{3\rho u}{r} = -\rho \frac{\partial u}{\partial r} - 2\frac{\rho u}{r} \qquad (188)$$

The solution of this equation for u, using conditions at the shock to evaluate the constant, is then

$$u = u_1 \frac{r}{R_s}\left[1 - \alpha \ln \frac{r}{R_s}\right] \qquad (189)$$

where

$$\alpha(t) = \frac{R_s}{u_1}\frac{d}{dt}\ln(q+3) = \frac{R_s}{u_1}\frac{d\ln\rho_1}{dt} = \frac{\dot{R_s}}{u_1}\frac{d\ln\rho_1}{d\ln R_s}\frac{d\ln\dot{R_s}}{d\ln R_s} \qquad (190)$$

69   AI-1821-A-2

The quantity α is always negative or zero, since ρ_1 increases with increasing $\dot{R}_s$, while the factor $d\ln \dot{R}_s / d\ln R_s$ is the decay coefficient (see Eq. (85)), which varies from $-3/2$ at infinite shock speed, to zero at $\dot{R}_s = C$. For a C, S medium, Eq. (190) takes the form

$$\alpha(t) = \frac{R_s \ddot{R}_s}{\dot{R}_s^2} \frac{SM}{(M-1)\left[1+(S-1)M\right]} \tag{191}$$

Zaker notes that α is small in the strong-shock region $\left(\alpha \approx \frac{R_s \ddot{R}_s}{\dot{R}_s^2} \frac{S}{S-1} \frac{1}{M}\right)$, and neglects it for that reason. The additional error introduced by this step during the weaker stages has not been studied.

The next step is to find the pressure distribution, from the momentum equation

$$\frac{\partial p}{\partial r} + \rho \frac{Du}{Dt} = 0 \tag{192}$$

Using Eq. (189) for u, it is possible to show that

$$\frac{Du}{Dt} = \frac{r}{R_s}\left(1 - \alpha \ln \frac{r}{R_s}\right)\left[\frac{du_1}{dt} + \frac{u_1^2}{R_s}\left(1 - \alpha \ln \frac{r}{R_s}\right) - \frac{u_1 \dot{R}_s}{R_s}\right]$$

$$- u_1 \frac{r}{R_s}\left[\frac{d\alpha}{dt}\ln \frac{r}{R_s} + \alpha \frac{u_1}{R_s}\left(1 - \alpha \ln \frac{r}{R_s}\right) - \alpha \frac{\dot{R}_s}{R_s}\right] \tag{193}$$

Integration of Eq. (192) then gives the pressure

$$\int_0^r \frac{\partial p}{\partial r} dr = p(r,t) - p(o,t) = -\int_0^r \rho \frac{Du}{Dt} dr \tag{194}$$

Use of the above expressions for ρ and Du/Dt then leads, after some manipulation, to

$$\frac{p(r,t) - p(0,t)}{R_s \rho_1} = \left[(1-\alpha)\left(\frac{u_1 \dot{R}_s}{R_s} - \frac{u_1^2}{R_s}\right) - \frac{du_1}{dt} \right] \frac{(r/R_s)^{q+2}}{q+2}$$

$$+ \left[\frac{d}{dt}(\alpha u_1) - \frac{\alpha u_1 \dot{R}_s}{R_s} + (2\alpha - \alpha^2)\frac{u_1^2}{R_s} \right] \left(\frac{r}{R_s}\right)^{q+2} \left[\frac{\ln r/R_s}{q+2} - \frac{1}{(q+2)^2} \right] \quad (195)$$

$$- \frac{\alpha^2 u_1^2}{R_s} \left(\frac{r}{R_s}\right)^{q+2} \left[\frac{(\ln r/R_s)^2}{q+2} - \frac{2}{(q+2)}\left(\frac{\ln r/R_s}{q+2} - \frac{1}{(q+2)^2}\right) \right]$$

By setting $r/R_s = 1$, this gives a formula for the pressure at the origin $p(0,t)$ in terms of conditions at the shock

$$\frac{p_1(t) - p(0,t)}{R_s \rho_1} = \frac{1}{q+2} \left[(1-\alpha)\left(\frac{u_1 \dot{R}_s}{R_s} - \frac{u_1^2}{R_s}\right) - \frac{du_1}{dt} \right]$$

$$\qquad\qquad\qquad\qquad\qquad\qquad\qquad\qquad\qquad\qquad\qquad (196)$$

$$- \frac{1}{(q+2)^2} \left[\frac{d}{dt}(\alpha u_1) - \frac{\alpha u_1 \dot{R}_s}{R_s} + (2\alpha - \alpha^2)\frac{u_1^2}{R_s} \right] - \frac{2}{(q+2)^3} \frac{\alpha^2 u_1^2}{R_s}$$

2. <u>Energy Field and Shock Trajectory</u>

All that is now required to complete the solution of the problem is a determination of the internal energy $e - e_o$ as a function of position and time. Once this has been done, the conservation of total energy can then be used to derive a differential equation for the shock trajectory. To find the internal energy, Zaker uses the Hugoniot curve to calculate, for any p and ρ, the "waste heat", or energy unavailable for

mechanical work. For the present formulation, it appears simpler to use the state equation derived above, since it gives $e - e_0$ explicitly in terms of p and ρ .

To illustrate how this can be done, and to show the type of differential equation for the shock trajectory that results, consider the case where α is neglected. The conservation of total energy, using the present C , S form of the state equation, can be written

$$\frac{E}{2\pi R_s^3} = \int_0^1 \left[\frac{p_1}{2S-2} - \frac{R_s \rho_1 A}{2S-2} \left(1 + \eta^{g+2} \right) \right.$$

$$\left. - \frac{\rho_1 c^2 \eta^g \left(\frac{\rho_1}{\rho_0} \eta^g - 1 \right)}{(2S-2)\left[s - (s-1)\frac{\rho_1}{\rho_0} \eta^g \right]} + \frac{1}{2} \rho_1 u_1^2 \, \eta^{g+2} \right] \eta^2 d\eta \tag{197}$$

where

$$A = \frac{1}{(g+2)} \left(\frac{u_1 \dot{R}_s}{R_s} - \frac{u_1^2}{R_s} - \frac{du_1}{dt} \right) \tag{198}$$

Carrying out the integration leads to

$$\frac{E}{2\pi R_s^3} = F\left(\dot{R}_s ; s \right) + G\left(\dot{R}_s ; s \right) R_s \frac{du_1}{dt} \tag{199}$$

where

$$F(\dot{R}_s ; s) = \frac{p_1}{6(s-1)} + \frac{\rho_1 u_1^2}{2(g+5)} - \frac{\rho_1 c^2}{2S-2} \int_0^1 \frac{\eta^{g+2}\left(\frac{\rho_1}{\rho_0} \eta^g - 1 \right)}{\left[s - (s-1)\frac{\rho_1}{\rho_0} \eta^g \right]} d\eta \tag{200}$$

$$- G\left(\dot{R}_s ; s \right)\left(u_1 \dot{R}_s - u_1^2 \right)$$

$$G\left(\dot{R}_s ; s \right) = \frac{\rho_1}{2S-2} \left(\frac{1}{3} - \frac{1}{g+5} \right)\frac{1}{g+2}$$

The last term in Eq. (199) can be rewritten as

$$R_s \frac{du_1}{dt} = R_s \frac{du_1}{dM} \frac{dM}{dt} = R_s \frac{c}{s} \frac{\ddot{R_s}}{c} = \frac{\dot{R_s}^2}{s} \frac{d \ln \dot{R_s}}{d \ln R_s} \qquad (201)$$

Thus, Eq. (199) can be solved, so as to give an explicit expression for $d\dot{R_s}/dR_s$ as a function of R_s and $\dot{R_s}$. After integration, the shock trajectory is then found by applying Eq. (173).[*]

If α is not neglected, the third-order derivative $\dddot{R_s}$ will appear -- for example, from the term $d\alpha/dt$. However, the differential equation for total energy conservation never contains the independent variable t explicitly. Thus, the complete solution simply requires a number of quadratures.

The integrations indicated above have not been carried out. The analysis given is intended only to show the contribution that an explicit form of the state equation can make to Zaker's solution. It would be very interesting to complete these integrations, and to compare the results more extensively with the Quasi-Steady theory.[**] Presumably, the shock trajectory would not be markedly different, but the distributions of p , ρ , and u behind the shock would undoubtedly be better approximations of the exact numerical solutions.

---

[*] All of these steps could, of course, be put in dimensionless form, using only the variables R_s/R_0 , M , and ct/R_0 .

[**] One of the points that needs further study is the early-time solution. Zaker uses initial conditions related to an equivalent sphere of water, and finds early radius-time variations of the form $R_s \sim t^N$, where N is approximately 2/8 to 2/9, instead of the value 2/5 that would be expected for a strong blast.

IV SHOCK PROPAGATION IN POROUS TARGETS

The potential utility of porous substances for achieving improved resistance to meteoroid puncture has often been cited -- for example, in Refs. 18 and 52. Recent experimental findings in substances such as foamed plastics,[53, 54] and fiber metals[55] tend to substantiate the expected improvement. One of the factors responsible for the improvement is that porous materials absorb more energy per unit mass than do solid materials. Thus they offer the possibility of more rapid attenuation of impact-generated shock waves. In this section, the Quasi-Steady method is used to derive a solution for the propagation of spherical waves in a porous medium. The purpose is partly to illustrate how easily this method can be applied to a somewhat unconventional situation, and partly to shed light on the degree of attenuation that may be achieved by porosity.[*]

A. Hugoniot of a Porous Material

The equation of state for the nonporous form of a given material can be used to predict the Hugoniot for any degree of porosity. This fact is pointed out in three recent Soviet publications,[57-59] and details are worked out in those references for specific state equations. For present purposes, it is useful to find the Hugoniot for substances whose equation of state is the form introduced above (Eq. (36)). This equation applies for any degree of porosity; the fact that the constants C and S were determined from experiments on the nonporous form is irrelevant. The

---

[*] Zaker applied his theoretical approach some time ago,[8] and concluded that porosity was effective in achieving a more rapid attenuation. Some aspects of plane-wave propagation in porous solids have been studied recently by Payton.[56]

constants, however, have no direct relationship to the shock-wave proper-

ties of the porous substance. For example, c will not in general be

the weak-wave speed.

The initial density of the porous material is designated by ρ_p ,

and the porosity is defined as

$$m = \frac{\rho_o}{\rho_p} > 1 \tag{202}$$

The Rankine-Hugoniot equations for the porous solid are

$$e_H - e_o = \frac{p_H}{2}\left(\frac{1}{\rho_p} - \frac{1}{\rho_H}\right); \quad p_H = \rho_p u_s u_1 ; \quad \rho_p u_s = \rho_H (u_s - u_1) \tag{203}$$

Eliminating the energy between the first of these and the state equation

gives, for the Hugoniot,

$$\frac{p_H}{\rho_o c^2} = \frac{\frac{\rho_H}{\rho_o}\left(\frac{\rho_H}{\rho_o} - 1\right)}{\left[s - (s-1)\rho_H/\rho_o\right]\left[s - (s-1)m\,\rho_H/\rho_o\right]} \tag{204}$$

With this relation between ρ_H and p_H , the other Rankine-Hugoniot

equations can then be used to find u_s and u_1 . Figure 19 shows

typical results, for $S = 1.5$, and three values of the porosity param-

eter, $m = 1$, 2 and 4. To provide a common standard of reference,

all quantities are made dimensionless with respect to the values ρ_o and

C . Several features are worthy of notice. The first is that a weak

wave ($u_1 \rightarrow 0$) compresses the material back to its normal density, con-

sistent with the fact that a porous solid has very little compressive strength,

and is returned to its solid form by even a slight disturbance. The most

AI-1821-A-2

striking feature, however, is the behavior of strong shocks. A limiting density ratio is achieved, equal to

$$\frac{\rho_+}{\rho_0} \longrightarrow \frac{1}{m} \frac{s}{s-1} \qquad (205)$$

If the initial porosity m is greater than $s/(s-1)$, even an infinitely strong shock will not compress the material back to its normal density, although an extremely weak wave will do so. The reason is that the temperatures achieved in a shocked porous medium increase with increasing porosity. At high enough porosity, the decrease in density associated with these high temperatures is sufficient to keep ρ_+ less than ρ_0 . This phenomenon has been observed in the Soviet experiments,[57, 58] and was also reported recently[60] in this country.

A detailed analysis of the weak-wave limit shows that the shock speed and particle speed are proportional to each other

$$u_1 \approx \frac{m-1}{m} u_s \qquad (206)$$

and both are approaching zero.

B. Solution for Shock Trajectory

Having determined the Hugoniot for a porous c , s medium, it is now possible to find a solution for impact-generated shock propagation by using the Quasi-Steady solution. Conservation of energy in a spherical blast requires

$$E = \int_0^{R_s} \left(e + \tfrac{1}{2} u^2\right) 2\pi \rho r^2 dr = \frac{2\pi \rho_0 c^2}{m} M^2 R_s^3 \, I\left(M; m, s\right) \qquad (207)$$

where

$$M = \dot{R}_s/c \qquad I = \int_0^1 \left(g + \frac{1}{2}\phi^2\right)\psi\eta^2 \, d\eta$$

(208)

$$\eta = r/R_s \;, \quad g = e/\dot{R}_s^2 \;, \quad \phi = u/\dot{R}_s \;, \quad \psi = \rho/\rho_p$$

In terms of the usual scaling length, $R_0 = \left(E/2\pi\rho_0 c^2\right)^{1/3}$, this becomes

$$\frac{R_s}{R_0} = \left\{\frac{M^2 I(M; m, s)}{m}\right\}^{-1/3}$$

(209)

The integral I is now approximated by equating it to the value it would have for a perfect gas whose value of γ matches conditions at the shock

$$\gamma = \frac{\rho_H/\rho_p + 1}{\rho_H/\rho_p - 1}$$

(210)

As the shock speed varies from infinity to zero, γ increases from $2s-1$ to $(m+1)/(m-1)$. The resulting variation of shock speed with shock radius is shown in Fig. 20 for $s = 1.5$, $m = 1$, 2 and 4. It should be noted that the wave speed at a given depth is reduced considerably by the porosity.

Another integration gives the shock trajectory, from

$$\frac{ct}{R_0} = \int_0^{R_s/R_0} \frac{1}{M} \, d\left(\frac{R_s}{R_0}\right)$$

(211)

77
AI-1821-A-2

which is shown in Fig. 21. The reference quantities c and R_0 depend only on the target material and impact energy; they are independent of the porosity. Thus the curves shown provide a direct measure of the increased attenuation caused by the porosity.

One interesting feature of the curves for $m > 1$ is that the solution has the form $R_s \sim t^{2/5}$ both at early and at late times. Thus it never departs by very much from the classical Taylor solution for a strong shock. Mathematically speaking, such behavior is due to the finite range of variation of γ. Whenever γ is constant, the solution is of the form

$$\frac{R_s}{R_0} = \left\{ \frac{5}{2} \sqrt{\frac{m}{I(\gamma)}} \; \frac{ct}{R_0} \right\}^{2/5} + \text{const} \tag{212}$$

At early time, $\gamma \approx 2s - 1$, while at late time, $\gamma \to \frac{(m+1)}{(m-1)}$. Physically speaking, both of these limits must be viewed with some reservation until experimental evidence becomes available. At early time, the pressures generated in a porous target are less than in a nonporous one; thus the point-source assumption of instant destruction of the projectile is not as easy to justify. At the late-time limit, inviscid theory does not apply, because of the low pressures involved.

In any event, the evidence suggests that a porous substance will decelerate an impact shock wave more rapidly than the nonporous form of the same material. Whether this can be a useful design concept in protecting against meteoroid penetration depends upon a number of other systems considerations, of course, but it would appear that further study of the concept is warranted. In particular, studies of wave attenuation by internally instrumented targets would be very informative.

V CONCLUDING REMARKS

Status of Analytical Theory

The main purpose of the research described above has been to develop analytical methods for predicting the history of an impact-generated shock wave as it travels through a target. The problem is made complex by two factors: first, it is multidimensional, and second, the state equation of solids renders similarity methods inapplicable.

The present results indicate that the multidimensional nature of the problem can safely be ignored, if attention is restricted to quantities such as the shock trajectory. This conclusion is based upon approximate solutions along the axis of symmetry, and their comparison with solutions which assume the impact-generated flow field to be equivalent to one half of a symmetric disturbance. Such a conclusion had been reached previously by Rae and Kirchner[5] in the limit of extremely high impact speed, where similarity applies; the present results extend this conclusion to the range where nonsimilar effects are felt.

To account for the nonsimilarity of the problem, three approximate approaches have been studied and extended. One of these, called the Quasi-Steady method, has been developed more completely than the other two. The result is a simplified prediction, based on energy scaling, from which the history of the shock location, shock speed, shock pressure, etc., can be found for any material whose Hugoniot is known. This theory has proven successful in correlating all of the measured and calculated shock-trajectory data available at present. The only remaining discrepancies occur either at very early time, due to the plane-wave nature of the problem in the near vicinity of the impact point, or at very late time, due possibly to the onset of material-strength effects.

AI-1821-A-2

One of the most important results of the Quasi-Steady theory has been the identification of the scaling parameter R_o , proportional to the cube root of the projectile kinetic energy divided by the characteristic pressure $\rho_o c^2$ of the target, and the demonstration, by comparison with experiment and with computed results, of the ranges of this variable in which various types of shock motion can be observed. Thus, the perfect-gas, or similarity solution, in which $R_s \sim t^{2/5}$, can be detected only for times less than $10^{-2} R_o/c$, while the acoustic, or stress-wave, limit is encountered at times greater than $10\ R_o/c$. The intermediate, or transitional, regime is the one in which most present-day results lie. In all three regimes, the shock trajectory begins with a constant-speed, plane-wave phase, and approaches the point-source solution only after the projectile has been destroyed.

Suggestions for Further Research

Future improvements in the state of analytical theory could most profitably be sought in two areas. The first is concerned with accounting for the two-dimensional nature of the flow field. When approximate descriptions of this feature of the flow are obtained, they will permit the restriction to pure energy scaling to be removed.

The second area in need of improvement is the late-time portion of the problem. Even in the inviscid approximation, the law of decay of the shock pressure should be firmly established. Looking beyond that stage, the problem of material-strength effects is amenable to analytical study. A great deal of computational effort is presently being directed at this aspect of hypervelocity impact, and such analytical developments would be helpful in interpreting the numerical results.

It should be reiterated that the solutions described above are capable of supplying, with very little effort, a considerable amount of information -- for example, concerning the shock trajectory. Their advantage, in this regard, lies in their ability to handle unconventional problems very quickly. A significant example is the treatment, given above, of shock propagation in porous solids. Another such example is the application of the Quasi-Steady theory to the problem of shock propagation due to irradiation of a solid by an intense laser beam.[61]

Implications for Damage Effects

No report on the mechanics of hypervelocity impact should close without indicating how the studies in question contribute to our understanding of impact damage. While shock-propagation phenomena are of great interest in themselves, nonetheless the subject of most intense practical concern is the configuration in which the target material finally comes to rest.

At least three types of damage may be considered, depending on the thickness of the target. For very thin plates, whose role is to spread out the impulse of the projectile over a wider area, the essence of the problem is to determine the momentum distribution of the material coming from the back of the plate. Although this case has not been specifically investigated here, nevertheless the present studies have called attention to the significant effect of the low-density portions of the state equation.

For somewhat thicker plates, the most serious mode of deformation is that of spall fracture. Here, the present analyses supply important information, since the shape and amplitude of the incident compression wave must be known before the occurrence of such fractures can be pre-

dicted. The companion publication to this one[62] discusses in greater

detail the application of the present results to the spallation problem.

Finally, for targets which are effectively semi-infinite in extent, it

is desired to know the crater depth. Unfortunately, no theory based on

the inviscid-fluid model can offer any direct evidence on this question.

Physically speaking, the crater boundary takes shape along that line

where the material strength predominates to such an extent over normal

and shear forces that further removal of material ceases. This occurs

long after the point where the strengthless model is no longer valid.

To remedy the situation, some auxiliary criterion for defining the

crater size must be chosen, and its choice is crucial. The current dis-

agreement over the scaling laws for crater size[63] can be traced almost

entirely to differences in crater-formation criteria,[5] since all of the

published shock trajectories comply with essentially the same scaling law.

The two most prominent crater-formation criteria in use are those pro-

posed by Bjork[1] and by Walsh,[3] and the present studies bear, indirectly,

on both of these.

Bjork[1] identifies the crater boundary as the locus of points where

the pressure is extremely low, and the particle velocities randomly

oriented. The existence, noted above, of negative pressures in the state

equation used by Bjork for iron[*] raises a question about the validity of

the low-pressure portions of his results. Use of the inviscid model at

---

[*] It should also be noted that the Hugoniot curve for iron given by Bjork
(Figs. 3 and 4 of Ref. 1) is in error. It should be compared with the
experimental results listed by Rice, McQueen, and Walsh (Ref. 16) and
by Altshuler et al (Ref. 64) or with the Hugoniot determined from the state
equation used by Bjork (Fig. 1 of Ref. 18).

low pressure is always a questionable procedure, and the uncertainty is compounded when the state equation itself is suspect. What is needed is a quantitative statement of the pressure levels involved, and of the extent to which they are affected by the state equation.

Walsh[3] bases his criterion on the late-stage equivalence which he observes. His argument is that, if two different impacts give rise to the same flow patterns during the late stages of the inviscid phase, then the subsequent deformation during the strength-affected phases must also be the same. Thus, crater size is scaled by the same parameters as those which govern the late-stage equivalence.

By comparison, Walsh's criterion appears to the present author to be preferable. However, certain features of the present studies suggest that further examination of this criterion may be profitable. In particular, much of the evidence on which late-stage equivalence is based comes from integrated quantities, such as the total fluid momentum. It has been observed above that such integrals (in the case of the energy distribution) are rather insensitive to conditions at points whose distances from the origin are less than about 1/3 of the shock radius. But these are the particles that will eventually form the crater boundary. It would be a more sensitive test of late-stage equivalence if some parameter could be chosen that does not heavily weight the influence of particles near the shock, but rather emphasizes the role of the relatively less dense material. It has been pointed out, in this connection (Ref. 5, page 43) that the time scales for shock propagation in different targets under identical impact conditions appear to be different from the time scales that govern the ejection of material from the crater.

AI-1821-A-2

In summary, it can be said that the approximate analytic solutions discussed above properly account for nonsimilarity, accurately predict the shock trajectory, and focus attention on the need for better information on the state equation at low pressure. Future improvements should seek a better description of the two-dimensional nature of the solution, and should begin to account for the influence of material-strength effects.

REFERENCES

1. Bjork, R. L., Effects of a Meteoroid Impact on Steel and Aluminum in Space. Tenth International Astronautical Congress Proceedings (Springer-Verlag, 1960), Vol. II, pp. 505-514.

2. Bjork, R. L., Analysis of the Formation of Meteor Crater, Arizona: A Preliminary Report. J. Geophys. Research 66, 3379-3387 (1961).

3. Walsh, J. M. and Tillotson, J. H., Hydrodynamics of Hypervelocity Impact. Proc. of the Sixth Symp. on Hypervelocity Impact, Vol. 2, Pt. 1, pp. 59-104 (Aug. 1963). Also available as General Atomic Div., General Dynamics Corp., Rept. GA-3827, AD 401023 (Jan. 22, 1963).

4. Walsh, J. M., Johnson, W. E., Dienes, J. K., Tillotson, J. H., and Yates, D. R., Summary Report on the Theory of Hypervelocity Impact. General Atomic Div., General Dynamics Corp., Rept. GA-5119, AD 436251 (March 31, 1964).

5. Rae, W. J. and Kirchner, H. P., A Blast-Wave Theory of Crater Formation in Semi-Infinite Targets. Proc. of the Sixth Symp. on Hypervelocity Impact, Vol. 2, Pt. 1, pp. 163-227 (Aug. 1963).

6. Oshima, K., Blast Waves Produced by Exploding Wire. Aeronaut. Res. Inst., Univ. of Tokyo, Rept. No. 358 (July 1960).

7. Porzel, F. B., Height of Burst for Atomic Bombs, 1954; Part I, The Free-Air Curve. Los Alamos Scientific Lab. Rept. LA-1664 (May 1954). Declassified Sept. 1, 1960.

8. Zaker, T. A., Point Source Explosion in a Solid. Armour Research Foundation, Illinois Inst. of Tech., Rept. ARF 4132-6 (Nov. 1959).

9. Eichelberger, R. J. and Gehring, J. W., Effects of Meteoroid Impacts on Space Vehicles. ARS J. *32*, 10, 1583-1591 (Oct. 1962).

10. Halperson, S. M. and Hall, D. A., Shock Studies in Transparent Plastic by High-Speed Photographic Techniques. Reports of NRL Progress, pp. 37-39 (Sept. 1961).

11. Kinslow, R., Observations of Hypervelocity Impact of Transparent Plastic Targets. AEDC-TDR-64-49 (May 1964).

12. Frasier, J. T., Hypervelocity Impact Studies in Wax. Ballistic Res. Lab. Rept. No. 1124 (Feb. 1961).

13. Frasier, J. T. and Karpov, B. G., Impact Experiments on Wax. Proc. of the Fifth Symp. on Hypervelocity Impact, Vol. 2, Pt. 2, pp. 371-388 (April 1962).

14. Kynch, G. J., Blast Waves, Modern Developments in Fluid Dynamics. (Ed. by L. Howarth, Oxford, Clarendon Press, 1953), Vol. I, Part IV, Section II.

15. Sedov, L. I., Similarity and Dimensional Methods in Mechanics. (Academic Press, New York, 1959).

16. Rice, M. H., McQueen, R. G., and Walsh, J. M., Compression of Solids by Strong Shock Waves, Solid State Physics, Advances in Research and Applications. (Academic Press, New York, 1958), Vol. 6.

17. Tillotson, J. H., Metallic Equations of State for Hypervelocity Impact. General Atomic Div., General Dynamics Corp., Rept. GA-3216 (July 18, 1962).

18. Rae, W. J. and Kirchner, H. P., Final Report on a Study of Meteoroid Impact Phenomena. Cornell Aero. Lab. Rept. RM-1655-M-4, N63-16887 (Feb. 1963).

19. Bull, G. V., Murphy, C. L., Zwarts, F., and Friend, W., Review of Hypervelocity Impact Studies at McGill University. McGill Univ. Rept. 63-15 (Dec. 1963).

20. Riney, T. D., Solution of Visco-Plastic Equations for Axisymmetric Hypervelocity Impact. Second Summary Rept., 3 Nov. 1961 - 2 Nov. 1962, APGC TDR-62-74, AD 294959 (Dec. 1962).

21. Shanfield, I., Lee, J. H. S., and Bach, G. G., A Finite Difference Solution for the Cylindrical Expansion of a Gas Cloud into Vacuum. McGill Univ. Rept., NASA CR-54254 (1965).

22. Benedek, G. B., The Temperature of Shock Waves in Solids. Harvard Univ., Cruft Lab., Tech. Rept. 316 (Jan. 1960).

23. Wackerle, J., Shock-Wave Compression of Quartz. J. Appl. Phys. 33, 922-937 (1962).

24. Walsh, J. M., and Christian, R. H., Equation of State of Metals from Shock Wave Measurements. Phys. Rev. 97, 1544-1556 (1955).

25. Enig, J. W., A Complete E, P, V, T, S, Thermodynamic Description of Metals Based on the P, u Mirror-Image Approximation. J. Appl. Phys. 34, 746-754 (1963).

26. Sakurai, A., On the Propagation and Structure of the Blast Wave, I. J. Phys. Soc. Japan 8, 662-669 (1953).

27. Kochina, N. N., On Particularities Near the Detonation Center and on the Appearance of Two Shock Waves. Sov. Phys. --Doklady 4, 3, 544-548 (Dec. 1959).

28. Oshima, K., Quasi-Similar Solutions of Blast Waves. Aeronaut. Res. Inst., Univ. of Tokyo, Rept. No. 386 (March 1964).

29.   Taylor, G. I., The Formation of a Blast Wave by Very Intense Explosion, I, Theoretical Discussion. Proc. Roy. Soc. A201, 159-174 (1950).

30.   Lewis, C. H., Plane, Cylindrical, and Spherical Blast Waves Based upon Oshima's Quasi-Similarity Model. AEDC-TN-61-157 (Dec. 1961).

31.   Cole, R. H., Underwater Explosions. (Princeton Univ. Press, 1948).

32.   Lees, L. and Kubota, T., Inviscid Hypersonic Flow over Blunt-Nosed Slender Bodies. J. Aeronaut. Sci. 24, 195-202 (1957).

33.   Oshima, K., Blast Waves Produced by Exploding Wires, Exploding Wires. (Ed. by W. G. Chace and H. K. Moore, Plenum Press, New York, 1962), Vol. 2, pp. 159-180.

34.   Bethe, H. A., Fuchs, K., Hirschfelder, J. O., Magee, J. L., Peierls, R. E., and von Neumann, J., Blast Wave. Los Alamos Scientific Lab. Rept. LA-2000 (Aug. 1947).

35.   Taylor, J. L., An Exact Solution of the Spherical Blast-Wave Problem. Phil. Mag. 46, 317-320 (1955).

36.   Latter, R., Similarity Solution for a Spherical Shock Wave. J. Appl. Phys. 26, 954-960 (1955).

37.   Sakurai, A., An Exact Solution of the Blast-Wave Problem. J. Phys. Soc. Japan 10, 827-828 (1955).

38.   Rayzer, Yu. P., Motion of a Gas Generated by a Concentrated Explosion on the Surface. Zhurnal Prikladnoi Mekhaniki i Tekhnicheskoi Fiziki, No. 1, 57-66 (Jan. - Feb. 1963) (In Russian). Translated by M. J. Nowak, as General Atomic Div., General Dynamics Corp., Rept. GA-tr-5081, AD 440513 (May 28, 1964) and also by the Foreign Technology Division, Air Force Systems Command, FTD-MT-63-80, AD 434954 (24 Sept. 1963).

39. Mirels, H., Hypersonic Flow over Slender Bodies Associated with Power Law Shocks. *Advances in Applied Mechanics* (Academic Press, New York, 1962), Vol. VII.

40. Anderson, D. C., Fisher, R. D., McDowell, E. L., and Weidermann, A. H., Close-In Effects from Nuclear Explosions. AFSWC-TDR-63-53, AD 411132 (May 1963).

41. Deribas, A. A. and Pokhozhaev, S. I., Problem of a Point Explosion on the Surface of a Liquid. Sov. Phys.--Doklady 7, 5, 383-384 (Nov. 1962).

42. Kang, Gi Mang, An Investigation of Some Problems in the Nonsteady Motion of Liquids. Lomonosov State Univ., Dissertation (1957).

43. von Neumann, J. and Richtmeyer, R. D., A Method for the Numerical Calculation of Hydrodynamic Shocks. J. Appl. Phys. 21, 232-237 (1950).

44. Brocher, E. F., On Similar Solutions for Strong Blast Waves and their Application to Steady Hypersonic Flow. J. Aerospace Sci. 29, 694-701 (1962).

45. Heyda, J. F. and Riney, T. D., Peak Axial Pressures in Semi-Infinite Media under Hypervelocity Impact. Gen. Elec. Co., Space Sciences Lab. Rept. R64SD87 (Nov. 1964).

46. Charest, J. A., Measurements of Shock-Wave Pressures Generated by Hypervelocity Impacts in Aluminum. Gen. Motors Corp., Defense Res. Labs, Tech. Rept. TR64-58 (Nov. 1964).

47. Karpov, B. G., Transient Response of Wax Targets to Pellet Impact at 4 Km/sec. Ballistic Res. Lab. Rept. No. 1226, AD 428221 (Oct. 1963).

48. Drummond, W. E., Multiple Shock Production. J. Appl. Phys. 28, 9, 998-1001 (Sept. 1957).

49. Bancroft, D., Peterson, E. L., and Minshall, S., Polymorphism of Iron at High Pressure. J. Appl. Phys. 27, 3, 291-298 (March 1956).

50. Curran, D. R., Nonhydrodynamic Attenuation of Shock Waves in Aluminum. J. Appl. Phys. 34, 9, 2677-2685 (Sept. 1963).

51. Nowak, M. J., Some Fundamental Properties of Shock Waves. General Atomic Div., General Dynamics Corp., Rept. GAMD-2288, AD 404646 (June 1, 1961).

52. Austing, J. L., Napadensky, H. S., Stresau, R. H., and Savitt, J., Strong Shocks in Porous Media. Proc. 3rd Symp. on Detonation, Princeton, Sept. 26-28, 1960. ONR Symposium Rept. ACR-52, Vol. 2, pp. 396-419, AD 242586.

53. Pipitone, S. J. and Reynolds, B. W., Effectiveness of Foam Structures for Meteoroid Protection. J. Spacecraft and Rockets 1, 1, 37-43 (Jan. - Feb. 1964).

54. Summers, J. L. and Nysmith, C. R., The Resistance of a Variety of Composite Space Structures to Hypervelocity Impact. NASA TM X-54,025 (Jan. 1964).

55. Zimmerman, F. J., Fiber Metals for Meteoroid Protection. AIAA 5th Annual Structures and Materials Conf., AIAA CP-8, pp. 402-413 (1964).

56. Payton, R. G., Shock-Wave Propagation in Solid and Compactible Media. J. Acoust. Soc. Am. 35, 4, 525-534 (April 1963).

57. Krupnikov, K. K., Brazhnik, M. I., and Krupnikova, V. P., Shock Compression of Porous Tungsten. Sov. Phys.--JETP 15, 470-476 (1962).

58. Kormer, S. B., Funtikov, A. I., Urlin, V. D., and Kolesnikova, A. N., Dynamic Compression of Porous Metals and the Equation of State with Variable Specific Heat at High Temperatures. Sov. Phys.--JETP 15, 477-488 (1962).

59. Altshuler, L. V., Krupnikov, K. K., Ledenev, B. N., Zhuchikhin, V. I., and Brazhnik, M. I., Dynamic Compressibility and Equation of State of Iron under High Pressure. Sov. Phys.--JETP 34, (7), 4, 606-614 (1958).

60. Bass, R. C., Hawk, H. L., and Chabai, A. J., Hugoniot Data for Some Geologic Materials. Sandia Corp. Rept. SC-4903 (RR) (June 1963).

61. Rae, W. J. and Hertzberg, A., On the Possibility of Simulating Meteoroid Impact by the Use of Lasers. Cornell Aeronaut. Lab. Rept. AI-1821-A-1, NASA CR-54029 (April 1964) N64-19788.

62. Rae, W. J., Comments on the Solution of the Spall-Fracture Problem in the Approximation of Linear Elasticity. Cornell Aeronaut. Lab. Rept. AI-1821-A-3, NASA CR-54250 (Jan. 1965).

63. Eichelberger, R. J., Summary: Theoretical and Experimental Studies of Crater Formation. Proc. of the Sixth Hypervelocity Impact Symp., Vol. 2, Pt. 2, pp. 683-705 (Oct. 1962).

64. Altshuler, L. V., Bakanova, A. A., and Trunin, R. F., Shock Adiabats and Zero Isotherms of Seven Metals at High Pressures. Sov. Phys.--JETP 15, 1, 65-74 (July 1962).

65. Cohen, A., *An Elementary Treatise on Differential Equations*. (Heath and Co., 1933), 2nd ed.

66. Brode, H. L. and Bjork, R. L., Cratering from a Megaton Surface Burst. Rand Corp., RM-2600 (June 30, 1960) AD 250380.

67. Lake, H. R. and Todd, F. C., Digital Computer Solution for the Propagation of a Spherical Shock Wave in Aluminum. Paper presented at the Oklahoma Academy of Science Meeting, Dec. 14-15, 1961. NASA Accession N62-11438.

68. Sodek, B. A. and Todd, F. C., Penetration of an Initially Radial Shock Wave Through an Aluminum-Glass Interface. Proc. Oklahoma Acad. Sci. 43, 173-182 (1962).

APPENDIX A

STATE EQUATIONS

In Ref. 2, Bjork presents the state equation which he uses for iron, crediting it to Dr. F. H. Harlow of the Los Alamos Scientific Laboratory. It has the form

$$p = \left\{ 7.780 \times 10^4 (\psi - 1) + 31.18 \times 10^4 (\psi - 1)|\psi - 1| \right.$$

$$+ \rho_0 (e - e_0) \left[959.1 + 1568 (\psi - 1) + 463.4 (\psi - 1)^2 \right] \qquad \text{(A-1)}$$

$$\left. + \rho_0^2 (e - e_0)^2 \left[0.3984 + 0.5306 (\psi - 1) \right] \right\} \frac{1}{900 + \rho_0 (e - e_0)}$$

where $\psi = \rho/\rho_0$ and where the megagram, millisecond, meter system of units is used. Thus the density ρ_0 is 7.86 gm/cm^3 = 7.86 Mgm/m^3. The internal energy $e - e_0$ has the units (m/msec)^2, or (km/sec)^2, and the pressure is in Mgm/(msec)^2-m or 10^{-2} Mbars. For $\psi \geqslant 1$, Riney[20] uses the same relation, and also credits it to Harlow.* For $\psi < 1$, Bjork apparently continues to use Eq. (A-1), while Riney's formulation -- Eq. (55) -- takes the form

$$p = \left\{ 7.780 \times 10^4 (\psi - 1) + \rho_0 (e - e_0) \left[959.1 + 1568 (\psi - 1) \right] \right.$$

$$\text{(A-2)}$$

$$\left. + \rho_0^2 (e - e_0)^2 \left[0.3984 + 0.5306 (\psi - 1) \right] \right\} \frac{1}{900 + \rho_0 (e - e_0)}$$

---

* Riney's version contains several factors involving parameters ξ_1 and ξ_2. Dr. Riney has informed the author in a private communication (September 15, 1964) that these parameters have been set equal to zero in all calculations to date. It should also be noted that the absolute value sign in the first line of Eq. (A-1) is absent from Riney's formula. For $\psi \geqslant 1$, its absence makes no difference.

The state equation used in Walsh's calculations has the form, for condensed states

$$p = \left\{ a + \frac{b}{\frac{e-e_0}{E_0 \psi^2} + 1} \right\} \rho(e-e_0) + A(\psi-1) + B(\psi-1)^2 \qquad (A-3)$$

while for expanded states it has the form

$$p = a\rho(e-e_0)$$
$$+ \left\{ \frac{b\rho(e-e_0)}{\frac{e-e_0}{E_0 \psi^2} + 1} + A(\psi-1) \, exp\left[-\beta\left(\frac{\rho_0}{\rho}-1\right)\right] \right\} exp\left[-\alpha\left(\frac{\rho_0}{\rho}-1\right)^2\right] \qquad (A-4)$$

In these relations, the pressure is in megabars, the internal energy in Mbar-cm^3/gm, and the constants, for iron, are[17]

$$a = 0.5$$
$$b = 1.5$$
$$A = 1.279 \text{ Mbar}$$
$$B = 1.05 \text{ Mbar}$$
$$E_0 = 0.095 \text{ Mbar-cm}^3/\text{gm}$$
$$\alpha = \beta = 5$$

APPENDIX B

ALTERNATE DERIVATION OF TEMPERATURE ON AN ISENTROPE

This Appendix contains an alternate derivation of Eq. (70). The method is due to Sedov (Ref. 15) who points out (p. 233) that because

$$d\Delta = \frac{de + p\, d\,(1/\rho)}{T} \tag{B-1}$$

is a perfect differential, it follows that a partial differential equation for T can be derived from the exactness condition. In general, if

$$du = M\,dx + N\,dy \tag{B-2}$$

is exact, then

$$\frac{\partial N}{\partial x} - \frac{\partial M}{\partial y} = 0 \tag{B-3}$$

If the state equation is given in the form

$$e = e(p,\rho) \tag{B-4}$$

then

$$d\Delta = \frac{1}{T}\left\{ \left(\frac{\partial e}{\partial p}\right)_{\rho} dp + \left(\frac{\partial e}{\partial \rho}\right)_{p} d\rho - \frac{p}{\rho^2}\, d\rho \right\} \tag{B-5}$$

and the exactness condition, after multiplication by $\rho^2 T^2$, has the form

$$T + \left(\frac{\partial T}{\partial p}\right)_{\rho} \left[\rho^2 \left(\frac{\partial e}{\partial \rho}\right)_{p} - p \right] - \rho^2 \left(\frac{\partial e}{\partial p}\right)_{\rho} \left(\frac{\partial T}{\partial \rho}\right)_{p} = 0 \tag{B-6}$$

This partial differential equation may be written in the form of three ordinary differential equations

$$\frac{dT}{T} = \frac{dp}{p - \rho^2 \left(\frac{\partial e}{\partial \rho}\right)_p} = \frac{dp}{\rho^2 \left(\frac{\partial e}{\partial p}\right)_\rho} \tag{B-7}$$

by using the method of Lagrange (see, for example, Ref. 65, p. 250). The method states that, in general, the problem of solving

$$P(x, y, z)\left(\frac{\partial z}{\partial x}\right)_y + Q(x, y, z)\left(\frac{\partial z}{\partial y}\right)_x - R(x, y, z) = 0 \tag{B-8}$$

is equivalent to the solution of the system of ordinary differential equations

$$\frac{dx}{P} = \frac{dy}{Q} = \frac{dz}{R} \tag{B-9}$$

If this set has the two solutions

$$u(x, y, z) = c_1 \quad \text{and} \quad v(x, y, z) = c_2 \tag{B-10}$$

then the general solution of (B-8) is

$$u = f(v) \tag{B-11}$$

where f is an arbitrary function.

For the Mie-Grüneisen equation

$$e = \frac{p}{\rho \Gamma(\rho)} - \Delta(\rho) \tag{B-12}$$

one of Eqs. (B-7) is

$$\frac{dT}{T} = \frac{\Gamma(\rho)\,d\rho}{\rho}$$

(B-13)

whose solution is

$$T = c_1 \exp\left[\int \frac{\Gamma(\rho)\,d\rho}{\rho}\right]$$

(B-14)

The second of Eqs. (B-7)

$$\frac{dp}{d\rho} = \frac{p - \rho^2\left(\frac{\partial \varepsilon}{\partial \rho}\right)_p}{\rho^2\left(\frac{\partial \varepsilon}{\partial p}\right)_\rho}$$

(B-15)

is a relation for the p, ρ coordinate of an isentrope, as can be seen by comparison with Eq. (56). Thus the solution of (B-15) is found to be

$$\frac{p}{\rho\Gamma(\rho)} = \Delta(\rho) + \exp\left[\int \frac{\Gamma(\rho)\,d\rho}{\rho}\right]\left\{\int \frac{\Gamma(\rho)\Delta(\rho)}{\rho}\exp\left[-\int\frac{\Gamma(\rho)\,d\rho}{\rho}\right] + c_2\right\}$$

(B-16)

which is the same equation for an isentrope already derived in Eq. (44). The general solution for the temperature field is therefore

$$T = \exp\left[\int \frac{\Gamma(\rho)\,d\rho}{\rho}\right] \times \text{fcn}(\Delta)$$

(B-17)

where Δ is the entropy. In particular, along an isentrope,

$$\frac{T}{T_H} = \exp\left[-\int_\rho^{\rho_H} \frac{\Gamma(\rho)\,d\rho}{\rho}\right]$$

(B-18)

which is the result presented above (Eq. (70)).

APPENDIX C

COLLECTION OF SHOCK-WAVE TRAJECTORY DATA

The data shown in Figs. 13 and 15 come from a variety of sources. This Appendix lists the measurements used, and the quantities employed in reducing the data.

Eichelberger and Gehring[9] present data for a Lucite target struck by a steel projectile. The data listed in Table III below were taken from Fig. 5 of their paper.

The second set of Lucite experiments was reported by Halperson and Hall.[10] They state that their results have the form $\dot{R}_s = 8 \, R_s^{-1/4}$, where $\dot{R}_s$ is in mm/μsec, and R_s is in millimeters. Integration leads to

$$R_s = (5.62 \times 10^5 t)^{4/5} \tag{C-1}$$

where R_s is in cm, and t in seconds. This formula has been used to calculate the R_s , t entries in Table IV.

The third set of measurements in Lucite was taken by Piacesi (see p. 65). The projectile was a 1/4-inch-diameter aluminum sphere. The measurements are listed in Table V.

The first set of numerical results was reported by Bjork.[1] The quantities listed below as R_s are actually the distance along the axis of symmetry from the impact point to the shock. Because the shock itself is spread out over several mesh sizes by the artificial viscosity technique, the precise location of the shock is uncertain by several percent. The numbers quoted below in Table VI lie about halfway between the points of minimum and maximum pressure.

The same comments apply to the data from Bjork's calculation of iron striking tuff. [2] In reducing these data, the value $C = 2.21$ km/sec was used. This was found from the equation of state given by Brode and Bjork. [66] At low pressure, it has the form

$$p \approx A \frac{\rho}{\rho_0} \sqrt{e - e_0} \qquad (C-2)$$

where, if cgs units are used, the constant A has the units 5.30×10^5 $\frac{\text{dynes}}{\text{cm}^2} \left(\frac{\text{gm}}{\text{erg}} \right)^{1/2}$. Equating (C-2) and Eq. (8) gives

$$\frac{p_1}{A^2} \left(\frac{\rho_0}{\rho_1} \right)^2 = \frac{1}{2\rho_0} \left(1 - \frac{\rho_0}{\rho_1} \right) = \frac{1}{2\rho_0} \frac{u_1}{u_s} \qquad (C-3)$$

Thus, using Eq. (7)

$$p_1 = \rho_0 u_s^2 \frac{u_1}{u_s} = \frac{A^2}{2\rho_0} \left(\frac{\rho_1}{\rho_0} \right)^2 \frac{u_1}{u_s} \qquad (C-4)$$

or

$$u_s^2 = \frac{A^2}{2\rho_0^2} \left(\frac{\rho_1}{\rho_0} \right)^2 \qquad (C-5)$$

as $\frac{\rho_1}{\rho_0} \longrightarrow 1$, $u_s \longrightarrow C$

$$C^2 = \frac{A^2}{2\rho_0^2} \qquad (C-6)$$

Using $A = 5.30 \times 10^5 \frac{\text{gm}}{\text{sec-cm}^2}$ and $\rho_0 = 1.7$ gm/cm^3 gives $C = 2.21$ km/sec. The data is given in Table VII.

The third computed trajectory is that for iron striking iron at 40 km/sec, given by Walsh and Tillotson.[3] The R_s, t points, given in Table VIII, were found from Fig. 12 of Ref. 3, which presents the pressure p_1 behind the shock as a function of R_s. These pressures were converted to shock speeds by use of the Hugoniot curve (Fig. 8 of Ref. 17). The resulting graph of $1/\dot{R}_s$ vs R_s was then integrated (by Simpson's rule) to give R_s vs t. The shock speed was taken to be constant, at its impact-point value of 3.05×10^6 cm/sec for $0 < R_s < 1.36$ cm. The resulting trajectory is listed in Table VIII.

Another set of calculated trajectory data has been given by Lake and Todd (Fig. 7 of Ref. 67). These calculations assume a spherical wave, and neglect the θ-variation.* The results, given in Table IX, are for an iron projectile of mass 10^{-3} gm, striking aluminum at 4.75 km/sec (15,600 ft/sec) but reveal an extremely rapid rate of shock propagation. For example, at the latest time shown (6.9×10^{-10} sec) the average shock Mach number $M_{avg} = R_s/ct$ is 82.7. These data have not been included on Fig. 13.

Charest[46] has recently presented a set of measurements of the shock pressures developed in an aluminum target when struck at 7.32 km/sec by 0.476 cm diameter aluminum spheres. His data have been reduced, and appear in Table X.

Finally, Heyda and Riney[45] have presented computed results for a series of aluminum-aluminum and lead-lead interactions. Measurements

---

* The θ-variation is included in the formulation of Ref. 68, but the continuity equation used there is in error. The equation in question -- Eq. (1) of Ref. 68 -- is presented for the case of cylindrical, not spherical, polar coordinates (cf Eq. (1) above).

taken from their figures, and the associated values of R_s/R_o ,

ct/R_o , $p_{SH}/p_o c^2$ are given in Tables XI through XVI.

ACKNOWLEDGMENT

During the research reported here, the author has had the benefit of discussions with Messrs. Martin Gutstein, James J. Kramer, Gordon T. Smith, and Francis S. Stepka, all of the Lewis Research Center.

Table I
QUASI-STEADY PREDICTION OF SHOCK RADIUS, SHOCK-SPEED RELATION

	$1/M$	γ	R_s/R_o	$p_1/\rho_o c^2$	ρ_1/ρ_o
S = 1.2	.1	1.667	.347	75	4
	.2	2	.636	16.7	3
	.3	2.43	.959	6.49	2.4
	.4	3	1.34	3.12	2
	.5	3.8	1.813	1.67	1.714
	.6	5	2.43	0.925	1.5
	.7	7	3.28	.511	1.333
	.8	11	4.667	.260	1.2
	.886	20	6.96	.121	1.105
	.9415	40	10.75	.0550	1.052
	.9662	70	15.10	.0301	1.029
	.9762	100	18.72	.0208	1.020
S = 1.5	.1	2.33	.449	60	2.50
	.2	2.75	.795	18.25	2.14
	.3	3.29	1.174	5.20	1.87
	.4	4	1.619	2.50	1.667
	.5	5	2.16	1.333	1.50
	.6	6.5	2.85	.734	1.36
	.7	9	3.80	.409	1.25
	.8	14	5.34	.208	1.154
	.858	20	6.80	.130	1.105
	.926	40	10.62	.0569	1.052
	.958	70	15.0	.0307	1.029
	.970	100	18.65	.0211	1.020
S = 2	.1	3.44	.581	45.0	1.82
	.2	4	1.017	10	1.667
	.3	4.714	1.475	3.89	1.54
	.4	5.667	2	1.88	1.428
	.5	7	2.62	1.0	1.333
	.6	9	3.44	.556	1.25
	.7	12.333	4.55	.306	1.178
	.8	19	6.35	.156	1.111
	.81	20	6.56	.145	1.105
	.9023	40	10.45	.0600	1.052
	.9436	70	14.85	.0317	1.029
	.9604	100	18.50	.0214	1.020

AI-1821-A-2

Table II
QUASI-STEADY SOLUTION FOR SHOCK TRAJECTORY

R_s/R_o	$ct/R_o)_S = 1.2$	$ct/R_o)_S = 1.5$	$ct/R_o)_S = 2$
.5	.0356	.0206	.0198
1	.153	.1128	.0887
1.5	.342	.2706	.2144
2	.586	.4826	.3908
2.5	.873	.7386	.6116
3	1.194	1.0319	.8703
3.5	1.543	1.3546	1.160
4	1.914	1.7016	1.476
4.5	2.302	2.0686	1.814
5	2.704	2.4526	2.171
5.5	3.119	2.8496	2.543
6	3.542	3.2576	2.927
6.5	3.975	3.6756	3.324
7	4.415	4.1026	3.732
8	5.312	4.974	4.571
9	6.225	5.867	5.437
10	7.151	6.778	6.324
11	8.086	7.702	7.226
12	9.029	8.635	8.140
13	9.981	9.577	9.064
14	10.939	10.526	9.997
15	11.901	11.480	10.938
16	12.868	12.440	11.882
17	13.839	13.403	12.833
18	14.812	14.369	13.789
19	15.788	15.339	14.734

Table III
EICHELBERGER AND GEHRING (REF. 9) IRON - LUCITE

$M = 0.18$ gm $\qquad V = 4.6$ km/sec $\qquad c = 2.59$ km/sec

$R_o = 0.338$ cm $\qquad R_o/c = 1.304 \mu$ sec $\qquad \rho_o c^2 = 7.92 \times 10^{10}$ dynes/cm^2

t, μ sec	R_s, cm	ct/R_o	R_s/R_o
.674	.334	.516	.988
1.06	.540	.813	1.598
1.55	.77	1.19	2.27
2.10	.92	1.62	2.72
2.40	1.07	1.84	3.16
3.20	1.40	2.45	4.15
4.30	1.59	3.30	4.70
5.6	1.93	4.30	5.70
6.9	2.23	5.30	6.60
8.2	2.56	6.30	7.60

Table IV
HALPERSON AND HALL (REF. 10) ALUMINUM - LUCITE

$M = 1.0$ gm $\qquad V = 5.31$ km/sec $\qquad c = 2.59$ km/sec

$R_o = .610$ cm $\qquad R_o/c = 2.35 \mu$ sec $\qquad \rho_o c^2 = 7.92 \times 10^{10}$ dynes/cm^2

t, μ sec	R_s, cm	ct/R_o	R_s/R_o
1.780	1	0.755	1.640
1.780×10^1	6.3	7.55	10.3

Table V
PIACESI (PRIVATE COMMUNICATION) ALUMINUM -LUCITE

M = 0.361 gm $\qquad$ V = 5.7 km/sec $\qquad$ c = 2.59 km/sec

R_0 = 0.490 cm $\qquad$ R_0/c = 1.90 μsec $\qquad$ $\rho_0 c^2$ = 7.92 x 10^{10} dynes/cm^2

t, μ sec	R_s, cm	ct/R_0	R_s/R_0
1.076	0.75	0.565	1.53
2.552	1.50	1.345	3.06
4.028	2.05	2.11	4.19
5.504	2.55	2.90	5.20
6.980	3.17	3.66	6.48
8.456	3.69	4.45	7.51
9.932	4.20	5.22	8.59
11.41	4.71	6.00	9.61
12.88	5.08	6.80	10.3

Table VI
BJORK (REF. 1) IRON - IRON

M = 6160 gm $\qquad$ V = 5.5 km/sec $\qquad$ c = 4.0 km/sec

R_0 = 4.90 cm $\qquad$ R_0/c = 12.25 μsec $\qquad$ $\rho_0 c^2$ = 1.259 Mbar

t, μ sec	R_s, cm	ct/R_0	R_s/R_0
3.5	3.1	.286	.632
8.7	7.9	.710	1.61
81.7	36	6.68	7.35

Table VII
BJORK (REF. 2) IRON - TUFF

M = 1.065 x 10^{10} gm $\qquad$ V = 30 km/sec $\qquad$ c = 2.21 km/sec

R_0 = 46.5 meters $\quad$ R_0/c = 2.10 x 10^{-2} sec $\quad$ $\rho_0 c^2$ = 8.30 x 10^{10} dynes/cm^2

t, sec	R_s, meters	ct/R_0	R_s/R_0
.17 x 10^{-3}	5.5	8.10 x 10^{-3}	.118
.36 x 10^{-3}	11	1.72 x 10^{-2}	.236
3.44 x 10^{-3}	65	1.64 x 10^{-1}	1.40
6.36 x 10^{-3}	89	3.02 x 10^{-1}	1.92
9.25 x 10^{-3}	105	4.40 x 10^{-1}	2.25
24.8 x 10^{-3}	165	1.18	3.55
61 x 10^{-3}	260	2.90	5.60

Table VIII
WALSH AND TILLOTSON (REF. 3) IRON - IRON

M = 38.6 gm $\qquad$ V = 40 km/sec $\qquad$ c = 4.0 km/sec

R_o = 3.4 cm $\qquad$ R_o/c = 8.5 μsec $\qquad$ $\rho_o c^2$ = 1.259 Mbar

t, μsec	R_s, cm	p_1, Mbar	ct/R_o	R_s/R_o	$p_1/\rho_o c^2$
.450	1.37	–	.053	.403	–
.678	2	–	.0798	.589	–
.894	2.5	–	.105	.735	–
1.150	3	–	.135	.881	–
1.449	3.5	–	.170	1.03	–
1.787	4	–	.210	1.18	–
2.160	4.5	–	.255	1.32	–
2.566	5	–	.303	1.47	–
3.012	5.5	–	.355	1.62	–
3.497	6	–	.410	1.76	–
4.019	6.5	–	.474	1.91	–
4.586	7	–	.540	2.05	–
5.186	7.5	–	.610	2.20	–
5.812	8	–	.685	2.35	–
–	1.34	47.5	–	.394	37.8
–	2.7	17.5	–	.795	13.9
–	3.8	8.4	–	1.12	6.67
–	6.2	2.9	–	1.82	2.30
–	6.5	2.6	–	1.91	2.06
–	7.25	2.0	–	2.13	1.59
–	8.2	1.5	–	2.41	1.19

Table IX
LAKE AND TODD (REF. 67) IRON - ALUMINUM

M = 10^{-3} gm $\quad$ V = 4.75 km/sec $\quad$ c = 5.85 km/sec

R_o = 2.695 x 10^{-2} cm $\quad$ R_o/c = 4.61 x 10^{-8} sec

t, μsec	R_s, cm	ct/R_o	R_s/R_o
5.2 x 10^{-11}	9.12 x 10^{-2}	1.13 x 10^{-3}	3.39
1.6 x 10^{-10}	1.52 x 10^{-1}	3.47 x 10^{-3}	5.65
3.9 x 10^{-10}	2.41 x 10^{-1}	8.46 x 10^{-3}	8.95
6.9 x 10^{-10}	3.35 x 10^{-1}	1.5 x 10^{-2}	12.4

Table X
CHAREST (REF. 46) ALUMINUM - ALUMINUM

$M = 0.1525$ gm $\qquad V = 7.32$ km/sec $\qquad c = 5.85$ km/sec

$R_0 = 0.187$ cm $\qquad R_0/c = 0.320\,\mu\,\text{sec} \qquad \rho_0 c^2 = 0.924$ Mbar

R_s, cm	p_1, Mbar	R_s/R_0	$p_1,\rho_0 c^2$
0.51	.352	2.73	.381
0.76	.206	4.05	.224
1.02	.150	5.45	.162
1.02	.130	5.45	.141
1.53	.0786	8.20	.0850
1.91	.0496	10.2	.0538
2.54	.0315	13.6	.0341
3.05	.0239	16.3	.0259
3.55	.0198	19.0	.0215
4.80	.0120	25.6	.0130
6.40	.0076	34.1	.00822
7.61	.0053	40.8	.00573

Table XI
HEYDA AND RINEY (REF. 45) ALUMINUM - ALUMINUM

$M = 0.1525$ gm $\qquad V = 7.6$ km/sec $\qquad c = 5.85$ km/sec

$R_0 = 0.197$ cm $\qquad R_0/c = 0.337\,\mu\,\text{sec} \qquad \rho_0 c^2 = 0.924$ Mbar

t,μ sec	R_s, cm	p_1, Mbar	ct/R_0	R_s/R_0	$p_1/\rho_0 c^2$
.340	.315	1.155	1.01	1.60	1.25
.380	.345	1.110	1.13	1.75	1.20
.420	.380	.865	1.25	1.93	.935
.510	.410	.695	1.52	2.09	.750
.750	.615	.540	2.23	3.13	.584
.915	.750	.240	2.71	3.81	.260
.985	.790	.225	2.92	4.01	.244
1.050	.850	.226	3.11	4.32	.245
1.180	.920	.210	3.50	4.68	.227
1.320	.990	.211	3.91	5.02	.229
1.450	1.110	.110	4.30	5.63	.119

Table XIII
HEYDA AND RINEY (REF. 45) ALUMINUM – ALUMINUM

$M = .1525$ gm $\qquad$ $V = 20$ km/sec $\qquad$ $c = 5.85$ km/sec

$R_0 = .375$ cm $\qquad$ $R_0/c = .642\,\mu$sec $\qquad$ $\rho_0 c^2 = .924$ Mbar

t, μsec	R_s, cm	p_1, Mbar	ct/R_0	R_s/R_0	$p_1/\rho_0 c^2$
.200	.320	–	.311	.854	–
.210	.350	4.88	.328	.935	5.29
.232	.380	4.30	.362	1.015	4.65
.260	.415	3.95	.405	1.11	4.28
.285	.435	3.60	.445	1.16	3.90
.375	.555	1.52	.585	1.48	1.64
.410	.630	1.53	.640	1.68	1.66
.505	.695	1.37	.786	1.86	1.48
.555	.770	–	.865	2.05	–
.632	.825	0.94	.986	2.20	1.02
.750	.955	0.73	1.170	2.55	.790
.860	1.075	0.78	1.34	2.87	.843
1.045	1.110	0.43	1.64	2.96	.465
1.555	1.370	0.52	2.42	3.65	.561
1.823	1.770	0.23	2.85	4.73	.250
2.076	2.025	0.20	3.22	5.40	.216

AI-1821-A-2

Table XIII
HEYDA AND RINEY (REF. 45) ALUMINUM - ALUMINUM

$M = .1525$ gm $\qquad$ $V = 40$ km/sec $\qquad$ $c = 5.85$ km/sec

$R_o = .595$ cm $\qquad$ $R_o/c = 1.020$ sec $\qquad$ $\rho_o c^2 = .924$ Mbar

t, μsec	R_s, cm	ct/R_o	R_s/R_o
.122	.315	.120	.530
.133	.340	.130	.570
.140	.370	.137	.622
.158	.410	.155	.690
.165	.44	.162	.740
.181	.465	.178	.783
.191	.500	.187	.840
.252	.62	.247	1.04
.280	.69	.275	1.16
.310	.74	.305	1.24
.366	.82	.360	1.38
.396	.87	.390	1.46
.43	.92	.421	1.54
.48	1.0	.470	1.68
.52	1.05	.510	1.76
.58	1.15	.570	1.94
.74	1.25	.725	2.10
.88	1.35	.863	2.27
1.03	1.5	1.01	2.52
1.60	2.10	1.57	3.54
1.74	2.20	1.70	3.70
1.90	2.40	1.86	4.04

Table XIV
HEYDA AND RINEY (REF. 45) ALUMINUM – ALUMINUM

$M = .1525$ gm $V = 60$ km/sec $c = 5.85$ km/sec

$R_0 = .780$ cm $R_0/c = 1.332 \mu$sec $\rho_0 c^2 = .924$ Mbar

R_s, cm	t, μ sec	ct/R_0	R_s/R_0
.311	.087	.0653	.400
.340	.090	.0675	.435
.377	.102	.0766	.485
.41	.110	.0826	.526
.445	.121	.0910	.570
.48	.131	.0982	.615
.51	.141	.106	.652
.63	.180	.135	.809
.70	.202	.152	.897
.76	.230	.173	.972
.83	.260	.195	1.06
.90	.282	.212	1.16
.95	.331	.249	1.22
1.0	.370	.278	1.28
1.15	.44	.330	1.48
1.26	.56	.420	1.62
1.40	.63	.474	1.80
1.50	.70	.526	1.92
1.67	.84	.630	2.14
1.80	.96	.720	2.30
1.95	1.11	.832	2.50
2.08	1.25	.940	2.66
2.17	1.40	1.05	2.79
2.34	1.52	1.14	3.00
2.50	1.74	1.31	3.20
2.60	1.90	1.43	3.34

AI-1821-A-2

Table XV
HEYDA AND RINEY (REF. 45) LEAD-LEAD

$M = .641$ gm $\qquad V = 7.6$ km/sec $\qquad c = 2.07$ km/sec

$R_0 = .394$ cm $\qquad R_0/c = 1.904\ \mu$ sec $\qquad \rho_0 c^2 = .484$ Mbar

t, μ sec	R_s, cm	p_1, Mbar	ct/R_0	R_s/R_0	$p_1/\rho_0 c^2$
.40	.285	4.21	.210	.722	8.70
.45	.310	3.33	.236	.788	6.88
.50	.335	2.87	.263	.850	5.92
.55	.375	2.69	.290	.950	5.56
.60	.405	2.53	.315	1.03	5.21
.70	.424	1.78	.367	1.08	3.67
.80	.485	1.98	.420	1.23	4.09
.87	.560	1.23	.456	1.42	2.54
.95	.620	.95	.500	1.58	1.96
1.30	.685	.81	.682	1.74	1.67
1.62	.885	.61	.850	2.25	1.26
1.80	.950	.57	.946	2.41	1.18
2.00	1.01	.43	1.05	2.56	.89
2.17	1.07	-	1.14	2.72	-
2.31	1.11	.33	1.22	2.81	.67
2.70	1.24	.37	1.42	3.15	.765
4.70	1.76	.125	2.46	4.46	.258
5.90	2.03	.135	3.10	5.15	.278
6.29	2.28	.06	3.30	5.80	.124

Table XVI
HEYDA AND RINEY (REF. 45) LEAD – LEAD

$M = 0.641$ gm $V = 20$ km/sec $c = 2.07$ km/sec

$R_O = .751$ cm $R_O/c = .363 \mu$ sec $\rho_o c^2 = .484$ Mbar

t, μ sec	R_s, cm	p_1, Mbar	ct/R_O	R_s/R_O	$p_1/\rho_o c^2$
.16	.315	21.2	.0441	.420	43.9
.24	.350	-	.0660	.465	-
.28	.385	16.3	.0770	.512	33.7
.30	.410	14.8	.0829	.545	30.5
.31	.435	13.85	.0855	.580	28.6
.36	.495	10.3	.0992	.660	21.3
.40	.560	6.1	.110	.745	12.6
.46	.625	5.3	.127	.830	11.0
.53	.690	5.45	.146	.920	11.2
.60	.755	4.1	.166	1.00	8.48
.75	.820	3.6	.207	1.09	7.42
.90	.950	2.9	.248	1.26	6.00
1.05	1.08	2.4	.290	1.44	4.95
1.27	1.12	1.4	.350	1.49	2.90
1.62	1.25	1.7	.446	1.66	3.51
2.0	1.50	0.65	.551	2.00	1.34
2.71	1.77	0.6	.748	2.34	1.24
3.10	1.895	-	.856	2.52	-
3.37	2.025	0.45	.930	2.70	.93
4.20	2.280	0.40	1.16	3.04	.83

AI-1821-A-2

$$\frac{\rho_1}{\rho_0}$$

$$1 + \frac{2}{\Gamma}$$

$$\frac{1}{2\Gamma^2 + 4\Gamma}$$

$$\frac{\Gamma + 2}{\Gamma + 1}$$

$$\Delta / u_s^2$$

3

2

$$\frac{\rho_1}{\rho_0}$$

$\Gamma = 1$

$\Gamma = 2$

$\Gamma = 3$

1

0   .04   .08   .12   .16   .20

$$\frac{\Delta(\rho_1)}{u_s^2}$$
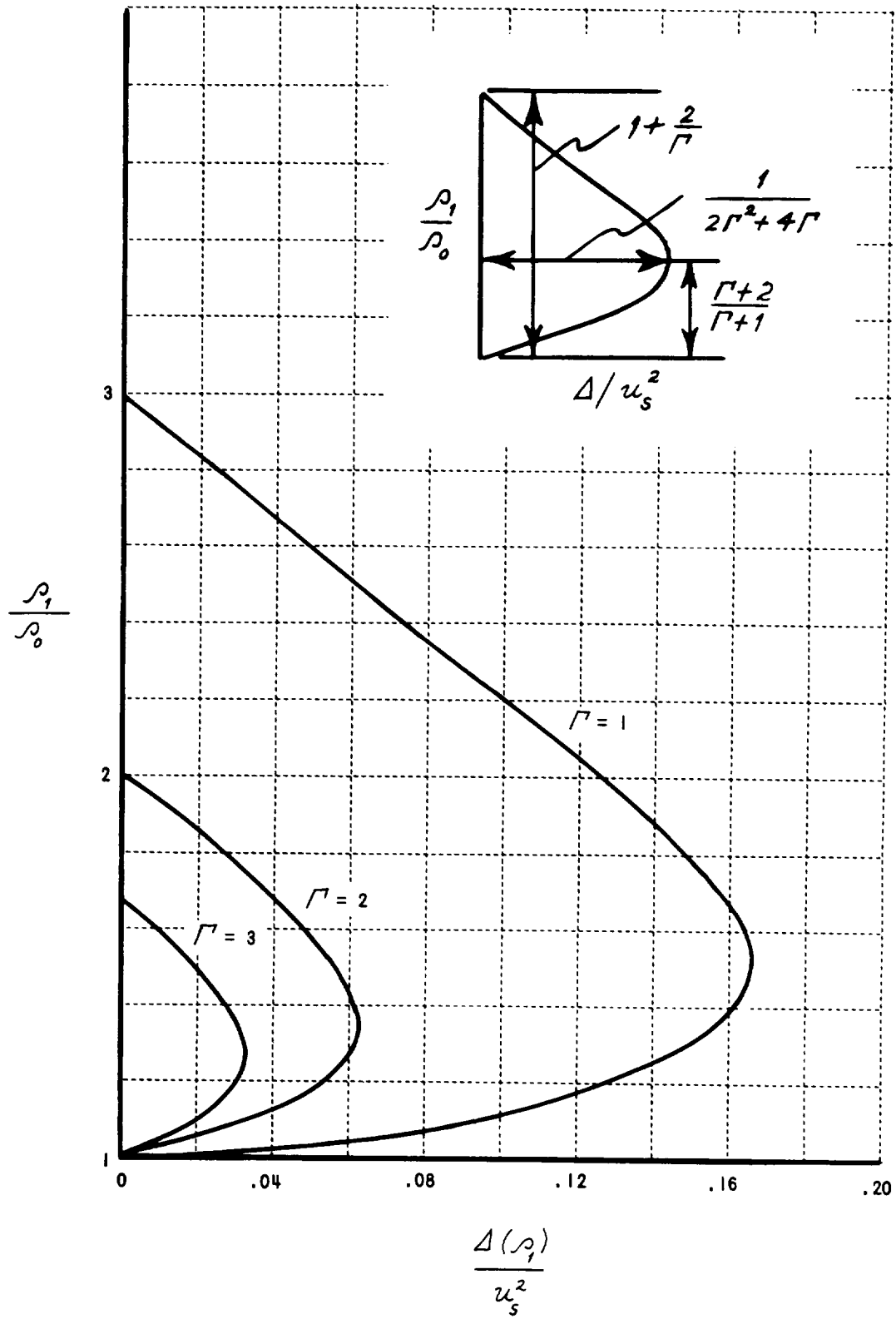
Figure I   GENERAL SHOCK-WAVE RELATIONS FOR THE MIE-GRÜNEISEN
EQUATION OF STATE
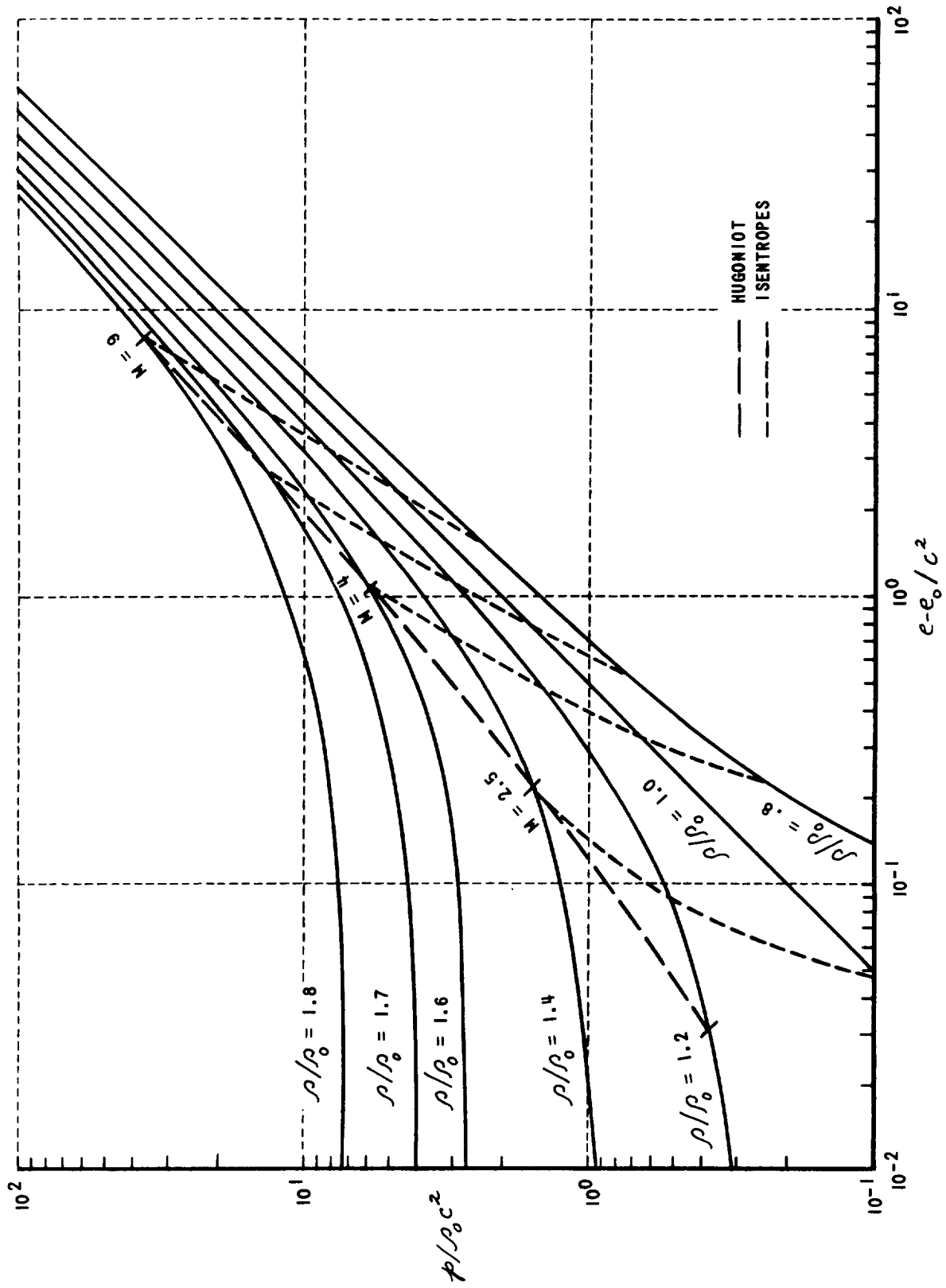
Figure 2a STATE EQUATION OF A C,S MEDIUM; S = 2
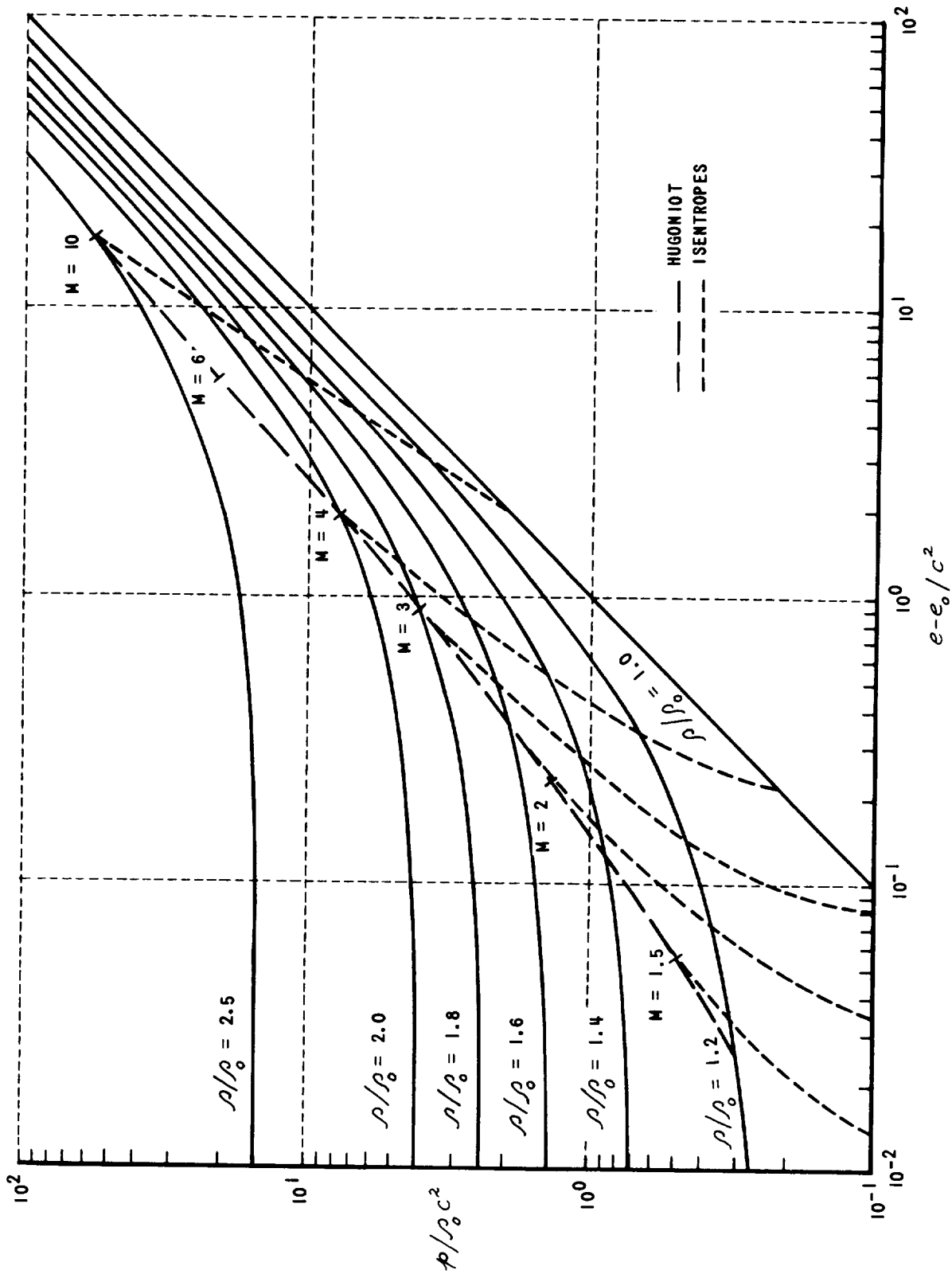
Figure 2b STATE EQUATION OF A C, S MEDIUM; S = 1.5

116
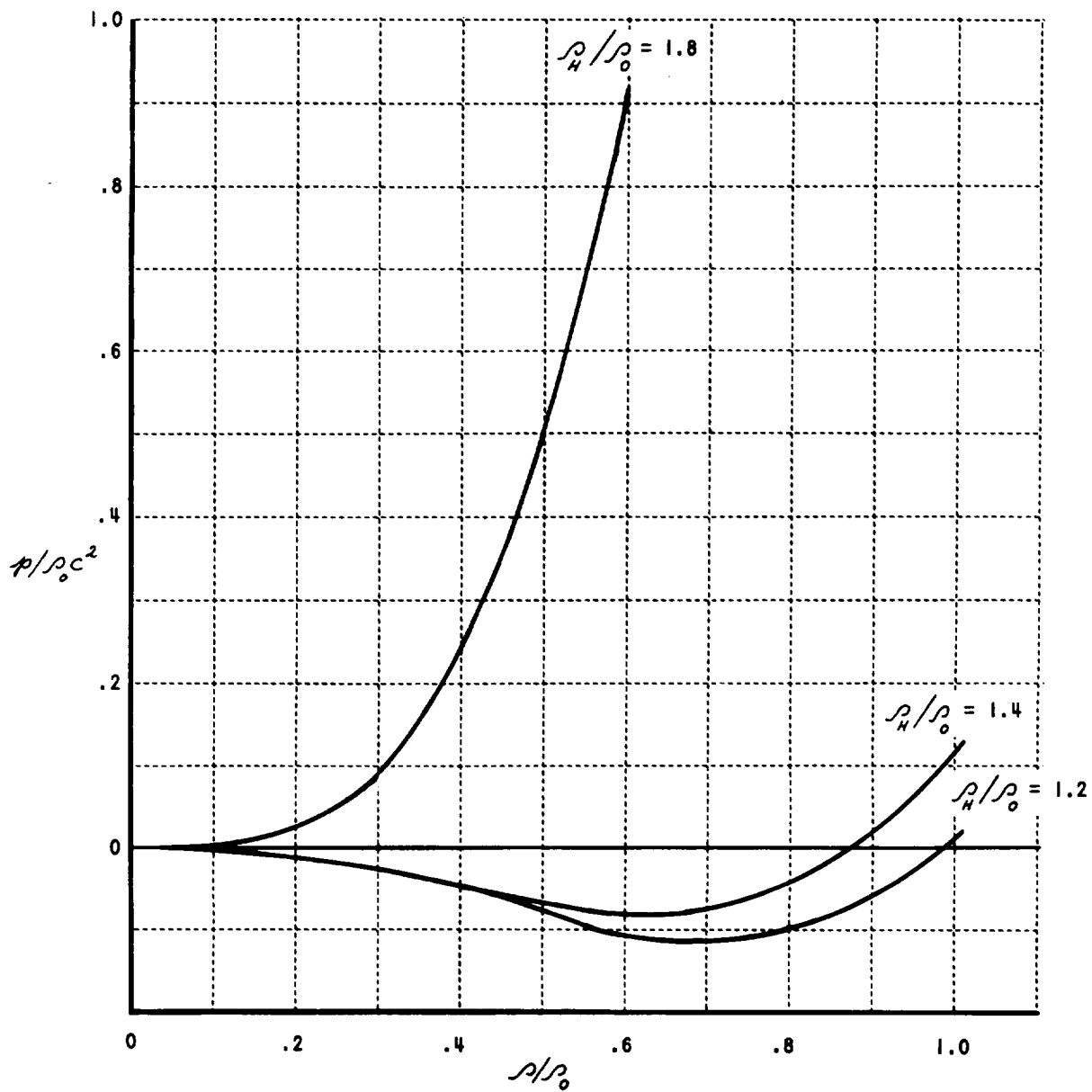
Figure 3   LOW-PRESSURE ISENTROPES IN THE C,S APPROXIMATION

AI-1821-A-2
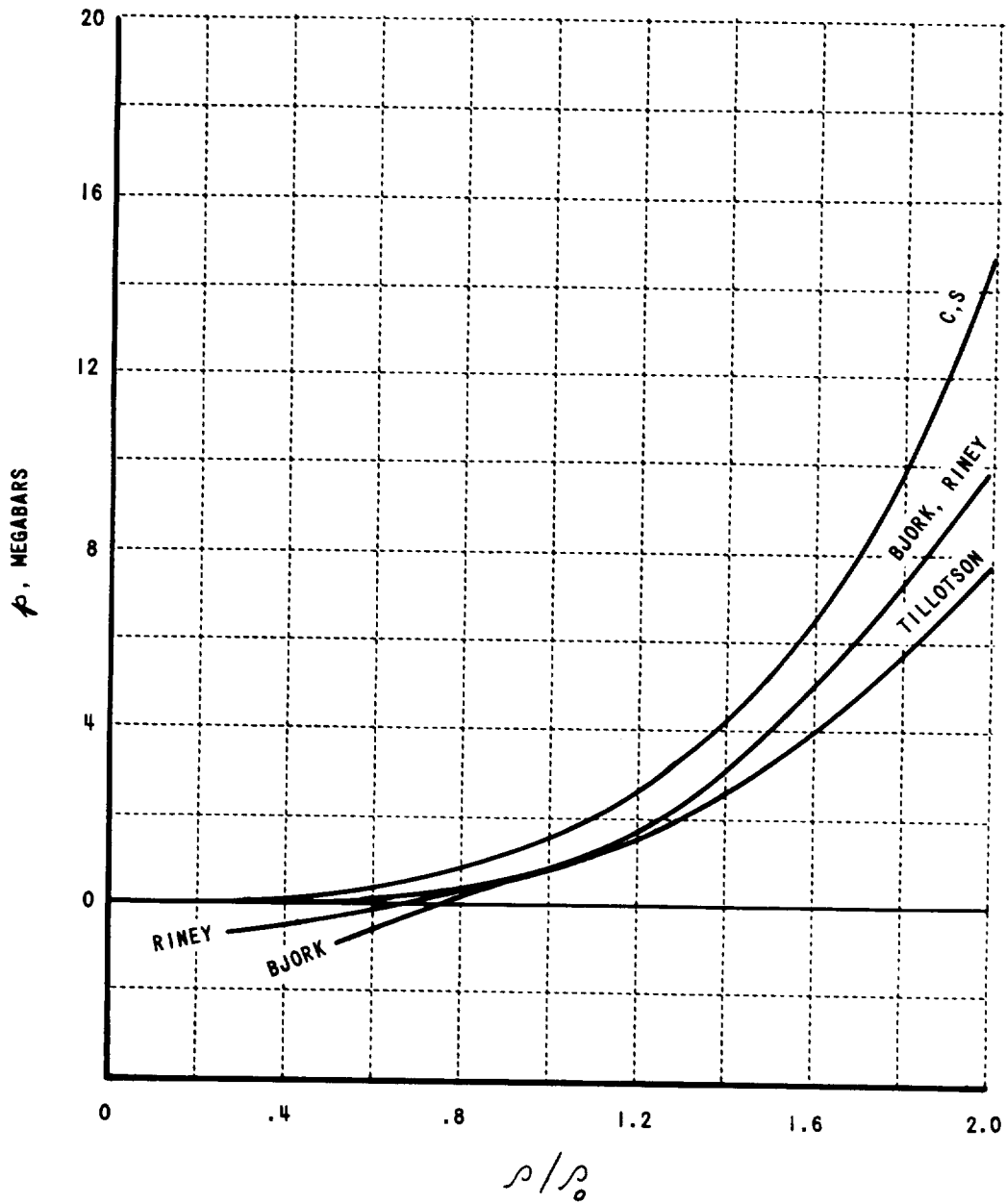
Figure 4 ISENTROPIC STATES OF IRON, ACCORDING TO SEVERAL STATE EQUATIONS

$$\rho_H / \rho_0 = 2.0$$

BROKEN LINE IS THE HUGONIOT; SOLID LINES ARE LINES OF CONSTANT $S\left(\frac{\rho_o}{\rho}-1\right)$

TABLE BELOW GIVES REPRESENTATIVE VALUES OF $\frac{\rho_o}{\rho}$ AND S

FOR SELECTED VALUES OF $S\left(\frac{\rho_o}{\rho}-1\right)$.

Ψ	S	$S\left(\frac{\rho_o}{\rho}-1\right)$
1.8	2	−8/9
1.7	2	−14/17
2	1.5	−3/4
1.6	2	−3/4
1.8	1.5	−2/3
1.6	1.5	−9/16
1.4	1.5	−3/7
1.2	2	−1/3
1.2	1.5	−1/4
1	−	0
.8	2	.5

Curve labels: −8/9, −4/17, −3/4, −2/3, −9/16, −3/7, −1/3, −1/4, 0, 0.5

Vertical axis: $S p / \rho_o c^2$

Horizontal axis: $S^2(e-e_o)/c^2$
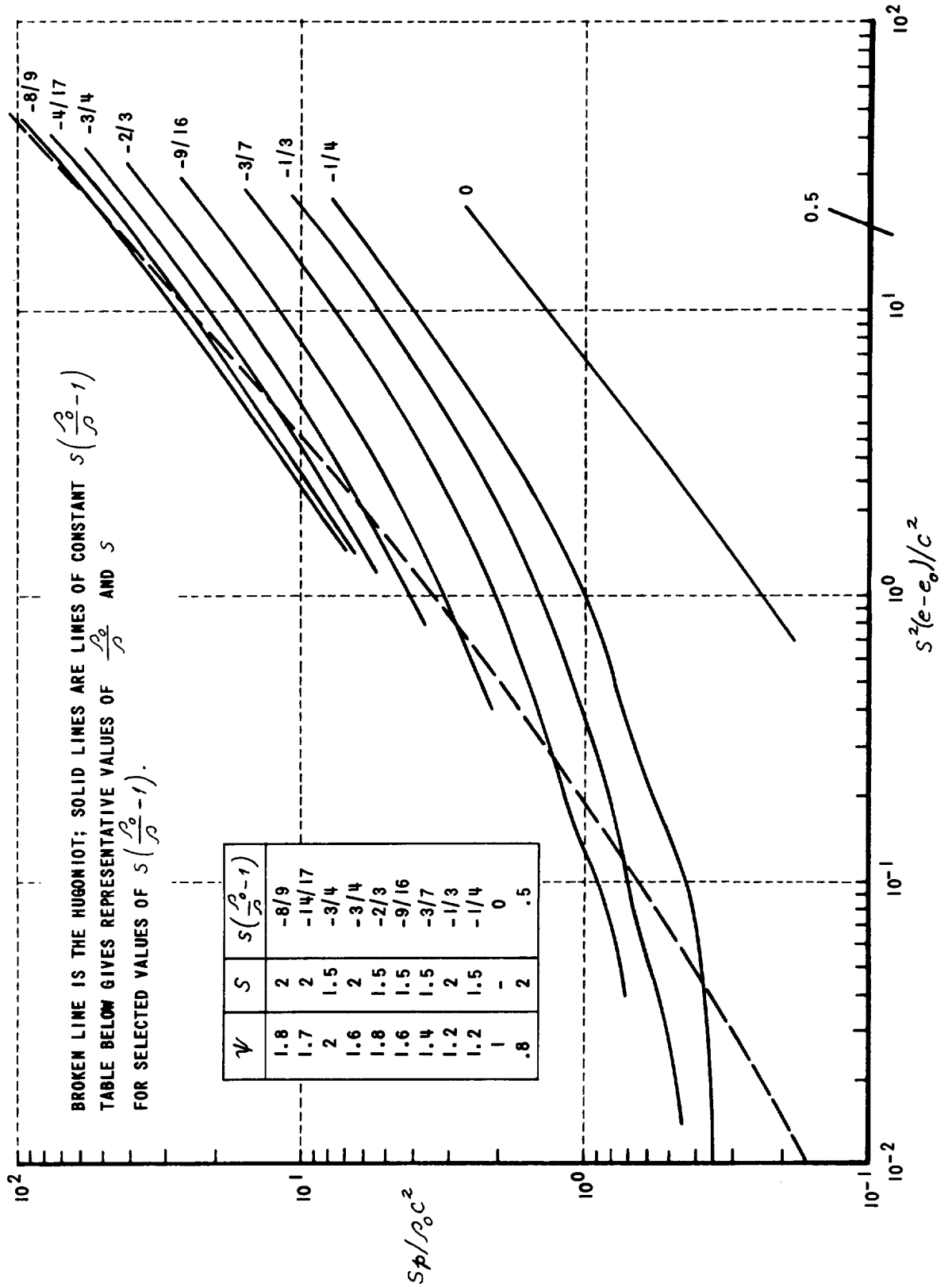
Figure 5 ENIG'S EQUATION OF STATE

119

AI-1821-A-2
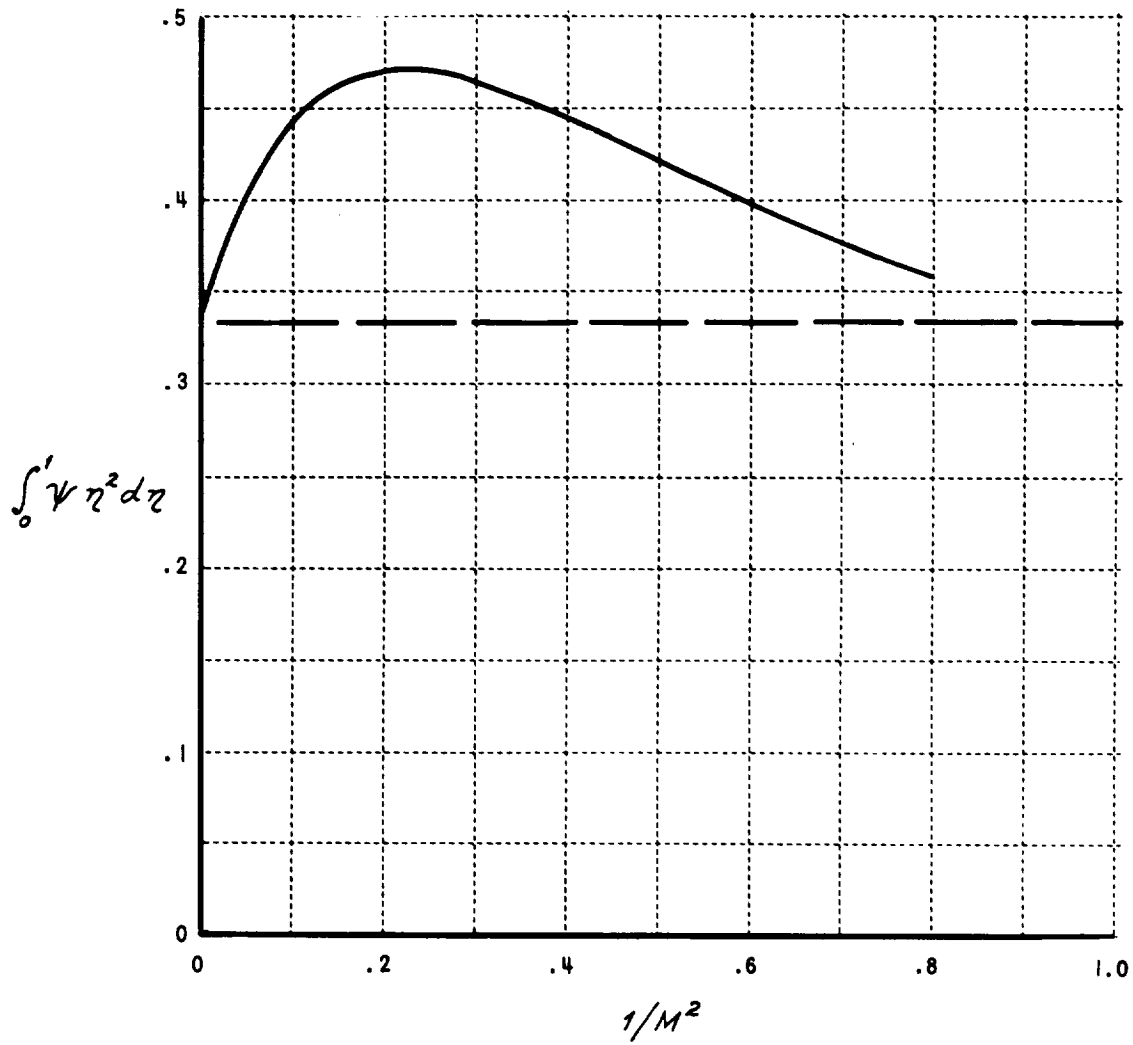
Figure 6   MASS-CONSERVATION ERROR IN OSHIMA'S PERFECT-GAS SOLUTION
(SPHERICAL CASE)
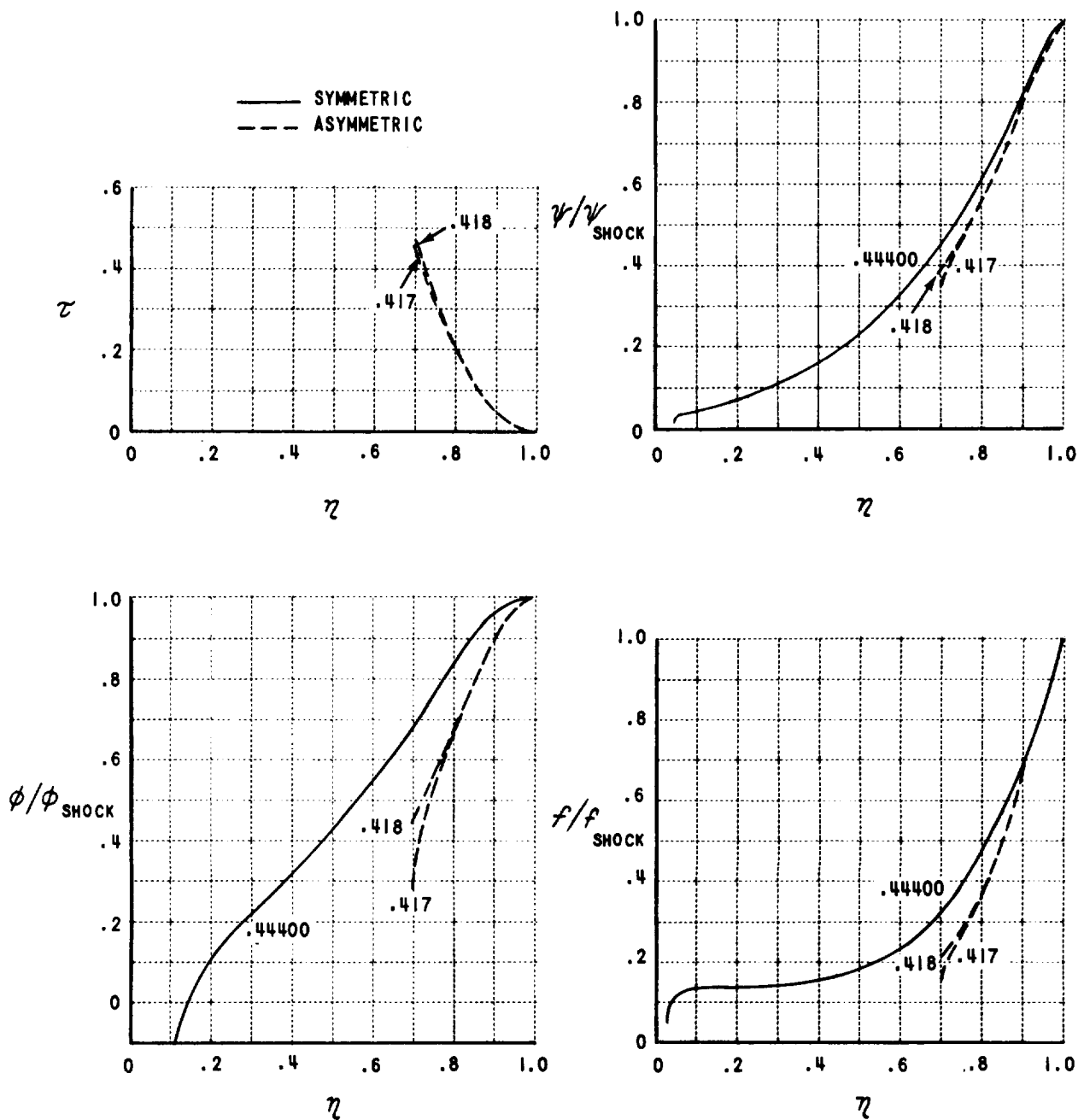
Figure 7a   QUASI-SIMILAR BLAST WAVE SOLUTION
$\nu = 2$ $S = 2$ $M = 8$
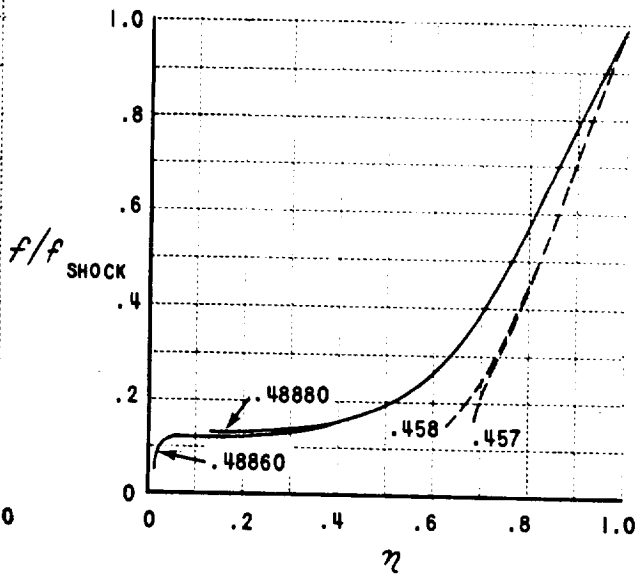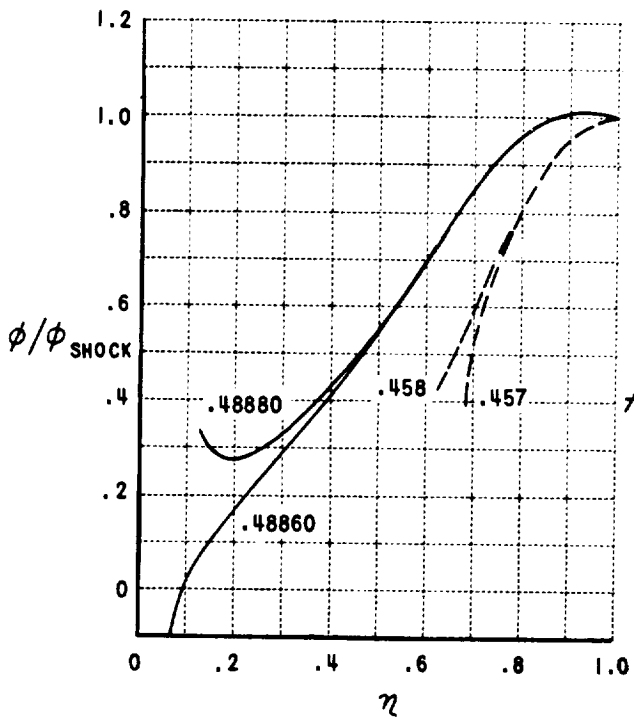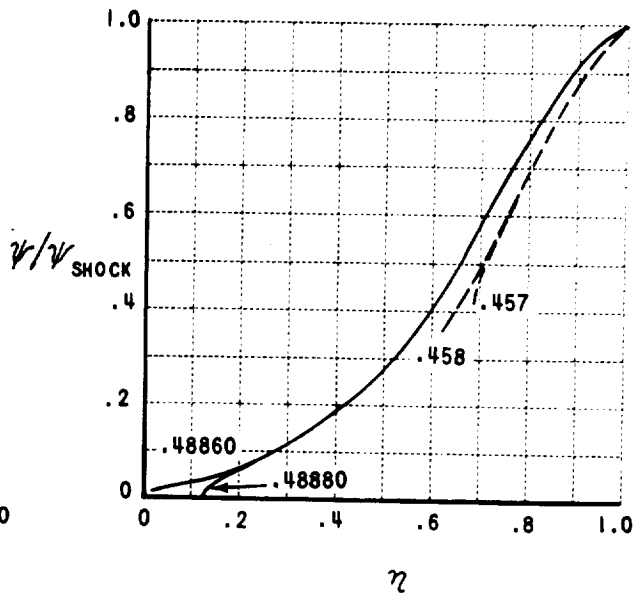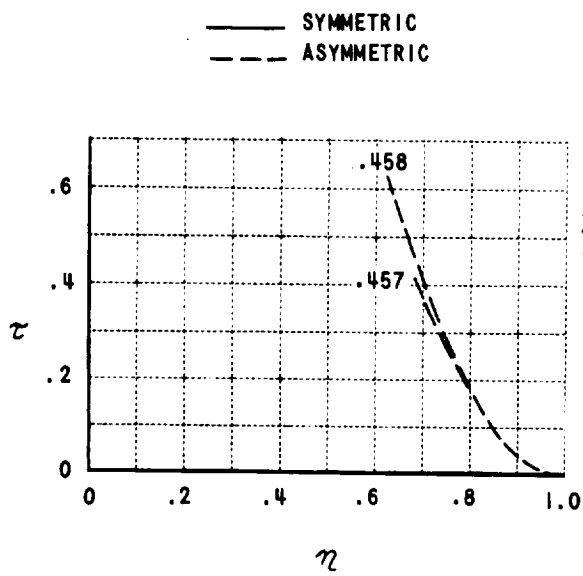
Figure 7b QUASI-SIMILAR BLAST WAVE SOLUTION
$\nu = 2$ $S = 2$ $M = 4$
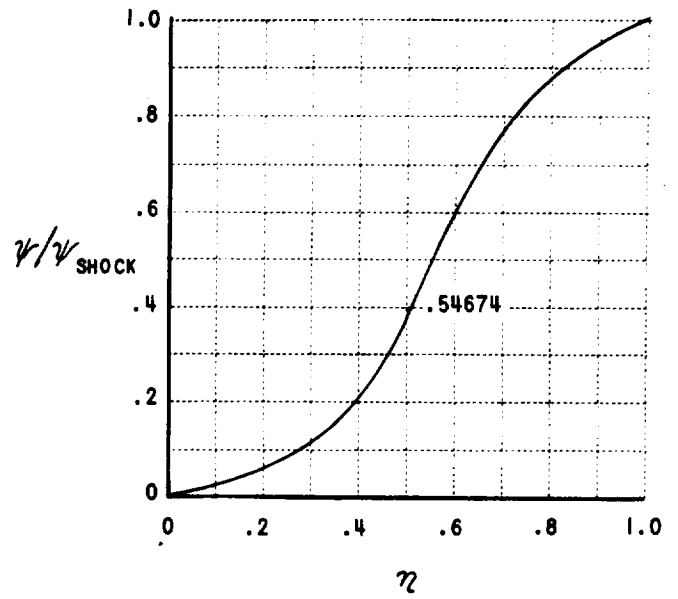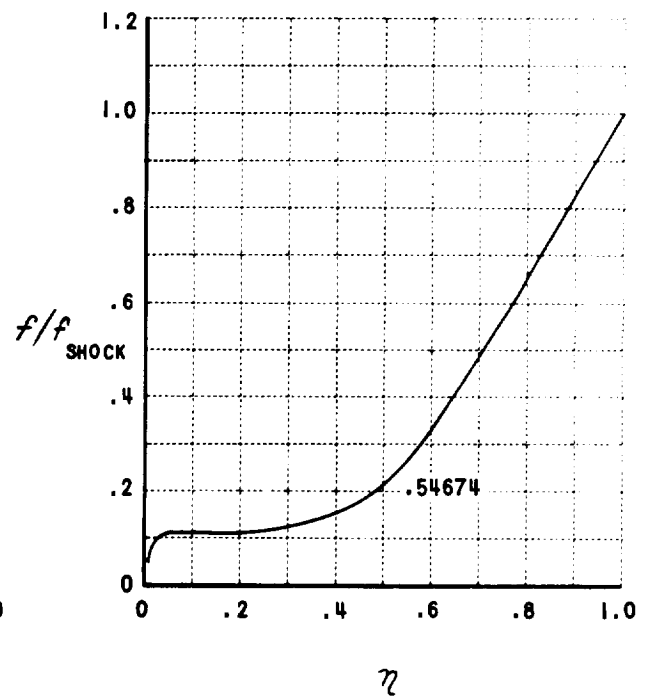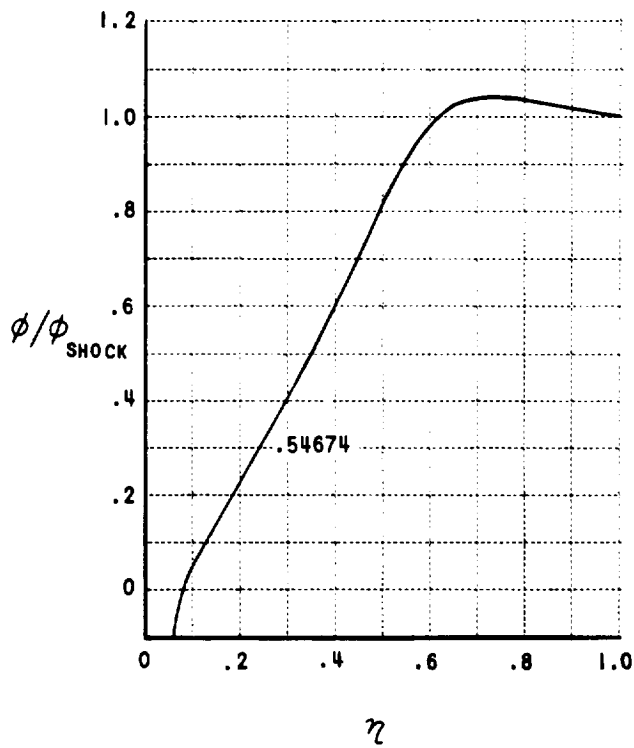
Figure 7c QUASI-SIMILAR BLAST WAVE SOLUTION
$\gamma = 2$ S = 2   M = 2.5
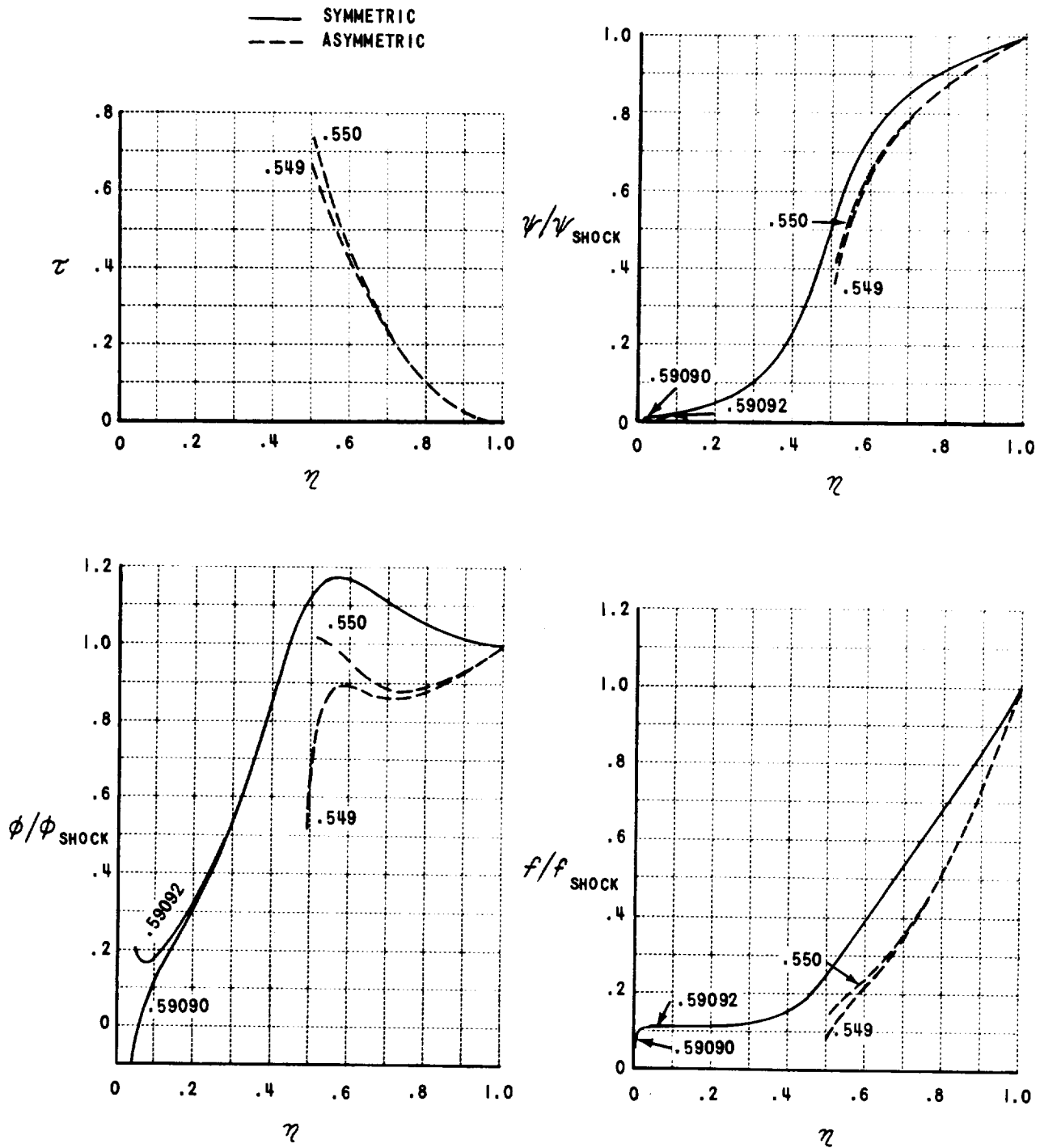
Figure 7d   QUASI-SIMILAR BLAST WAVE SOLUTION
$\nu = 2$ $S = 2$ $M = 2$
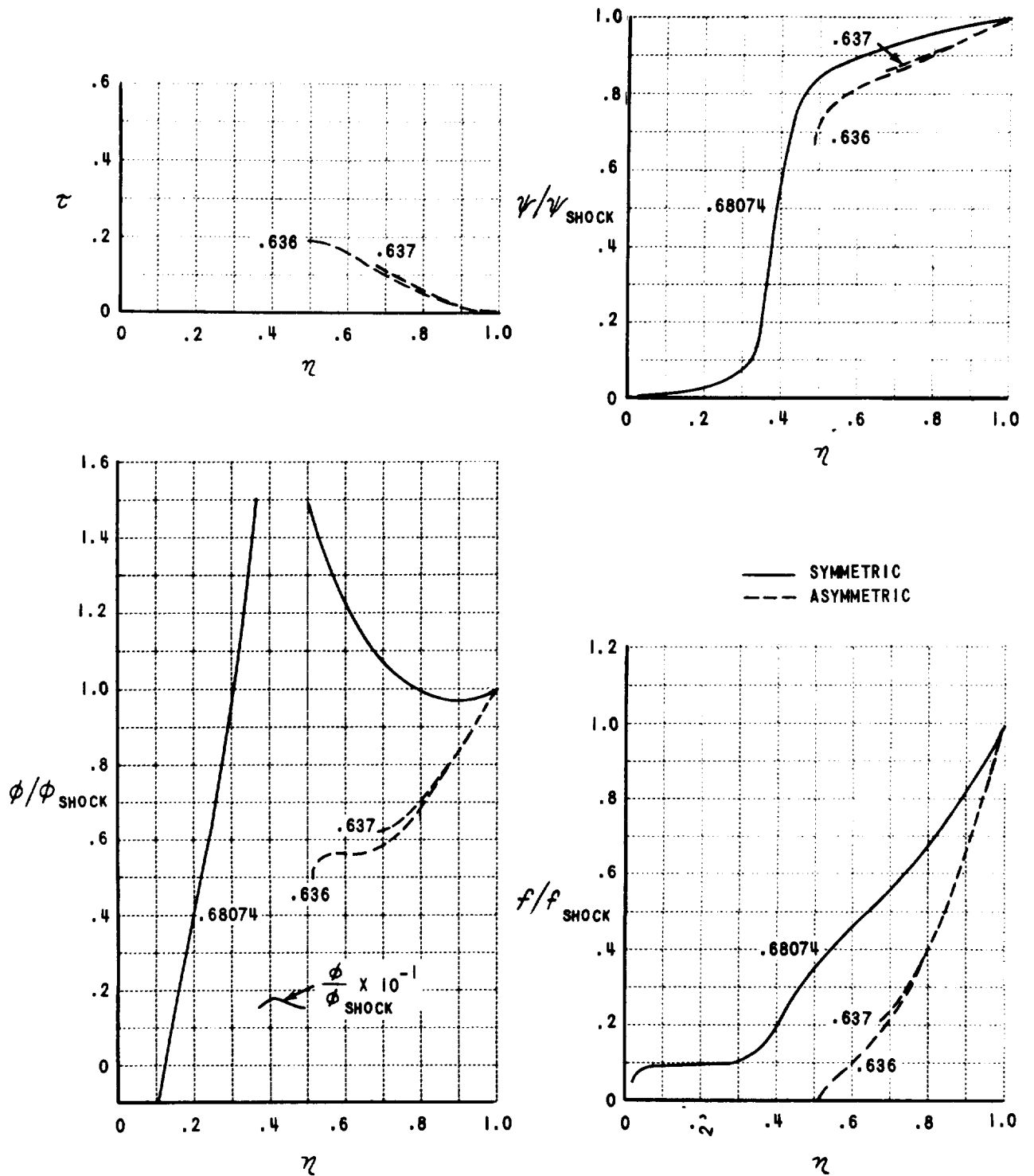
Figure 7e QUASI-SIMILAR BLAST WAVE SOLUTION
$\mathcal{V} = 2$ $S = 2$ $M = 1.5$

125
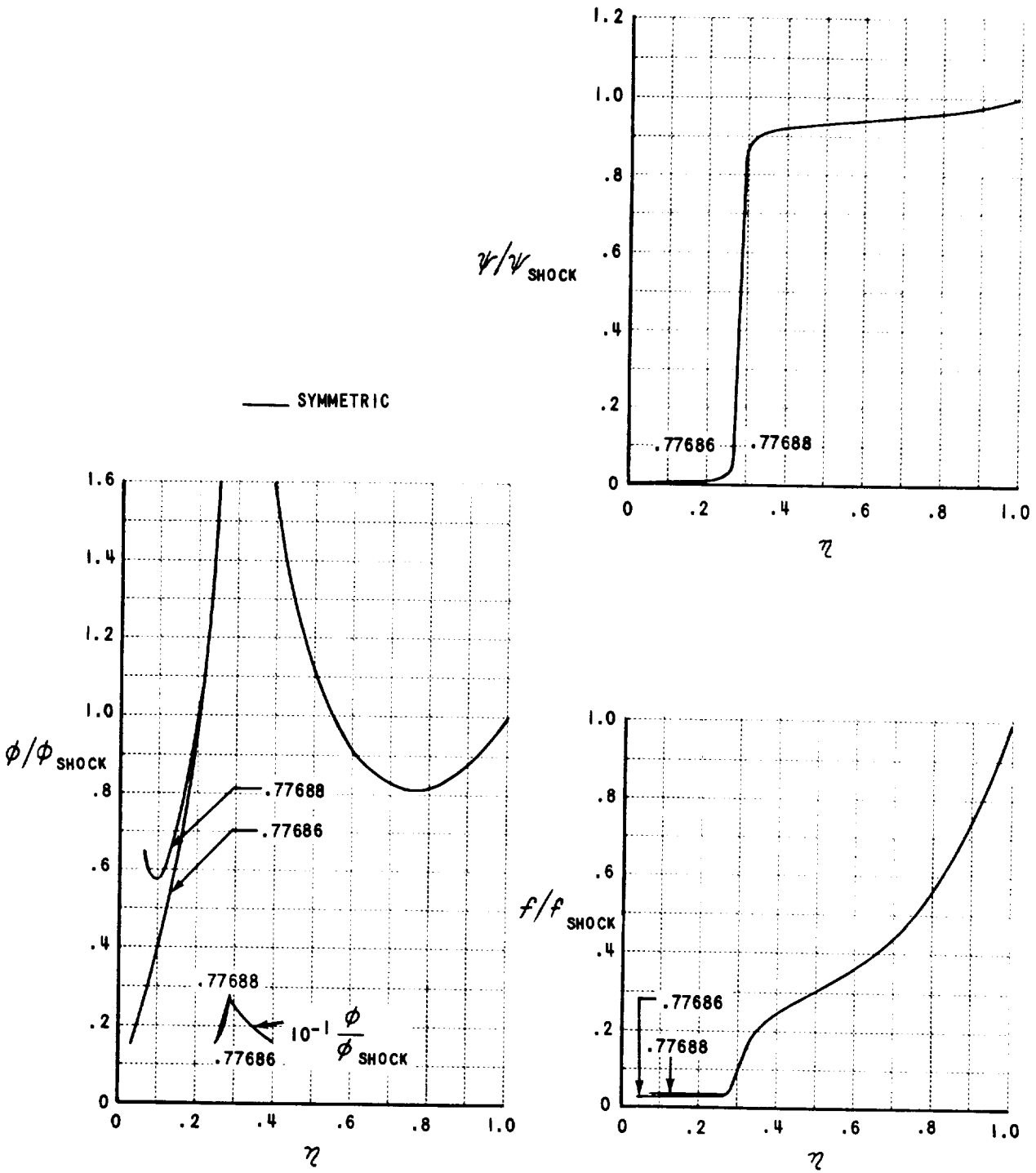
Figure 7f QUASI-SIMILAR BLAST WAVE SOLUTION
$\gamma = 2$ $S = 2$ $M = 1.25$
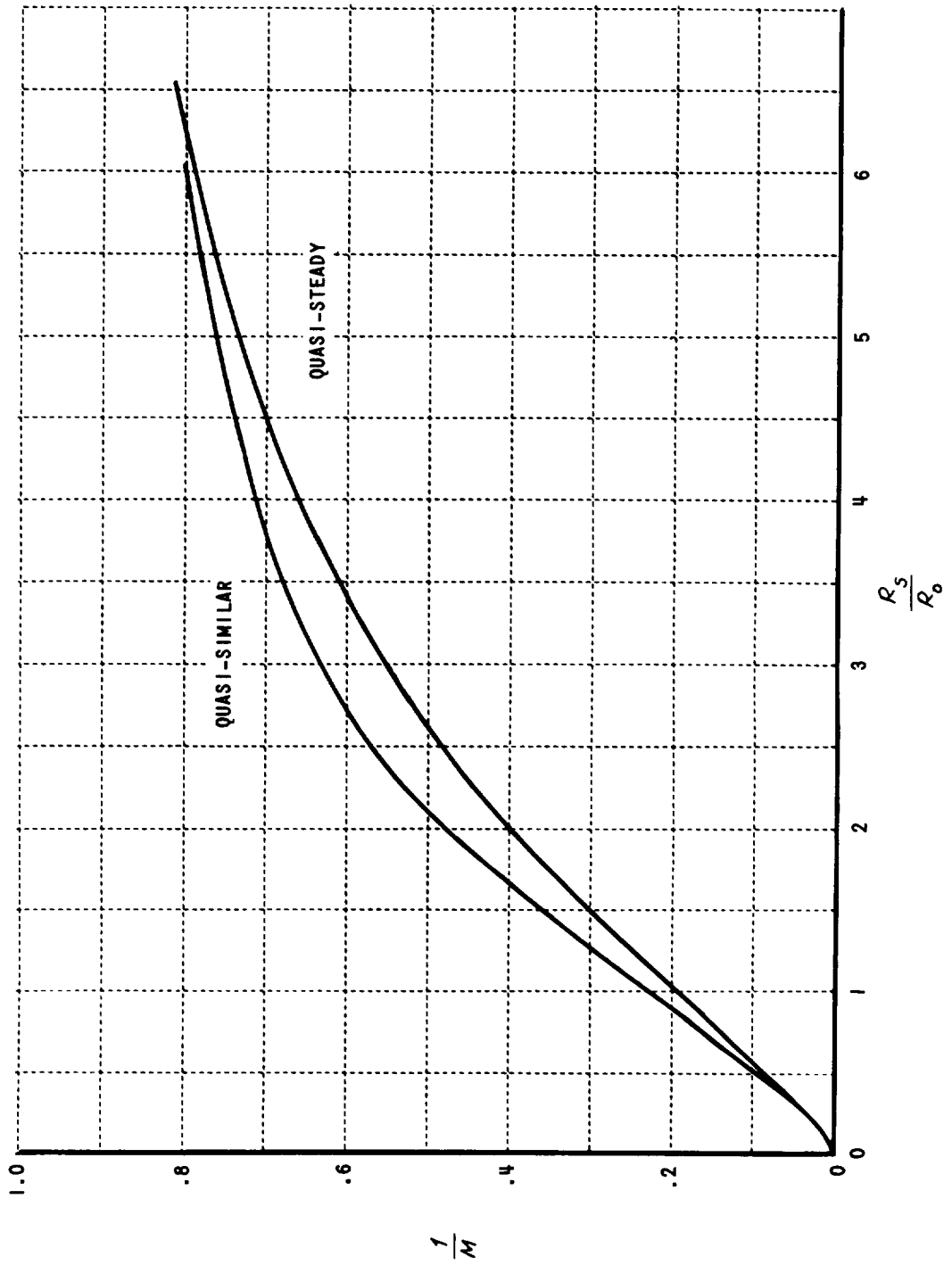
Figure 8 SHOCK SPEED-SHOCK RADIUS RELATION FOR QUASI-STEADY SOLUTION
AND QUASI-SIMILAR SOLUTION; $\nu = 2$, $S = 2$

127
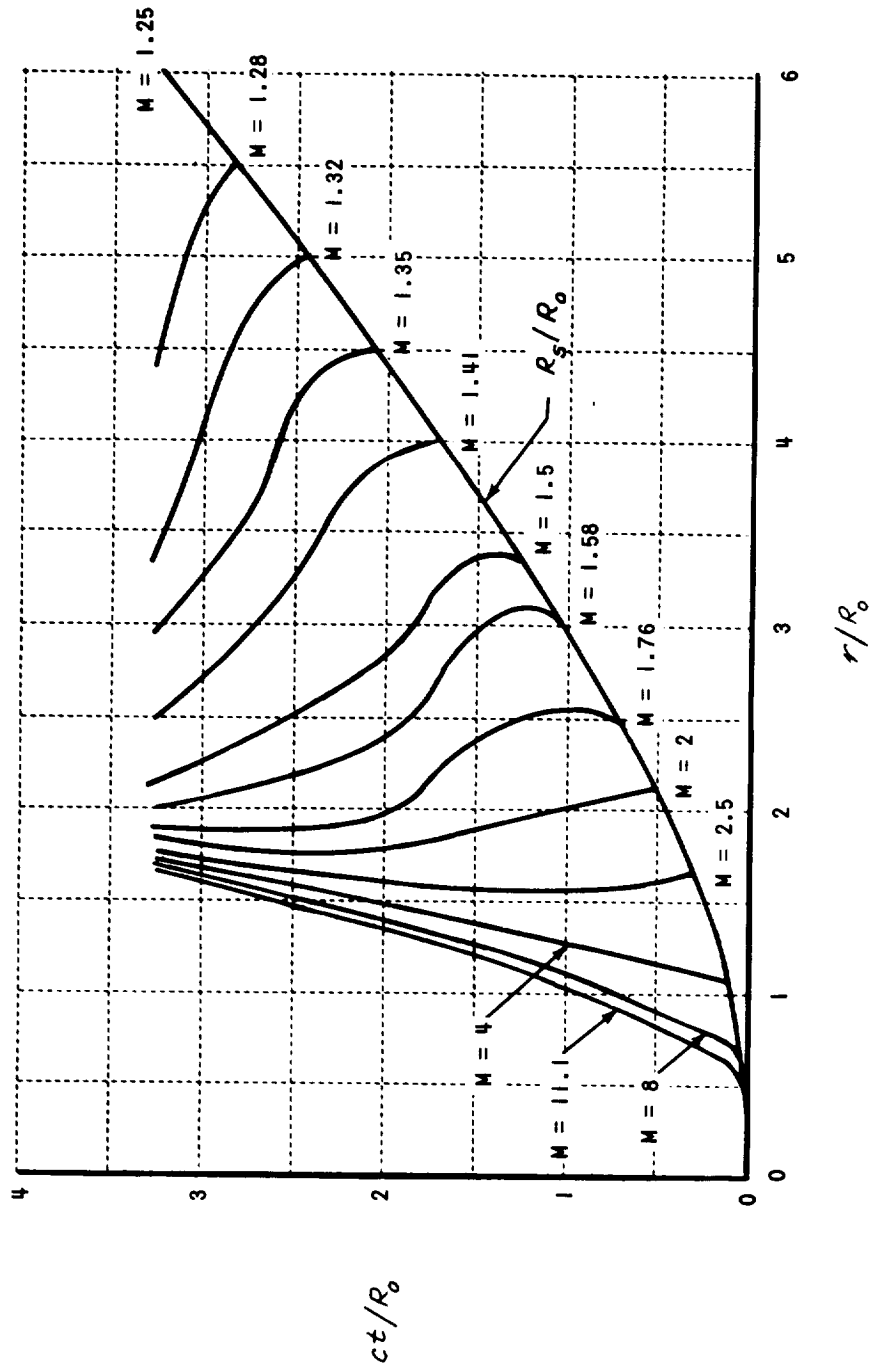
Figure 9 SHOCK AND PARTICLE TRAJECTORIES; $\nu = 2$, $S = 2$
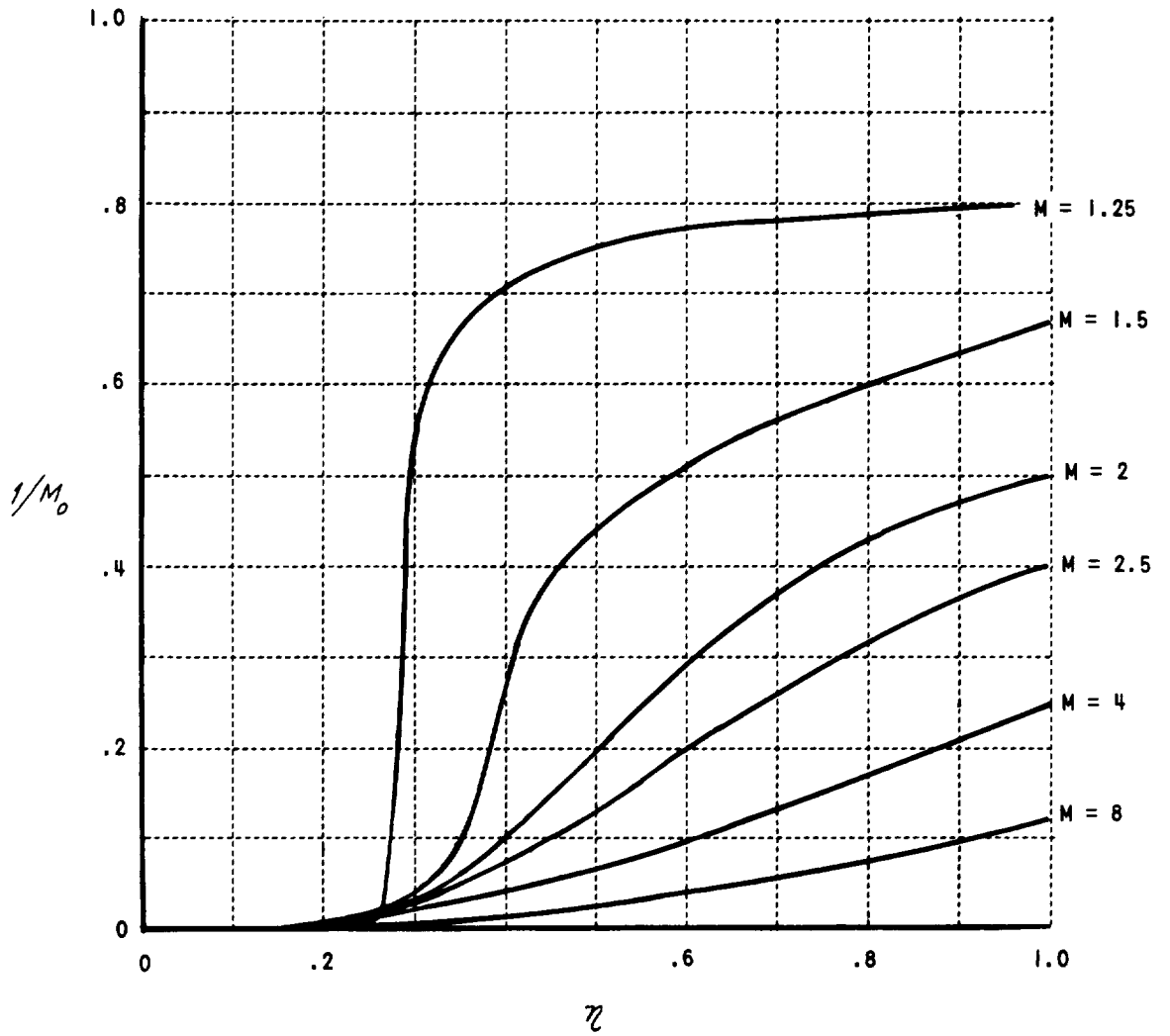
Figure 10   VALUES OF THE SHOCK MACH NUMBER AT SHOCK CROSSING; $\gamma = 2$, S = 2
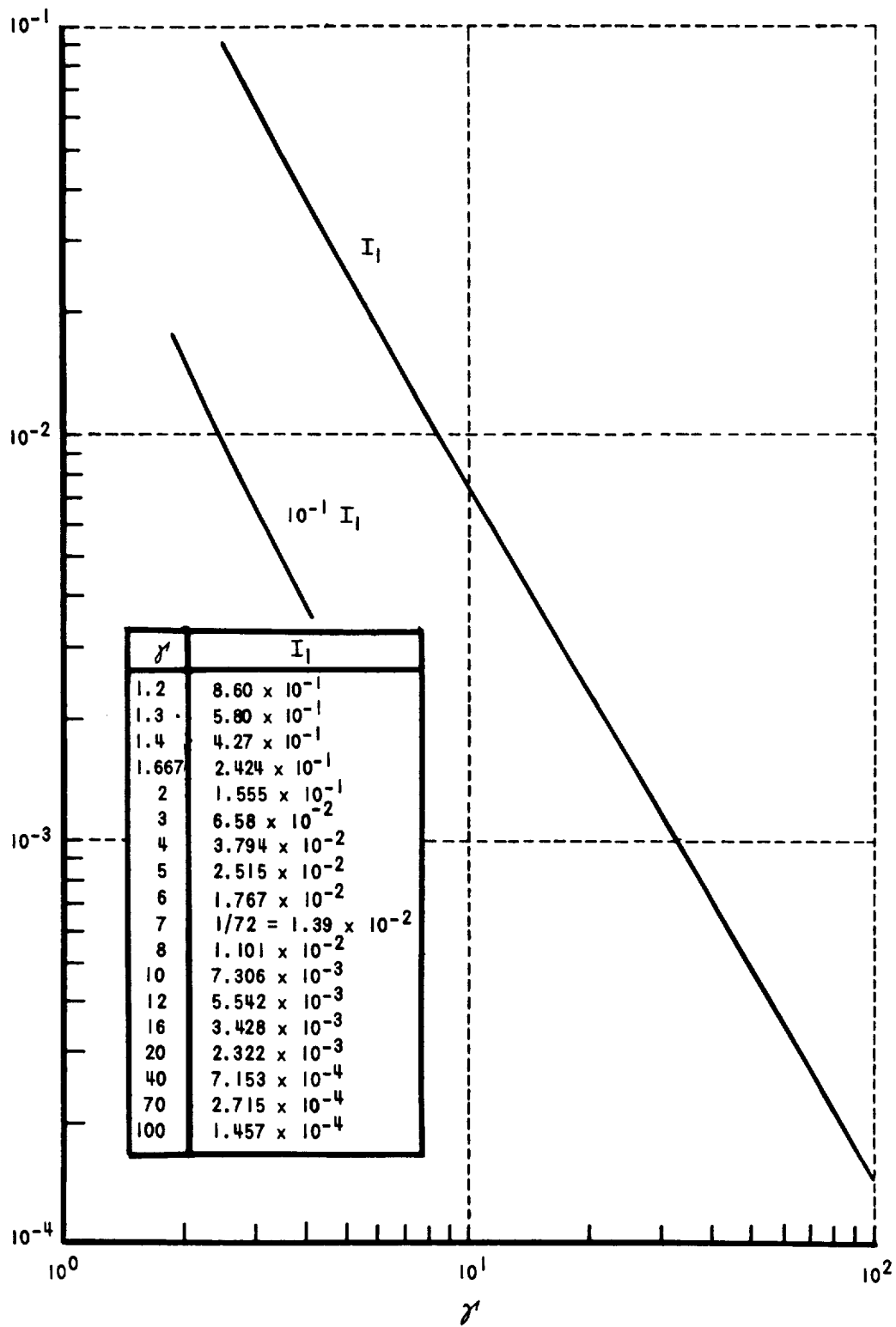
Figure II   THE FUNCTION I_1 (γ) FOR SPHERICALLY SYMMETRIC BLAST WAVES
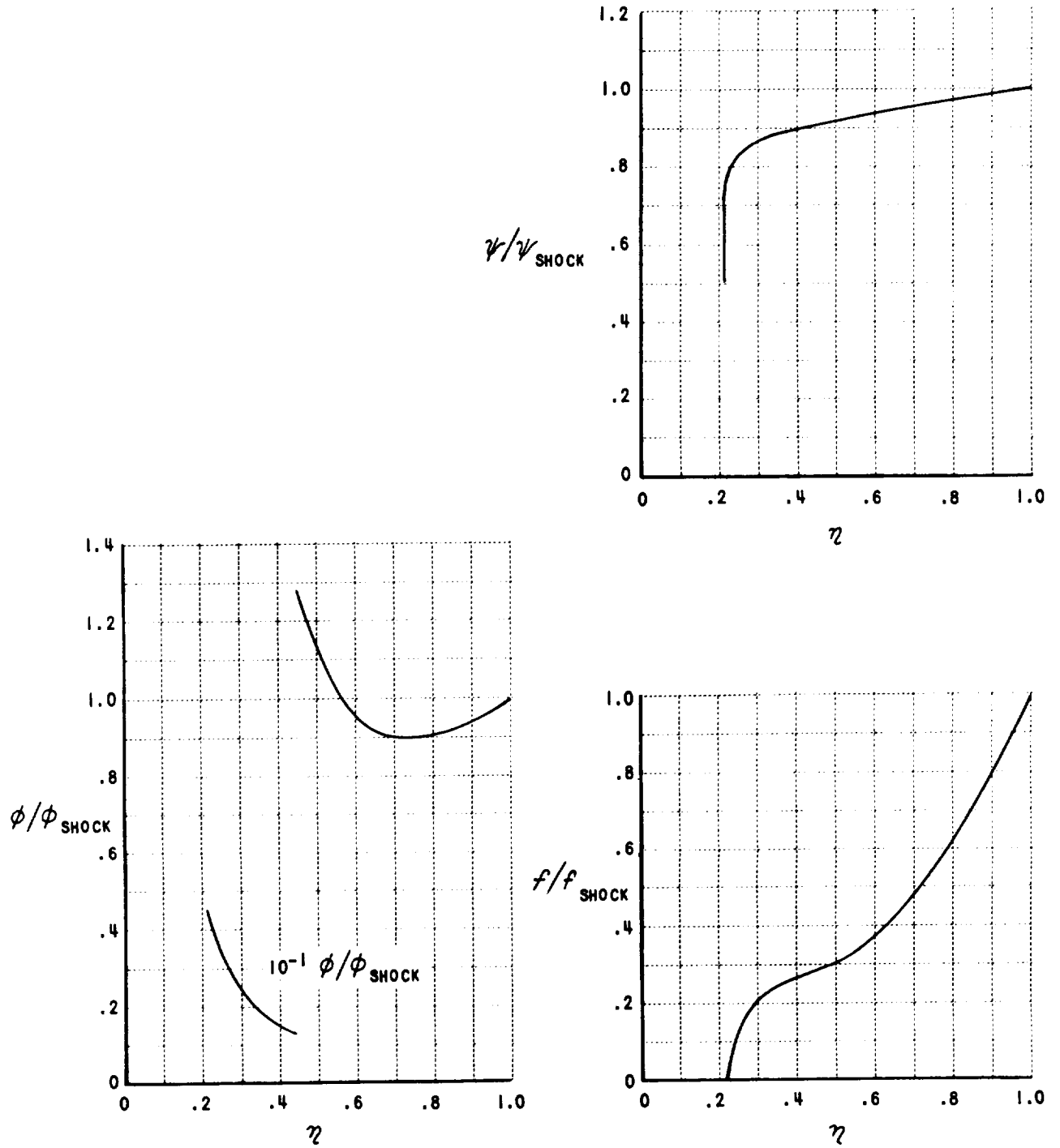
Figure 12a   DISTRIBUTION OF DENSITY, PARTICLE VELOCITY, AND PRESSURE
FOR A SPHERICAL BLAST WAVE; $\gamma = 40$

131
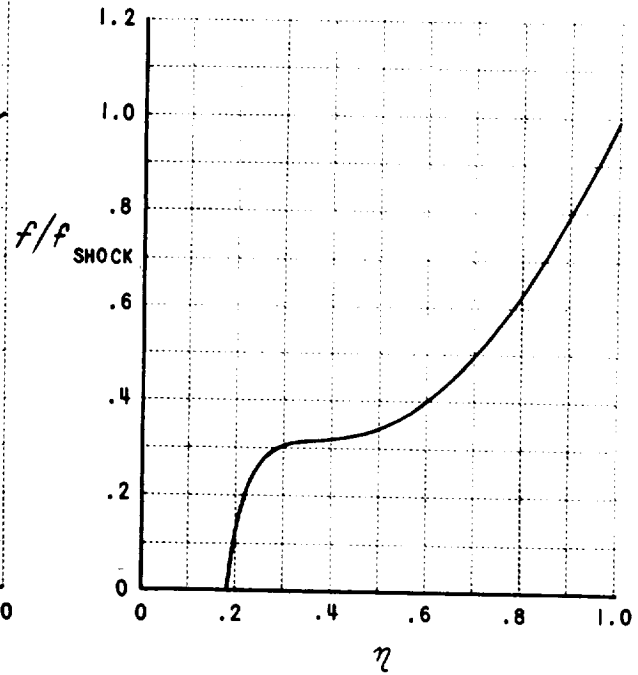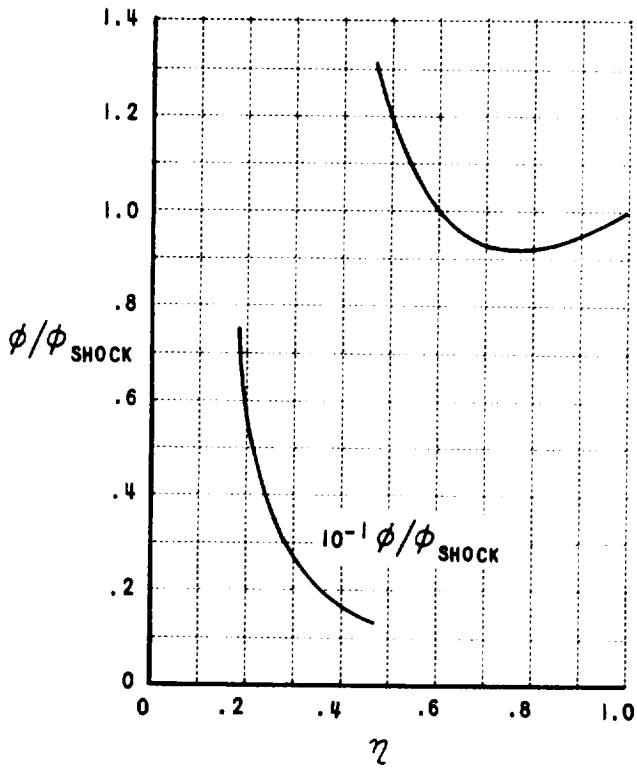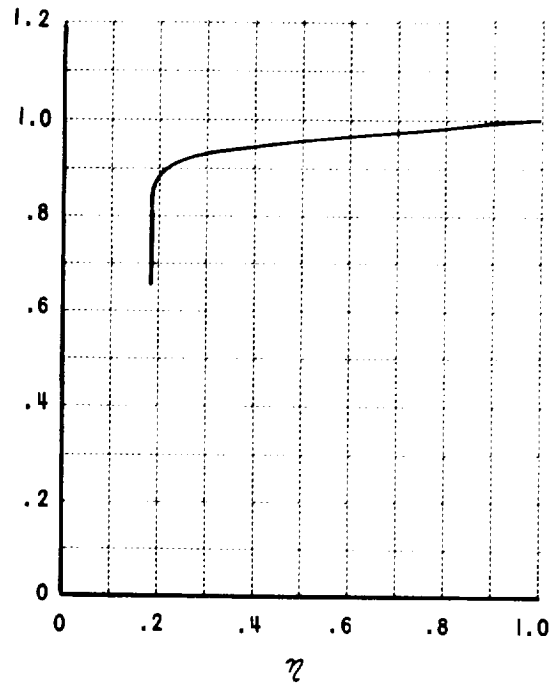
Figure 12b   DISTRIBUTION OF DENSITY, PARTICLE VELOCITY, AND PRESSURE
FOR A SPHERICAL BLAST WAVE; $\gamma = 70$
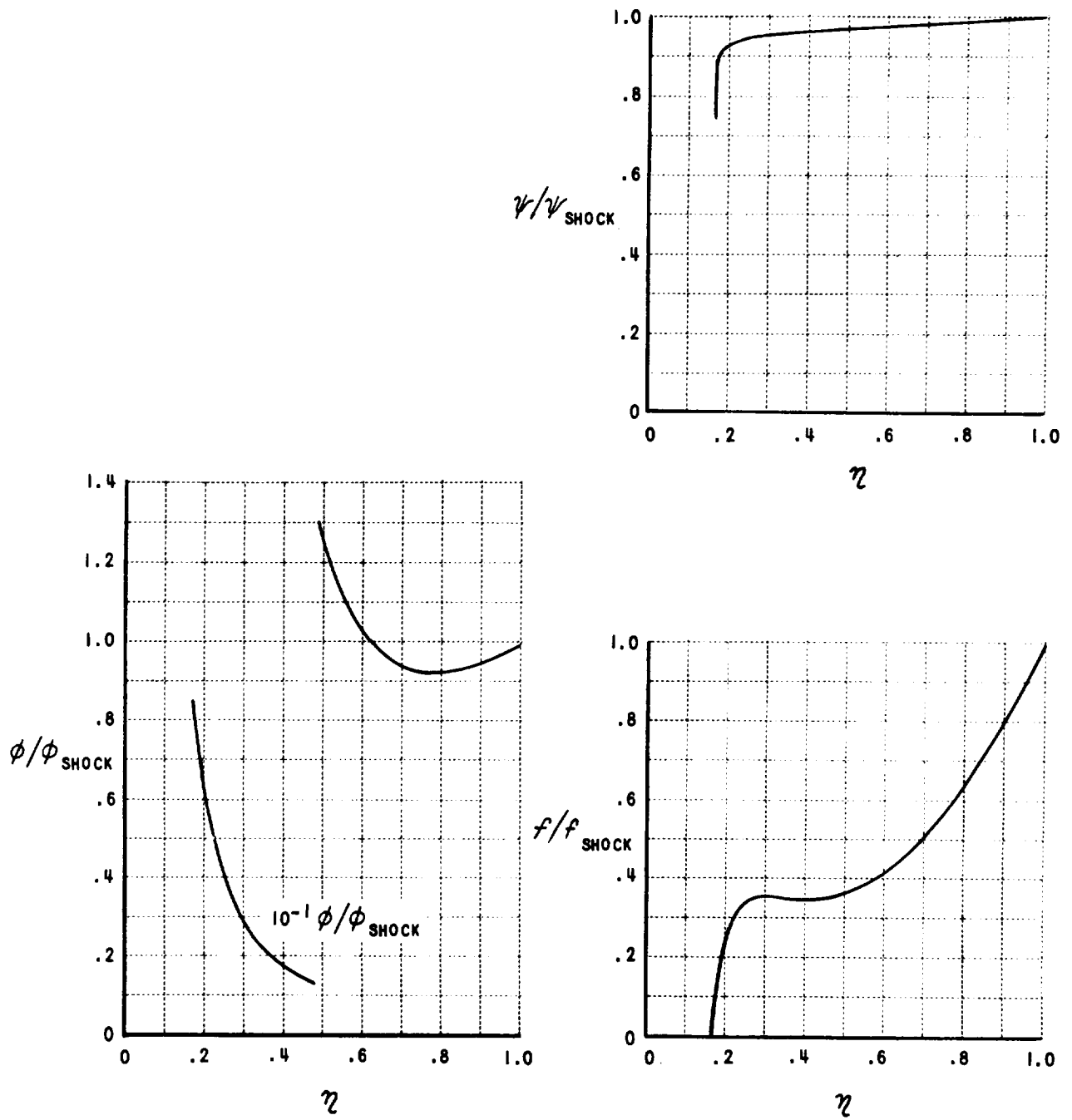
Figure 12c   DISTRIBUTION OF DENSITY, PARTICLE VELOCITY, AND PRESSURE
FOR A SPHERICAL BLAST WAVE; γ = 100

SYM	SOURCE	PROJ→TARGET	V, km/sec
○	EICHELBERGER & GEHRING	Fe→LUCITE	4.6
△	BJORK	Fe→Fe	5.5
□	"	Fe→TUFF	30
◇	HALPERSON & HALL	Al→LUCITE	5.31
◇	PIACESI	Al→LUCITE	5.7
◇	WALSH & TILLOTSON	Fe→Fe	40
▷	HEYDA & RINEY	Al→Al	7.6
△	"	"	20
▽	"	"	40
◇	"	"	60
▱	"	Pb→Pb	7.6
▱	"	"	20
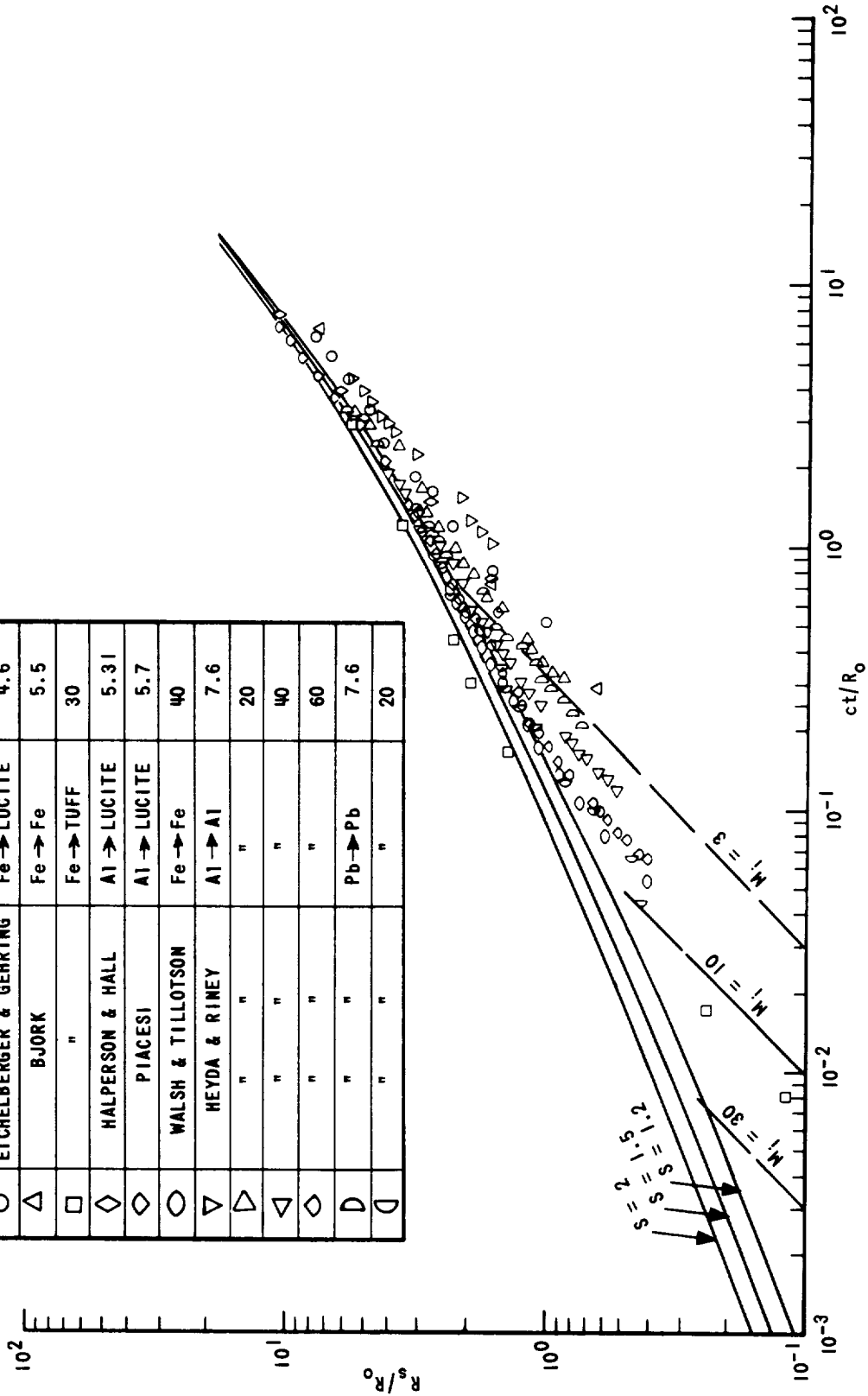
Figure 13 SHOCK-TRAJECTORY DATA COMPARED WITH QUASI-STEADY SOLUTION

$M_i = 3$

$M_i = 10$

$M_i = 30$

$S = 2$, $S = 1.5$, $S = 1.2$

ct/R_o

R_s/R_o
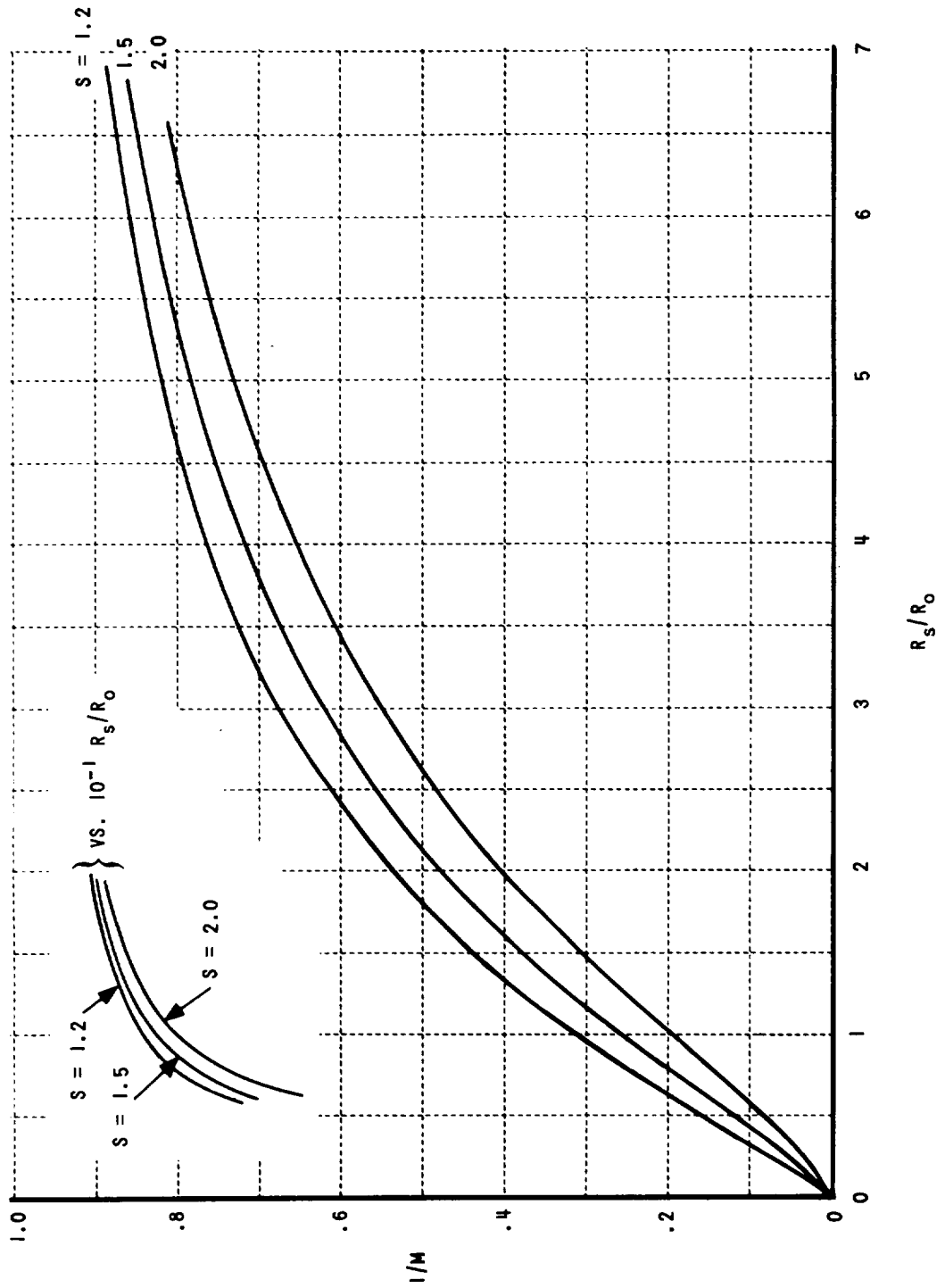
Figure 14 SHOCK SPEED – SHOCK RADIUS RELATION FOR QUASI–STEADY SOLUTION

AI-1821-A-2
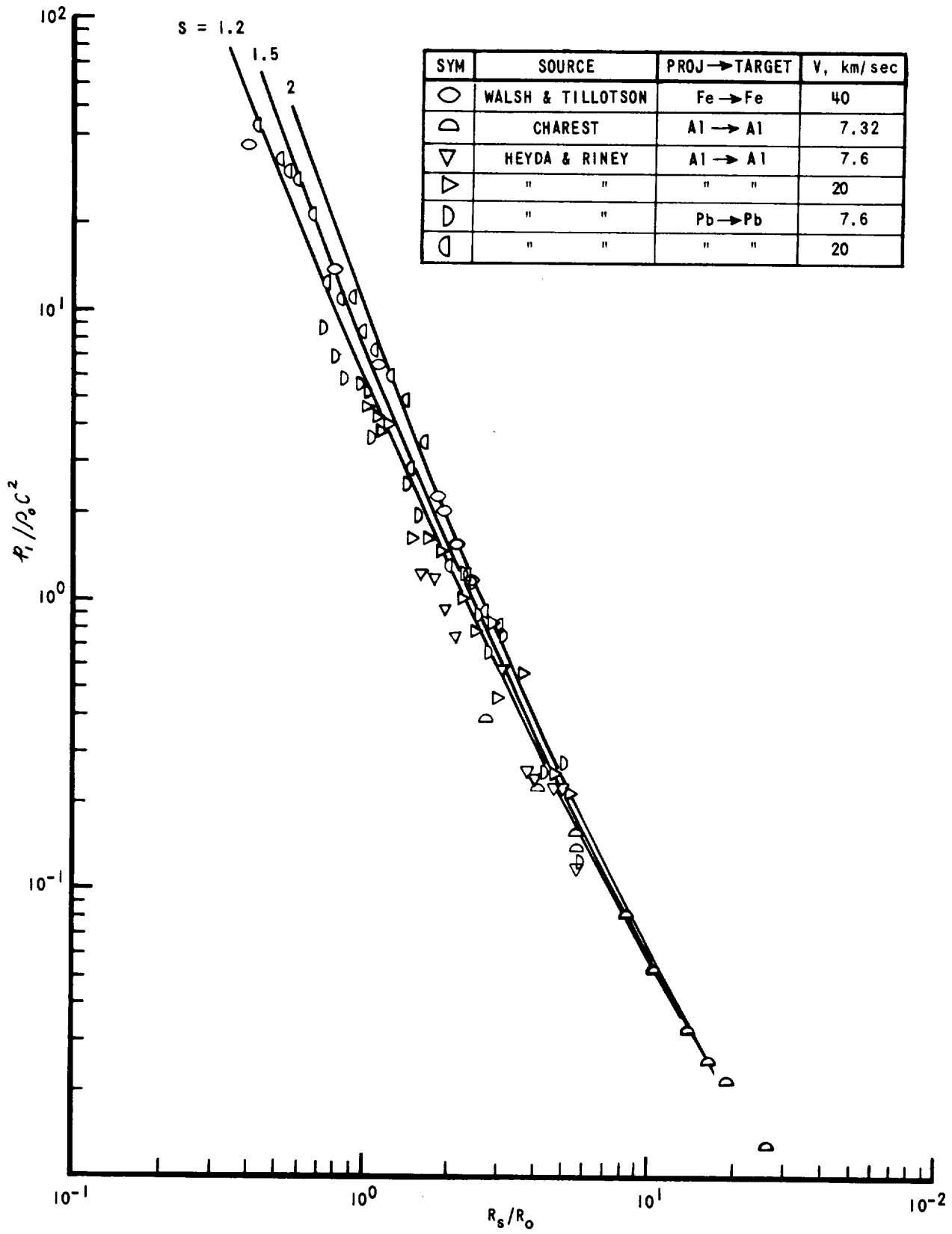
Figure 15 SHOCK PRESSURE VARIATION ACCORDING TO QUASI-STEADY THEORY
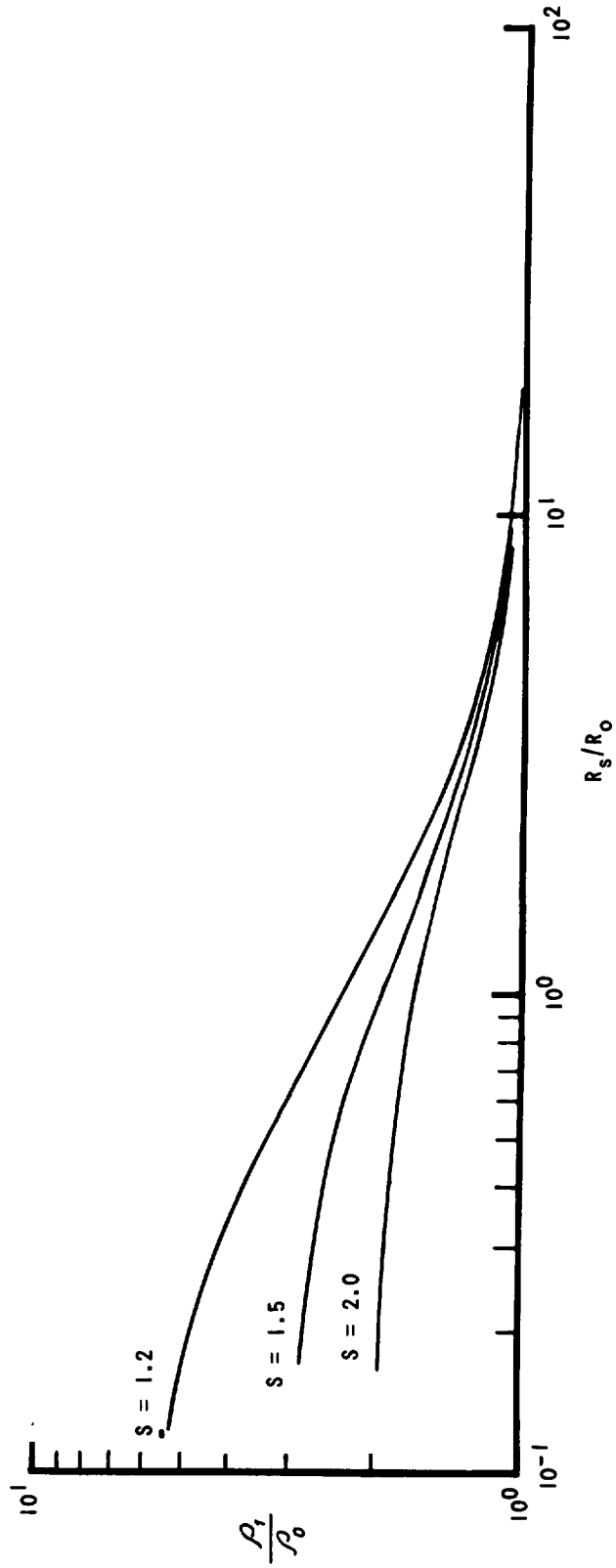
Figure 16 SHOCK DENSITY VARIATION ACCORDING TO QUASI-STEADY THEORY

137
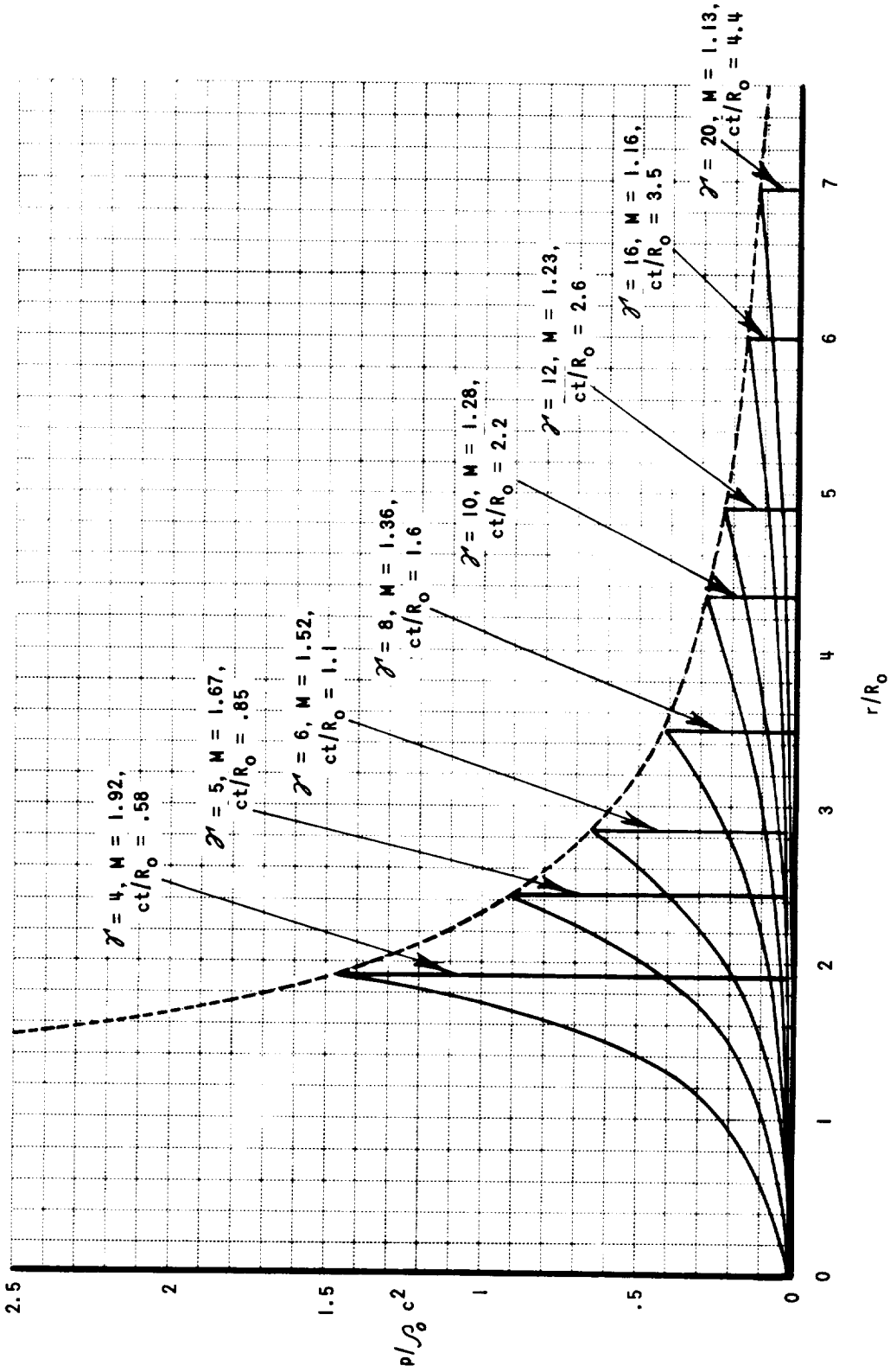
Figure 17a PRESSURE DISTRIBUTION ACCORDING TO QUASI-STEADY THEORY, S = 1.2

$R_o \equiv (E/2\pi \rho_o c^2)^{1/3}$
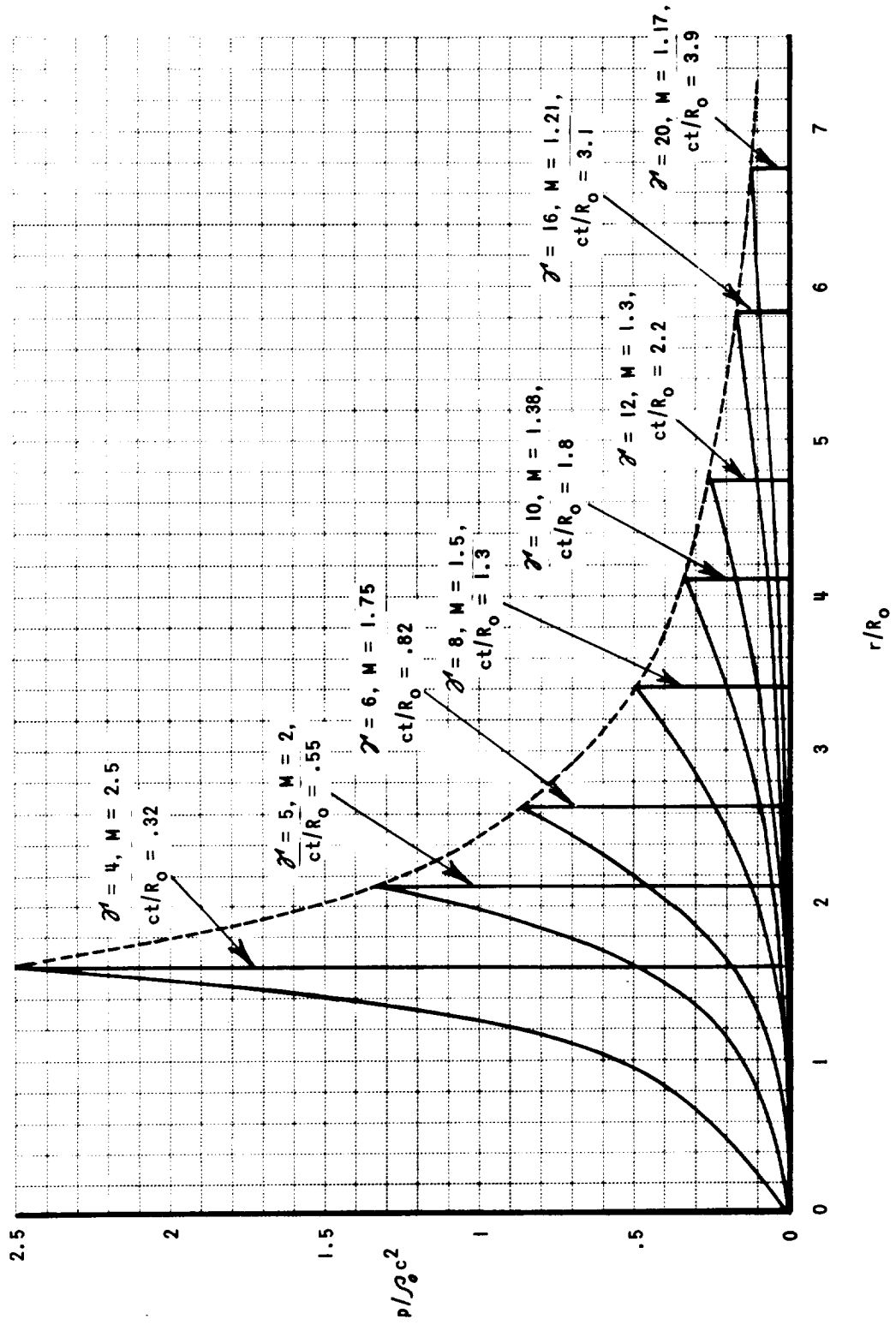
Figure 17b PRESSURE DISTRIBUTION ACCORDING TO QUASI-STEADY THEORY, S = 1.5

$$R_o \equiv (E/2\pi \rho_o c^2)^{1/3}$$
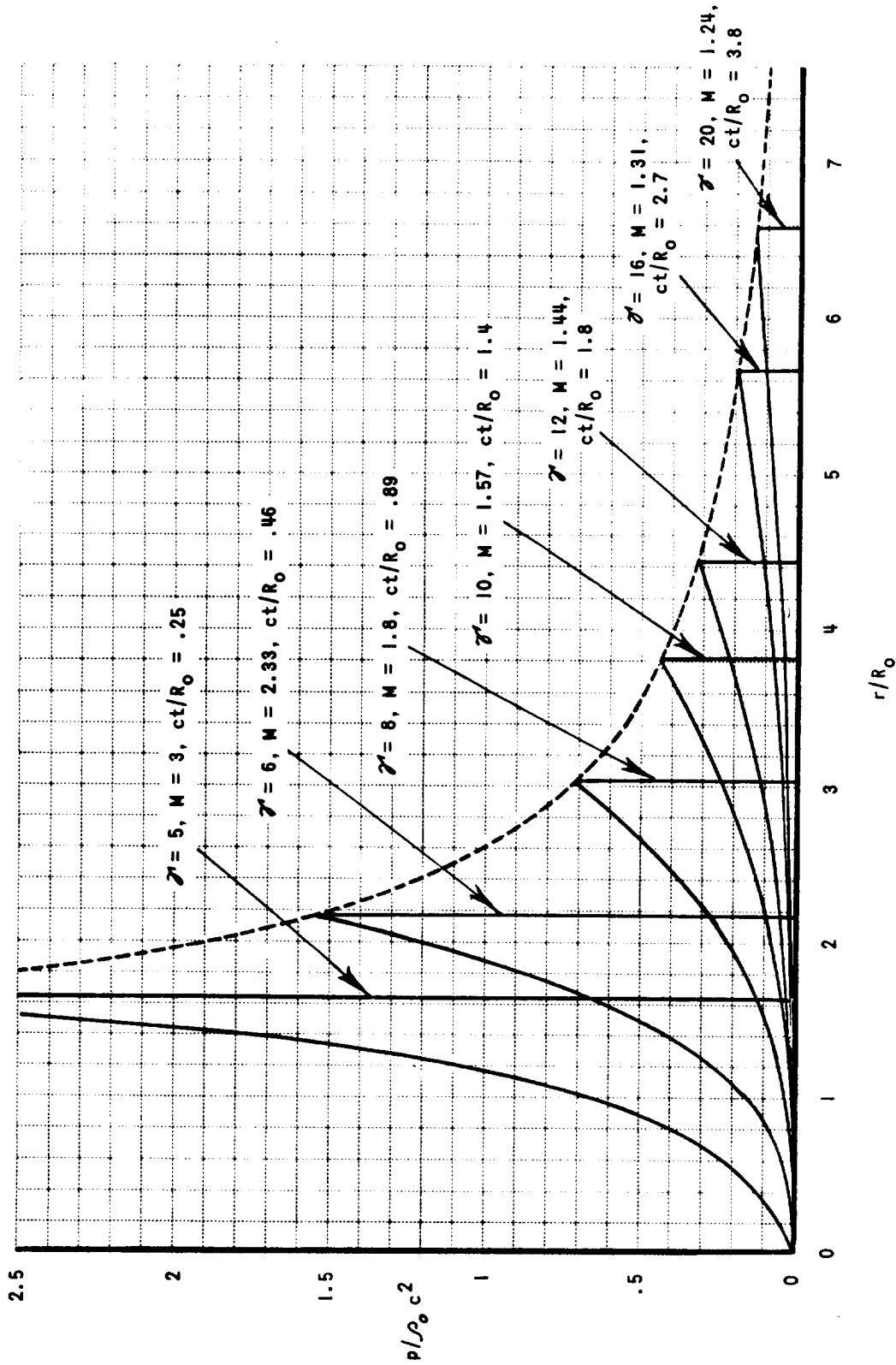
Figure 17c PRESSURE DISTRIBUTION ACCORDING TO QUASI-STEADY THEORY, S = 2

$R_o \equiv (E/2\pi\rho_o c^2)^{1/3}$
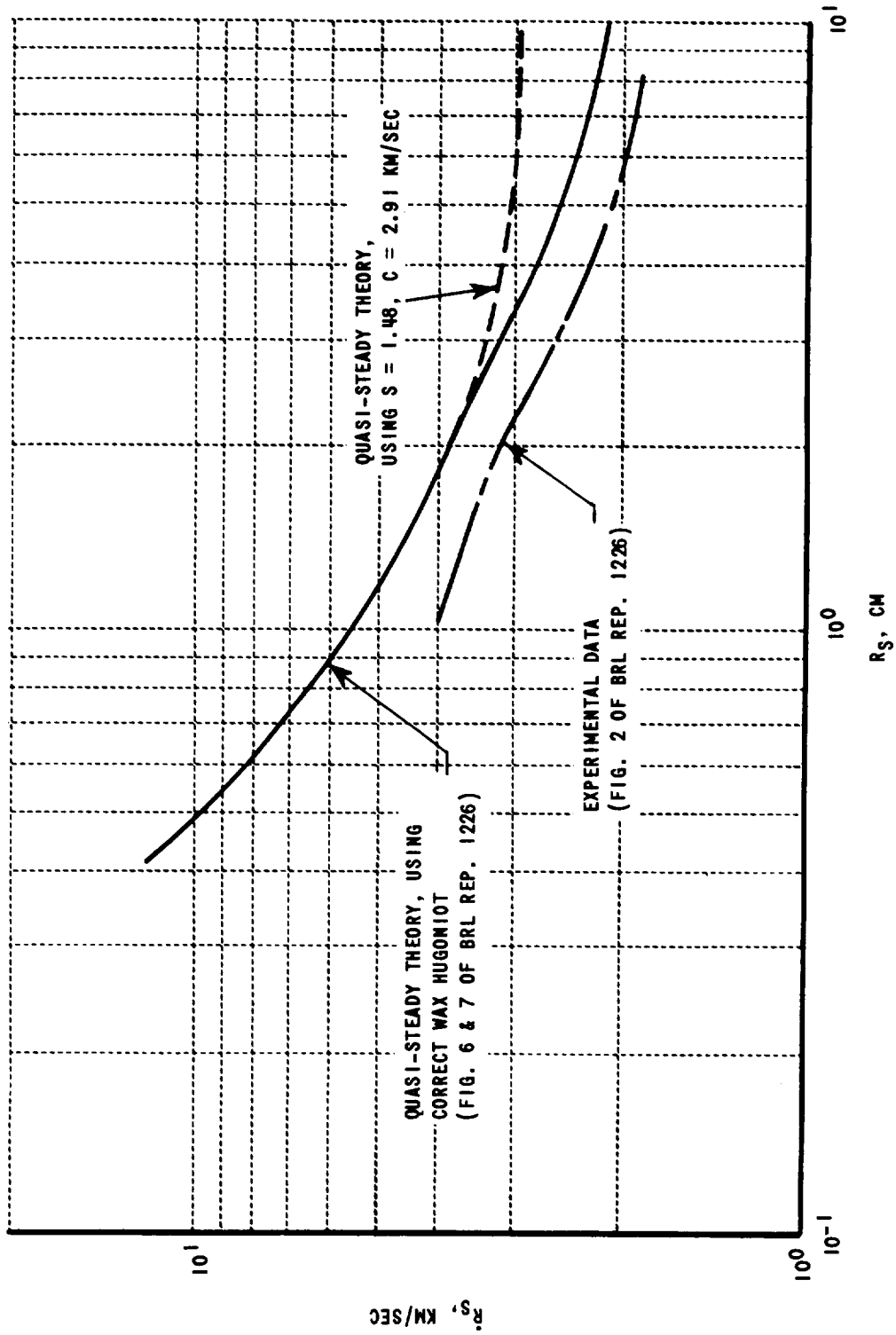
Figure 18 BLAST-WAVE THEORY COMPARED WITH NEW DATA IN WAX TARGETS

AI-1821-A-2

$$m = \frac{\rho_o}{\rho_p} = \frac{\text{INITIAL DENSITY OF NONPOROUS SOLID}}{\text{INITIAL DENSITY OF POROUS SOLID}}$$
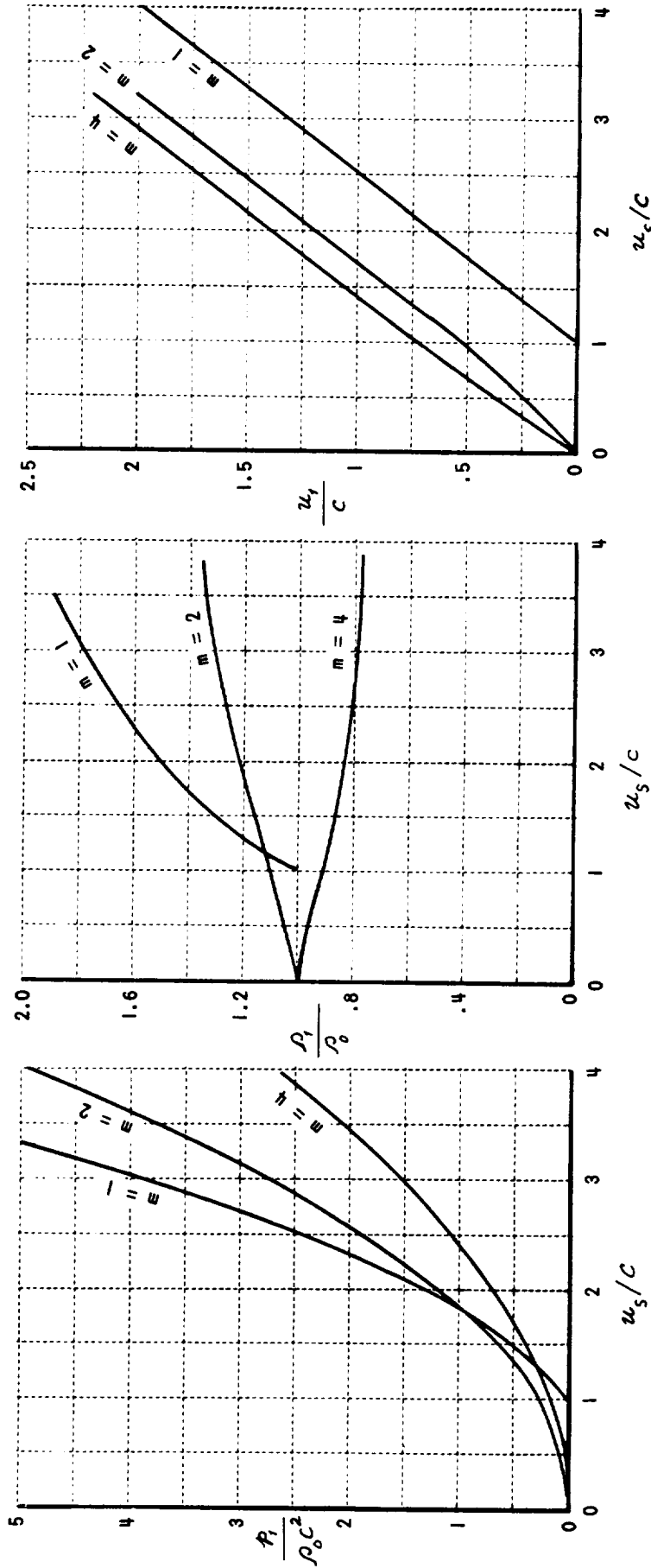
Figure 19   HUGONIOT OF A POROUS MEDIUM; S = 1.5
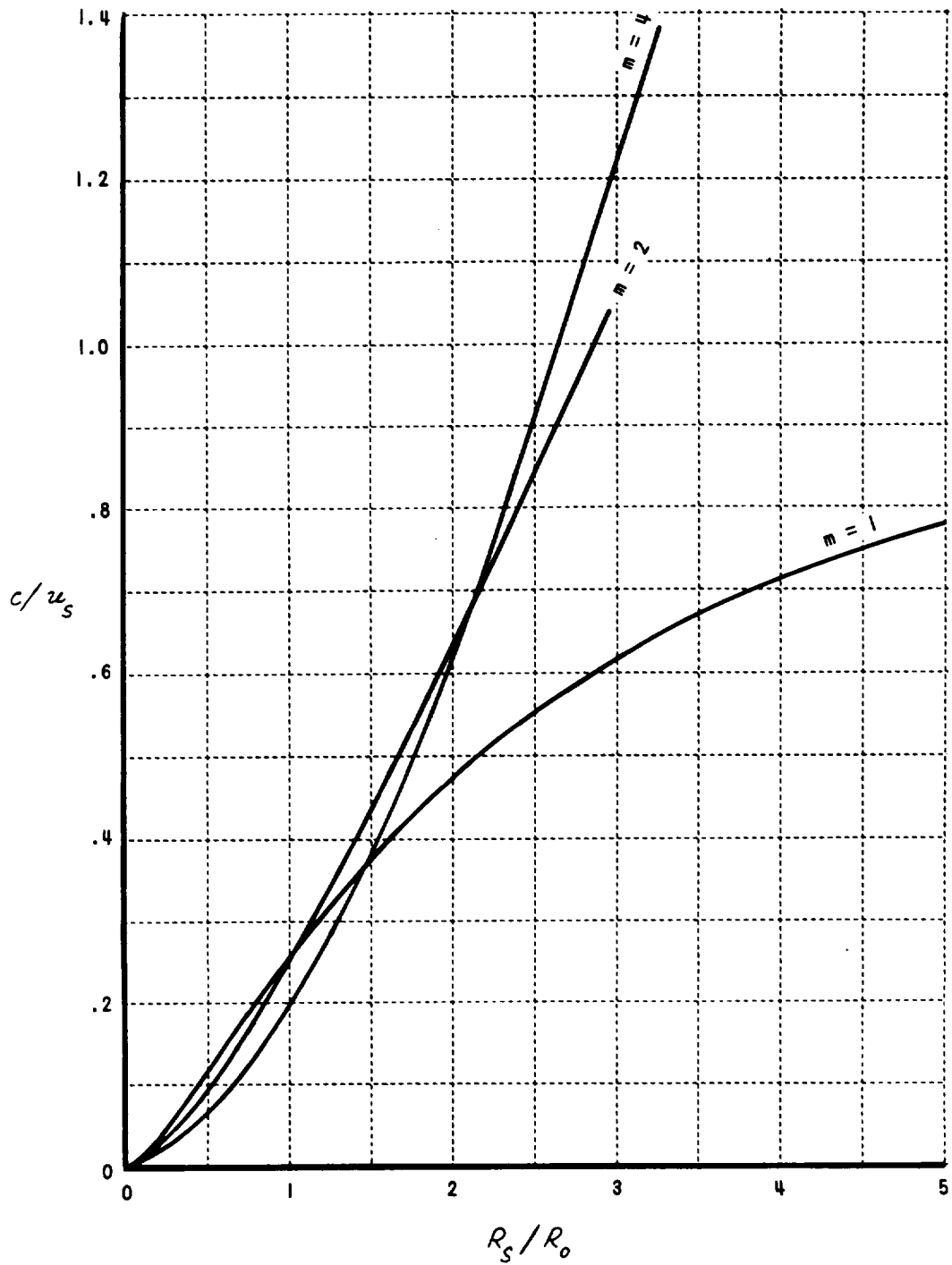
Figure 20   QUASI-STEADY SOLUTION FOR SHOCK-SPEED, SHOCK-RADIUS
RELATION IN POROUS MEDIA;   S = 1.5

AI-1821-A-2
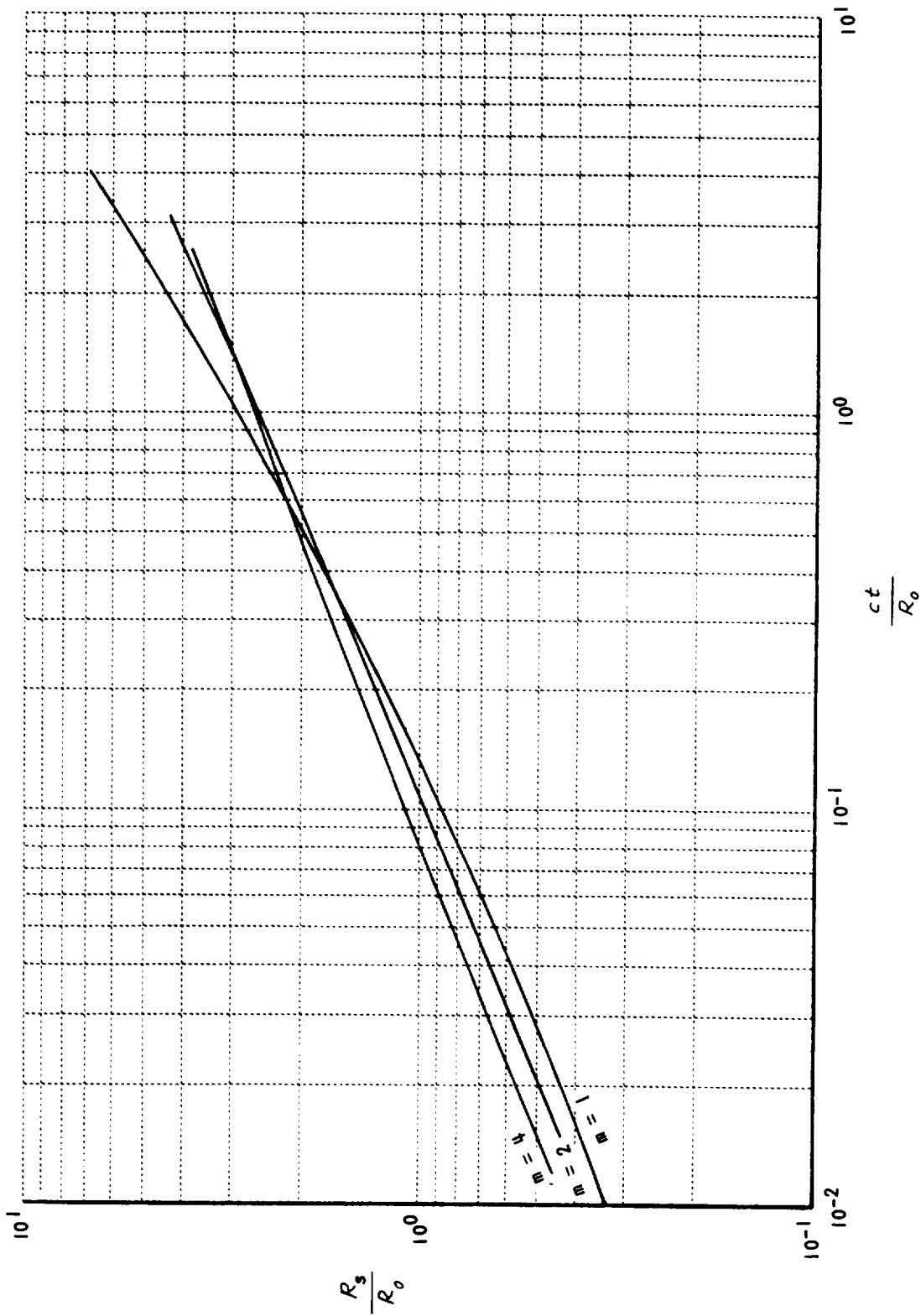
Figure 21 QUASI-STEADY SOLUTION FOR SHOCK TRAJECTORY IN A POROUS MEDIUM; S = 1.5